UNIVERSITÀ DEGLI STUDI DI TRIESTE

DOTTORATO DI RICERCA IN INGEGNERIA CIVILE
DIPARTIMENTO DI INGEGNERIA ED ARCHITETTURA (DIA)
XXXI CICLO

Numerical modelling and design methods for CLT structures

SSD: ICAR/09 – Tecnica delle costruzioni

DOTTORANDO
Gabriele TAMAGNONE

COORDINATORE DOTTORATO
Chiar.mo Prof. Ing. Diego MICHELI

FIRMA: _____

SUPERVISORE DI TESI
Chiar.mo Prof. Ing. Massimo FRAGIACOMO

FIRMA: _____

SUPERVISORE DI TESI
Dr. Ing. Giovanni RINALDIN

FIRMA: _____

ANNO ACCADEMICO 2017 - 2018

ABSTRACT

Since its conception in the mid 90's, cross-laminated timber, known also as CLT or X-Lam, has achieved a great popularity as construction material thanks to its numerous intrinsic qualities, worldwide effort to erect reliable structures in seismic-prone areas and necessity to build a more eco-friendly environment.

Many tests have been carried out in the last 15 years, aimed to better understand the behavior of connections in CLT buildings, CLT assemblies and CLT structures in order to provide reliable rules for designers to calculate structures made of CLT in any loading condition.

Based on these tests, many numerical models have been suggested through the years. They represent a fundamental tool for the design of CLT structures when specific design problems arise.

Despite many years of efforts, reliable design rules are still missing in almost every code worldwide and many are still the unknown related to CLT structures behavior at many levels (connections, assemblies, structures).

This thesis summarizes three years of numerical investigations, which have faced different problems related to the comprehension of CLT assemblies and structures behavior under dynamic loading conditions. The first part of this path focused on the continuation of a previous study made within the Master Degree thesis, which was the formulation of a simplified method to obtain an axial-load/bending moment limit domain for a CLT panel connected to the supporting surface through hold-down and angle bracket connections.

Without test results of interest, the focus of the study returned to be the formulation of simple methods for CLT assemblies design. The problem of panel-to-panel connections was investigated. In particular, the stiffness of such connections related to the rocking behavior of 2-panel wall assemblies was studied through full-scale tests and FE numerical analyses. A formula for the design of these connections was firstly suggested and then, after further analyses, revised and corrected.

In order to extend the analyses and consider more complex assemblies, the influence of diaphragm and wall-to-diaphragm connections stiffness on the rocking behavior of wall assemblies was numerically investigated, taking into account configuration with and without diaphragm, varying several parameters to obtain statistically significant results.

In the summer of 2017 the candidate actively participated to the NHERI TallWood

Project, an American research project intended to test CLT structures in order to provide design rules for these structures in the future US codes. Sponsored by the Colorado State University, in the person of Professor John W. van de Lindt, the candidate collaborated to the setup of a 2-story CLT building that was tested on the UCSD shaking table located in San Diego (California).

In order to assess the most proper value of damping for CLT structures under low-intensity seismic events and to better investigate the potential of the component approach for the modelling of CLT structures, the 0,15 g shaking table tests of the 3-story building within the SOFIE Project were reproduced and analyzed. Further considerations on the role of friction for this type of structure have been made together with the problem of linear analyses for CLT structures (non-symmetric response for tension-compression loaded connections).

Keywords: Cross-laminated timber, Seismic behavior, Seismic design, Finite Element, Non-linear analysis

SOMMARIO

Dalla sua concezione a metà degli anni novanta, il legno lamellare a strati incrociati, anche noto come CLT o X-Lam, ha raggiunto grande popolarità tra i materiali da costruzione grazie alle numerose innate qualità, gli sforzi a livello mondiale per costruire strutture affidabili in zone a rischio sismico e la necessità di costruire un ambiente più eco-sostenibile.

Molti test sono stati fatti negli ultimi 15 anni, volti a comprendere meglio il comportamento delle connessioni in edifici in CLT, di parti strutturali o di intere strutture in CLT, in modo da fornire regole affidabili per i progettisti per progettare strutture in CLT sotto ogni condizione di carico.

Sulla base di questi test, molti sono stati i modelli numerici che sono stati suggeriti negli anni. Questi rappresentano uno strumento fondamentale per la progettazione di strutture in CLT quando insorgono specifiche problematiche ed un approccio analitico da solo non è sufficiente.

Nonostante i molti anni di sforzi, non esistono ancora affidabili metodologie di progetto nella quasi totalità dei codici a livello mondiale e ancora molte sono le incognite relative al comportamento delle strutture in CLT a molti livelli (connessioni, parti strutturali, strutture).

Questa tesi riassume tre anni di ricerche numeriche, le quali hanno affrontato diversi problemi relativi al comportamento di elementi strutturali e strutture in CLT sotto azioni dinamiche. Durante la prima parte di questo percorso l'attenzione è stata posta sulla continuazione di un precedente studio, portato avanti durante la tesi di laurea magistrale, il quale era incentrato sulla formulazione di un metodo semplificato per la costruzione di un dominio resistente sforzo normale-momento flettente per pannelli in CLT connessi alla base da connessioni tipo hold-down e angle bracket.

In mancanza di risultati di test di interesse, la concentrazione è stata rivolta ancora alla formulazione di metodi semplificati per la progettazione di elementi strutturali in CLT. È stato analizzato il problema delle connessioni pannello-pannello all'interno di una stessa parete. In particolare, è stata studiata la rigidezza di queste connessioni in relazione al comportamento ribaltante di pareti a due pannelli attraverso l'analisi di test a scala reale indipendenti e analisi numeriche agli elementi finiti. Una formula per il calcolo di queste connessioni è stata dapprima proposta e poi, dopo ulteriori analisi, rivista e corretta.

Per estendere l'analisi e considerare elementi strutturali più complessi, è stata investigata, a livello di analisi numerica, l'influenza del solaio e delle connessioni parete-solaio superiore sul comportamento ribaltante delle pareti, prendendo in considerazione configurazioni con e senza solaio, variando diversi parametri di modo da ottenere risultati statisticamente

significativi.

Nell'estate del 2017 il candidato ha partecipato attivamente al NHERI TallWood Project, una ricerca statunitense intesa a testare strutture in CLT per fornire regole di progettazione per tali strutture nei futuri codici nazionali. Sponsorizzato dalla Colorado State University, nella persona del Prof. John W. van de Lindt, il candidato ha collaborato alla preparazione di un edificio con due orizzontamenti fuori terra testato sulla tavola vibrante della UCSD a San Diego (California)

Per valutare il più corretto valore di smorzamento per strutture in CLT sotto l'azione di eventi sismici di bassa intensità, sono stati riprodotti numericamente ed analizzati i test su tavola vibrante del progetto SOFIE a 0,15 g. Ulteriori considerazioni sono state fatte sul ruolo dell'attrito su questo tipo di strutture e sul problema delle analisi lineari per strutture in CLT (risposta non simmetrica di connessioni caricate in tensione-compressione)

Parole chiave: Legno lamellare a strati incrociati, Comportamento sismico, Progettazione sismica, Analisi non lineare, elementi finiti

TABLE OF CONTENTS

LIST OF FIGURES

LIST OF TABLES

LIST OF PUBLICATIONS

G. Tamagnone, G. Rinaldin, M. Fragiacomo. A simplified non-linear procedure for seismic design of CLT wall systems. 14th World Conference on Timber Engineering (WCTE 2016), Technische Universität Wien, Wien, Austria, 2016.

G. Tamagnone, G. Rinaldin, M. Fragiacomo. A novel method for non-linear design of CLT wall systems. Engineering Structures. 167(2018):760–771. DOI:10.1016/j.engstruct.2017.09.010. 2017.

G. Tamagnone, M. Fragiacomo. Sul Progetto in Zona Sismica di Strutture a Pareti Lignee in Xlam. Convegno ANIDIS 2017. Pistoia, Italia.

G. Tamagnone, M. Fragiacomo. On the rocking behavior of CLT wall assemblies. 15th World Conference on Timber Engineering (WCTE 2018). COEX exhibition and convention center. Seoul, South Korea, 2018.

J. W. Van de Lindt, J. Furley, M. O. Amini, S. Pei, **G. Tamagnone**, A. R. Barbosa, D. Rammer, P. Line, M. Fragiacomo, M. Popovski. Experimental Seismic Behaviour of a Two-Storey CLT Platform Building: Design and Shake Table Testing. 16th European Conference on Earthquake Engineering (ECEE 2018). The Thessaloniki Concert Hall, Thessaloniki, Greece, 2018.

J. W. Van de Lindt, J. Furley, M. O. Amini, S. Pei, **G. Tamagnone**, A. R. Barbosa, D. Rammer, P. Line, M. Fragiacomo, M. Popovski. Experimental seismic behavior of a two-story clt platform building: shake table testing results. 15th World Conference on Timber Engineering (WCTE 2018). COEX exhibition and convention center. Seoul, South Korea, 2018.

C. Bedon, M. Fragiacomo, **G. Tamagnone**. Numerical Investigation on Timber-to-Timber Joints and Composite Beams with Inclined Self-Tapping Screws. 15th World Conference on Timber Engineering (WCTE 2018). COEX exhibition and convention center. Seoul, South Korea, 2018.

J. W. Van de Lindt, J. Furley, M. O. Amini, S. Pei, **G. Tamagnone**, A. R. Barbosa, D. Rammer, P. Line, M. Fragiacomo, M. Popovski. Experimental seismic behavior of a two-story clt

platform building. Engineering Structures. 183(2019): 408–422 https://doi.org/10.1016/j.engstruct.2018.12.079

G. Tamagnone, G. Rinaldin, M. Fragiacomo. Influence of the floor diaphragm on the rocking behavior of CLT. Undergoing revision. ASCE Journal of Structural Engineering.

I. Christovasilis. L. Riparbelli, G. Rinaldin, **G. Tamagnone**. Methods for Practice-oriented Linear Analysis in Seismic Design of Cross Laminated Timber Buildings. Undergoing revision, Soil Dynamics and Earthquake Engineering.

NOTATIONS

A	Cross-section area
C	Damping matrix
E	Elastic modulus/Young modulus
E_0	Modulus of elasticity parallel to grain
E_{90}	Modulus of elasticity perpendicular to grain
E_L	Modulus of elasticity in the longitudinal direction
E_N	Modulus of elasticity in the normal direction
E_T	Modulus of elasticity in the transverse direction
F	Lateral force applied at the top of the wall
F_{AB}	Reaction force in each angle bracket due to the load condition
F_c	Value of the reaction force in compression in the contact zone between panel and supporting surface
F_{HD}	Reaction force in the hold-down due to the load condition
F_{max}	Maximum force of the connection
$F_{Rd,AB}$	Design resistance of the angle brackets
$F_{Rd,HD}$	Design resistance of the hold-down
F_i	Value of the reaction force in the i^{th} connection
F_u	Force corresponding to the ultimate displacement of the connection
F_y	Yielding force of connections
G_0	Shear modulus in planes parallel to grain
G_{90}	Shear modulus in planes perpendicular to grain
K	Stiffness matrix
LTN	Longitudinal Transverse Normal
M	Bending moment
M	Mass matrix
N	Axial force
R	Compressive reaction force at the interface between the first panel and the supporting surface during the rocking mechanism
R_p	Reaction force at the interface between panels during the rocking mechanism
S	Modal matrix
T	Period
U_{ult}	Ultimate displacement of connections

$U_{ult,max}$	Maximum ultimate displacement among the two available
$U_{ult,min}$	Minimum ultimate displacement among the two available
V	Shear force
V_i	Reaction force in the i^{th} connection during the rocking mechanism
W	Self-weight of the panel
b	Length of the panel
d	Uplift of the uncompressed edge of the panel
d_{bottom}	Lateral displacement of the bottom corner of the assembly
d_{rock}	Lateral displacement of the top corner of the assembly due to rocking
d_{slip}	Lateral displacement of the top corner of the assembly due to slip
d_{top}	Lateral displacement of the top corner of the assembly
f_c	Ultimate compressive strength in CLT
h	Height of the wall
k	Compressive stress distribution coefficient
k	Modal stiffness matix
k_{el}	Elastic stiffness of the backbone
k_{pl}	Hardening stiffness of the backbone
k_s	Elastic stiffness of connections in the resistant domain calculation
k_i	Vertical stiffness of the i^{th} connection
l	Length of the wall
m	Modal mass matrix
n	Number of connections
n_{AB}	Number of angle brackets
n_p	Number of connections between wall panels
q_v	Axial load per linear meter applied to the assembly
s	Thickness of the panel
u_c	Fictitious displacement underneath the foundation surface
$u_{c,max}$	Maximum fictitious displacement underneath the foundation surface
u_i	Vertical displacement of the i^{th} connection
v_{max}	Displacement corresponding to the maximum force in the connection
v_u	Ultimate displacement of the connection
v_y	Yielding displacement
$\bar{x}$	Distance of the neutral axis from the bottom right corner
x_i	Distance of the i^{th} connection from the compressed panel corner
$x_{i,dx}$	Distances of the i^{th} connection from the bottom right corner of the wall
$x_{i,sx}$	Distances of the i^{th} connection from the bottom left corner of the wall

x_{max}	Position of the farthest connection from the bottom right corner having $U_{ult,max}$ as ultimate displacement
x_{min}	Position of the farthest connection from the bottom right corner having $U_{ult,min}$ as ultimate displacement
α	Mass-proportional damping coefficient
β	Stiffness-proportional damping coefficient
ζ	Damping
ξ_n	Critical damping ratio
θ	Angle between the panel and the supporting surface during the rocking mechanism
ν	Poisson's ratio
σ_c	Compressive stress at the bottom right corner of the wall
σ_d	Compressive stress at the bottom left corner of the wall
φ	Diameter
ω_n	Natural frequency of the system

INTRODUCTION

1.1. Research background and motivation

The use of Cross-Laminated Timber as structural material has increased rapidly in the last fifteen years for low- and mid-rise buildings, as it proved to be a good and more environmental-friendly alternative to more common materials, such as concrete or masonry.

However, few codes provide design formulas for the design of this type of structures, not accounting for all the possible scenarios the structure could undergo during its lifetime. Many aspects still need to be investigated in order to predict efficaciously the behavior and structural capacity of CLT assemblies and structures. Moreover, designers who deals with the project of buildings in seismic-prone areas needs to be provided with rules for a reliable numerical modelling of such structures to predict their dynamic response and possible critical issues, which could not be directly deducible from a not detailed investigation considering every load scheme.

For these reasons, it is evident how crucial is to keep on studying these type of structure and all the different parts, their behavior and how elements interact with each other, to find a proper design procedure specifically devised for CLT buildings, Among the different aspects that needs to be clarified, the thesis proposes a procedure to calculate the rocking capacity of a single-panel CLT wall, giving information on the most probable failure mechanism for a given set of external loads. After that, the vertical connection between panels in a same wall is considered, suggesting a formula for its design in order to give a determined type of behavior to the wall assembly. Furthermore, the influence of an overlaying diaphragm is investigated in terms of rocking behavior and capacity.

Full-scale tests are a very useful mean to collect data in structural engineering, and CLT structures are no exception. This thesis presents results of the tests carried out on a 2-story CLT platform building made for the validation of a specific design procedure. Results of this type of tests can also give information on the behavior and how to predict it when a numerical model needs to be created. Numerical analyses are a powerful tool that helps designers to test the capacity of a structure that needs to be built and check the goodness of the design. In this thesis, results of several full-scale tests are used to study, with two different modelling approaches, the influence of different parameters on the most proper value of damping to be implemented in FE analyses in CLT structures for low intensity motion, for which the effect of friction have proven to be more important.

1.2. Thesis structure

The focus of this PhD thesis is not unique and the studies made encompass different fields. The general topic is the research of formulations and tools to properly design and predict the behavior of CLT structures and their singular parts (e.g. walls, connections, etc)

The thesis itself is a collection of journal articles written during the last three years of research. After an introductive chapter (chapter 2), four studies (chapters 3 to 6) are presented. Each of the latter four chapters opens with few lines summarizing the content of that chapter, then an introductive chapter gives information on the topic under discussion and previous research in the same field. In the subsequent sections, experimental, analytical, and numerical results are compared and discussed.

Chapter 2 introduces the CLT as wood product. Its structural use is described and the most common connection systems, together with few of novel conception, are presented. The second part of this chapter addresses the problem of the numerical modeling of CLT structures and components, discussing the possible approaches and presenting the ones considered within this work.

Chapter 3 presents a simplified non-linear method to calculate the rocking capacity of a single-panel CLT wall connected to the supporting surface through angle brackets and hold-downs. The method, basing on the mechanical properties of the connections and the geometry of the system, calculates, for a given value of axial force applied, the most probable failure mechanism (i.e. crushing of CLT or failure of connections) and the position of the neutral axis in the corresponding ultimate state condition.

In chapter 4, a formula for the prediction of the rocking behavior (i.e. coupled or uncoupled) of a two-panels CLT wall is derived and validated against unrelated full scale tests and numerical analyses. The method accounts for external loads, mechanical properties of the connections and geometry of the system. In the second part of this chapter, the influence of the upper diaphragm and the wall-to-floor slab connections on the rocking behavior of a two-panel CLT wall assembly is investigated through several numerical analyses varying different parameters (e.g. stiffness of the connections, stiffness of the diaphragm, axial load applied).

Chapter 5 analyzes the findings of different shaking-table tests on a two-story CLT platform building with three different type of shear wall to compare the various responses depending on the system utilized. Several parameters are investigated, such as the slip between panels composing a wall, the uplift and lateral displacement of the wall or the presence of an orthogonal wall.

Finally, chapter 6 discusses two different modelling approaches for the linear modelling of CLT buildings and the influence of the value of damping set, when low-intensity seismic action is considered, upon the global response of the model compared to the results of a full-

scale building tested on a shaking-table.

CLT: PRODUCT, APPLICATIONS AND MODELLING APPROACHES

2.1. Product description

Cross Laminated Timber (CLT) is a wood-based product, which structure is depicted in Figure 2.1.1. As shown, CLT is composed of overlapping layers of wood lamellas, glued together to form a massive panel. The peculiarity of CLT is that lamellas of adjoining layers have grains running orthogonally to each other.

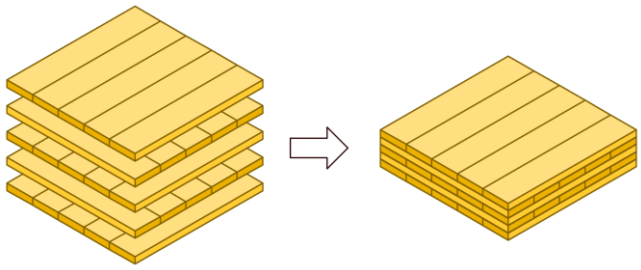

Figure 2.1.1 – CLT panel structure.

Lamellas used are generally 20 to 40mm thick and 80 to 250mm wide, they are dried to a moisture content of 12%, to ensure a perfect bond between layers and to avoid biological damages (pests, fungi or insects), graded and, if necessary, finger-jointed to create longer pieces or to avoid knots and reach higher performances; they are usually arranged in odd layers from three to seven. Species typically used are softwood qualities like spruce, pine and fir.

The glues utilized are the polyurethane-based glues (PUR), in some cases formaldehyde-based resins (RF and MUF) can be used too.

Once the layers are ready, panels are pressed. The equipment used can vary depending on the thickness of the panel and the type of adhesive used. Typical pesses utilized are: hydraulic press, compressed air press and vacuum press. Panels' thickness ranges from 60 to 300mm, but panels thick up to 500mm can be produced for specific purposes. The size, length and hight, is limited by factory equipment or transportation restrictions, but usually they are produced oversize, up to over 30m, and then cut to the disred geometry, especially in length, rather than be tailored manufactured.

The cross-laminating process provides the final product with high dimensional stability, in- and out-of-plane stiffness and strength, with the possibility of having comparable characteristics in two directions (in-plane directions), depending on number and thickness of

layers in each direction.

In Europe, the standard regulating CLT manufacturing is the UNI EN 16351:2015 (Timber structures – a Cross laminated timber – Requirements). In the US, there is the ANSI/APA PRG 320-2018 (Standard for Performance-Rated Cross-Laminated Timber).

2.1.1. Panels for structural applications

Panels are produced for general purposes. Different uses requires different panels' dimensions, but no significant difference is encountered during the production process.

CLT panels can be utilized for different purposes within a structure: walls, floor slabs, roofs, stairways and shafts. Panels can undergo different post-production processing, such as the cutting for openings, as door, windows, stairs and service channels, or to allow the proper installation of specific connections (see Chapter 2.2). Cuts and other manufacturing are usually performed by CNC machining tools, such as saws, drills, boring tools or lathes, at the production site, but some specific non-precision works can be made manually on-site.

Panels are usually placed matching the orientation of the grains of the outer layers with the direction of maximum stress in the specific element: walls have grains of outer layers running vertically; diaphragms have grains of outer layers running in the direction of maximum span. This is made because panels are manufactured in odd layers, so the majority of lamellas have grains parallel to those of the outer layer, thus this is the direction having the best characteristics within the panel.

For diaphragm applications, depending on the span between walls or thickness of panels, panels can be used alone or coupled to beams, in order to satisfy deformation, structural and vibration requirements.

2.2. Connections in CLT structures

Structures made of CLT panels can be of two different type: platform type and balloon type structures. The main difference between the two is that platform type structures have walls height coinciding with the inter-story height, that is that all the wall at a certain level have a diaphragm on the top of them, diaphragm that serve as supporting level for walls of the upper floor, etc.

In balloon type structures, walls height coincides with the height of the building. In this case, diaphragm can be placed following two structural approaches:

- Diaphragms are directly supported by walls, which bear axial and shear loads;
- Diaphragms can be supported by columns, which bear vertical loads, and be connected to the walls through special connections that allow exchanging only shear loads between the

two. In this case, the wall act exclusively as shear wall.

Connections play a crucial role in every timber structure. CLT is no exception. In this chapter, several connections are presented. Figure 2.2.1 shows the position of the connections within a platform type construction, as it is the type analyzed in this thesis. Balloon type structures presents differences in some connections, especially in wall-to-diaphragm connections, as diaphragms lean on the side of continuous wall rather than lay on the top of them, as occurring in the platform type buildings.

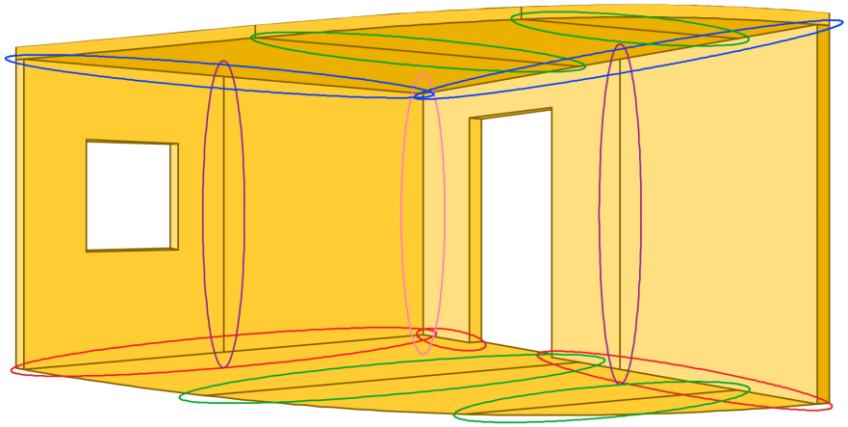

Figure 2.2.1 – Type of connections in CLT structures: wall-to-lower diaphragm / wall-to-foundation (red line), panel-to-panel in a wall (purple line), wall-to-wall (pink line), wall-to-upper diaphragm (blue line), panel-to-panel in a diaphragm (green line).

2.2.1. Typical connection systems

2.2.1.1. Wall-to-foundation connections

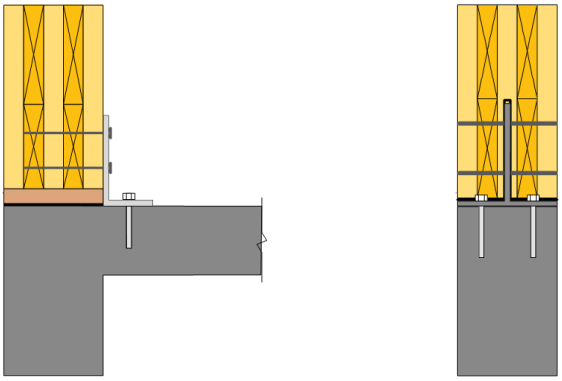

(a) (b)

Figure 2.2.2 – Examples of wall-to-foundation connections: metal bracket (a), concealed metal plate (b) [32].

Usually, foundations in wood structures are made of Reinforced Concrete (RC). In order to link together the two materials, threaded bars are embedded in concrete in correspondence with the position of the connections. In some specific cases, especially in balloon type structures with shear walls, this solution can be unfeasible for uplift preventing connections, depending on the connection used or the load to be born. In such cases, steel plates underneath the concrete

slab are used.

In platform structures, typical connections consist in metal plates fixed to the foundation through a bolt and linked to the wall through nails or screws (Figure 2.2.2.a). Another option is to hide the connection within the panel. This is made to improve the fire resistance of the connection and for aesthetic (Figure 2.2.2.b). The process here requires more attention in the preparation of the panel and selection of fasteners than in ordinary connections.

2.2.1.2. Panel-to-panel connections

Panel-to-panel connections can be performed in many ways. The two more used are the spline joint and the half-lapped joint. This joint can be a single or double, internal or surface joint, depending if the spline is placed within or outside the panels and the number of strips used.

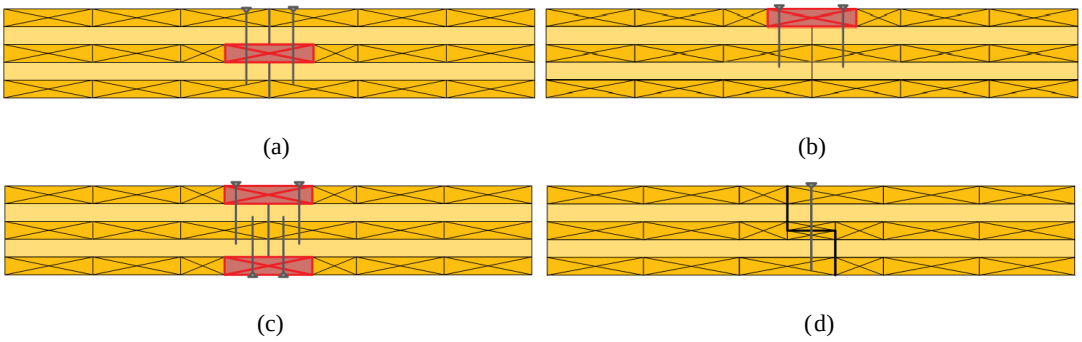

Figure 2.2.3 – Examples of panel-to-panel connections: internal spline (a), single surface spline (b), double surface spline (c), half-lapped joint (d) [32].

Materials used for splines are Laminated Veneer Lumber (LVL), Parallel Strand Lumber (PSL), Laminated Strand Lumber (LSL) or other Structural Composite Lumber (SCL) materials. The surface spline is a connection that can be performed completely on-site, as the profiling of the panel is superficial (Figure 2.2.3.b and c). Internal splines need the profiling to be made at the plant due to the position of the cut (Figure 2.2.3.a). Half spline is connected to a panel and the other half is connected to the other panel. Both sides are connected through metal fasteners, such as self-tapping screws, wood screws or nails. The main advantage of the internal spline is that it provides a double shear connection. On the other hand, profiling and fitting the different part together on-site could be challenging. Surface splines are easier to be made, even on-site manually, as the cut is exposed. The main disadvantages are the single shear connection type for single splines and the doubling in the number of fasteners and cut to be performed, increasing the time needed for this joint. On the other hand, double surface splines perform a double shear joint, increasing the resistance of the connection.

As suggested by the name, half-lapped joints are performed removing part of the edge of both panels involved (Figure 2.2.3.d). Self-tapping screws are usually utilized to perform this joint. The main disadvantage of this connection is the concentration of tension perpendicular to

the grain in the notched area.

2.2.1.3. Wall-to-wall connections

Wall-to-wall connections are designed to be over resisting compared to panel-to-panel in wall connections, as they have to maintain the box behavior of the structure though out the hypothetical loading event (e.g. strong wind, earthquake). The most common and fast way to link two walls together is to use self-tapping screws (Figure 2.2.4.a). They can be placed from outside or inside the structure. The main concern about this practice is that screws are driven in the narrow side of panels, thing that could result critical in case of strong seismic motions or high wind load. To optimize the performance of the connection, screws can be driven at an angle to avoid the direct installation of screws in the narrow side of the panel (toe-screwing) (Figure 2.2.4.b).

Other connections used can be metal brackets (Figure 2.2.4.c) or concealed metal plates (Figure 2.2.4.d). These last two connections are set as seen in wall-to-foundation connections.

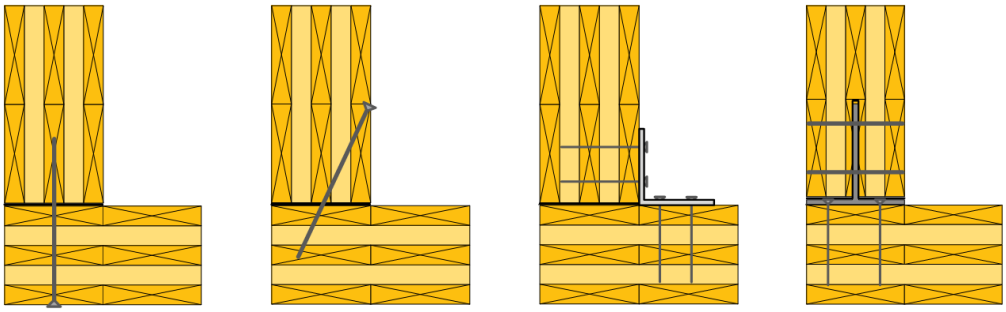

(a) (b) (c) (d)

Figure 2.2.4 – Examples of wall-to-wall connections: self-tapping screw connection (a), toe-screwing (b), metal bracket (c), concealed metal plate (d) [32].

2.2.1.4. Wall-to-diaphragm connections in platform type construction

Various can be the combinations of connections involving walls of two levels and the diaphragm in between. The same approaches seen for the wall-to-wall connections can be applied to this joint, merging them to find the best designing solution depending on expected external loads, availability of fasteners and degree of prefabrication.

The use of self-tapping screws is more common for linking together floors above and walls below than to joint upper walls to lower diaphragms (Figure 2.2.5.a and c). This solution, especially for 45° driven screws, maximize the strength of the connection to the detriment of its ductility.

Metal brackets represent a good solution in terms of strength and ductility and they are a more appropriate connection, compared to self-tapping screws, in high seismicity areas where a greater ductility needs to be achieved (Figure 2.2.5.b and c).

Concealed plates can be used to both for wall below to diaphragm above connection and

diaphragm below to walls above connection, screwing the plate to the floor slab first and then using fasteners, usually dowels, to connect the inner plate and the wall panel (Figure 2.2.5.d). As previously discussed, this solution requires a high degree of prefabrication, thing that make designers prefer other connections in ordinary CLT buildings.

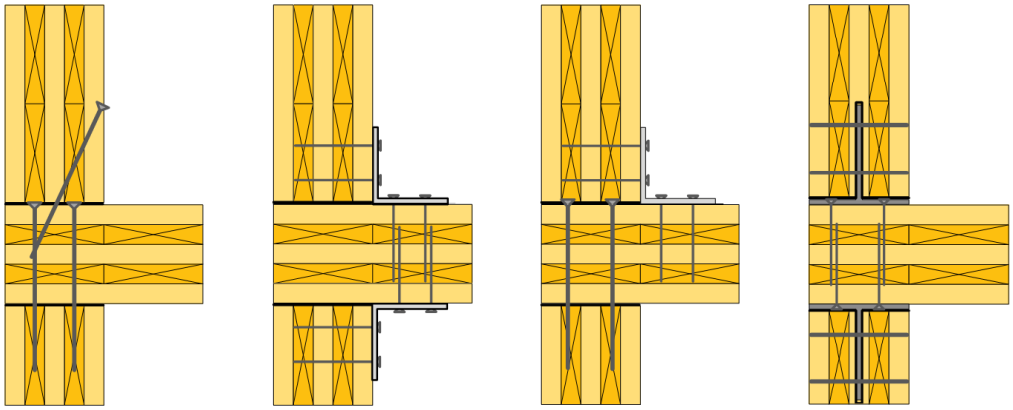

(a) (b) (c) (d)

Figure 2.2.5 – Examples of wall-to-diaphragm connections on platform type buildings: self-tapping screws (a), metal brackets (b), self-tapping screws and metal brackets (c), concealed metal plates (d) [32].

2.2.1.5. Wall-to-diaphragm connections in balloon type construction

While platform type structures are still the most common CLT constructions in Europe, due to ease and speed of erection and a quite simple design, balloon type structures are getting more and more attention in seismic-prone areas due to several studies made on CLT shear walls and the optimization, ductility and strength bearing capacity of related connections, examples of which are given in chapter 2.2.2.

In balloon type structures, when walls bear vertical and lateral loads, diaphragms lay on supports attached to the wall. Typical floor-to-wall connection solutions includes wood ledgers (Figure 2.2.6.a), made of LVL, LSL, PSL or even CLT, or metal brackets (Figure 2.2.6.b and c).

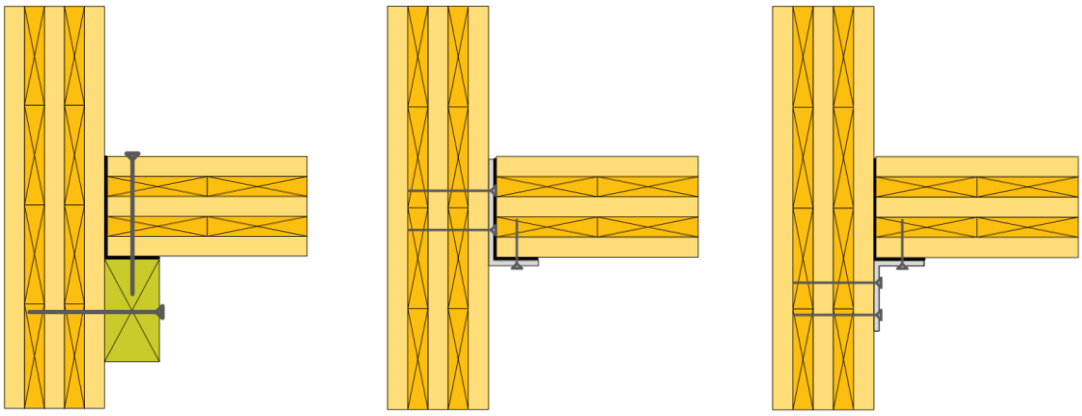

(a) (b) (c)

Figure 2.2.6 - Examples of wall-to-diaphragm connections on balloon type buildings: wood ledgers (a), metal brackets (b,c) [32].

In these kind of connections, it is important to account for detachment between wall and diaphragm, due to potential wind suction in external walls.

2.2.2. New connections for CLT buildings

The usual practice in CLT constructions is to use typical fasteners, such as screws, bolts and nails, and metal bracket connections like hold-down and angle brackets. Hold-downs (Figure 2.2.7.a) are placed in the corner of walls and are designed to prevent uplift and resist tension loads. On the other hand, angle brackets (Figure 2.2.7.b) are designed to prevent slip and resist shear loads, even if it is well known their tension strength has a non-negligible contribution [35].

(a) (b)

Figure 2.2.7 – Examples of a hold-down (a) and an angle bracket (b) (Rothoblaas).

This type of connections have been widely used and their behavior has been extensively studied by many academics.

In the last years, many have been the new connections and structural systems that have been devised in order to ease and speed up even more CLT construction, to simplify designing or to increase energy dissipation. In the following, some interesting findings are presented.

2.2.2.1. ATS Steel rods

In CLT constructions, a reliable designing process is still missing, despite CLT has been used as structural material for nearly 20 years. The main problem is that many are the different connections involved, and some of them, like hold-downs and angle brackets, have different parts composing the connection itself (i.e. metal plate with nails, screws or bolts). It is not entirely clear how nails, metal plate and screws, or bolts, act together to give a certain behavior and how it would vary once a parameter within the connection is changed. To ease the designing process, several connections have been devised to be a simpler solution than metal brackets.

One example is the use of steel rods instead of hold-downs. The working principles are the following: near the edge of a wall, on the upper and lower diaphragm a hole is cut, both on

the same vertical line; a steel rod, passing through both the holes, is then anchored to the intrados of the lower floor and to the extrados of the upper one (see Figure 2.2.8). In this way, the design for uplift is limited to the design of a steel rod, of which material and section are known. Furthermore, this approach makes it easy to replace the rod once it yields, if the strength hierarchy principles are adopted and the damage of other parts is prevented [67]. This connection has been recently used in the third part of the shaking table tests carried out in San Diego in 2017 within the NHERI TallWood Project (see chapter 5).

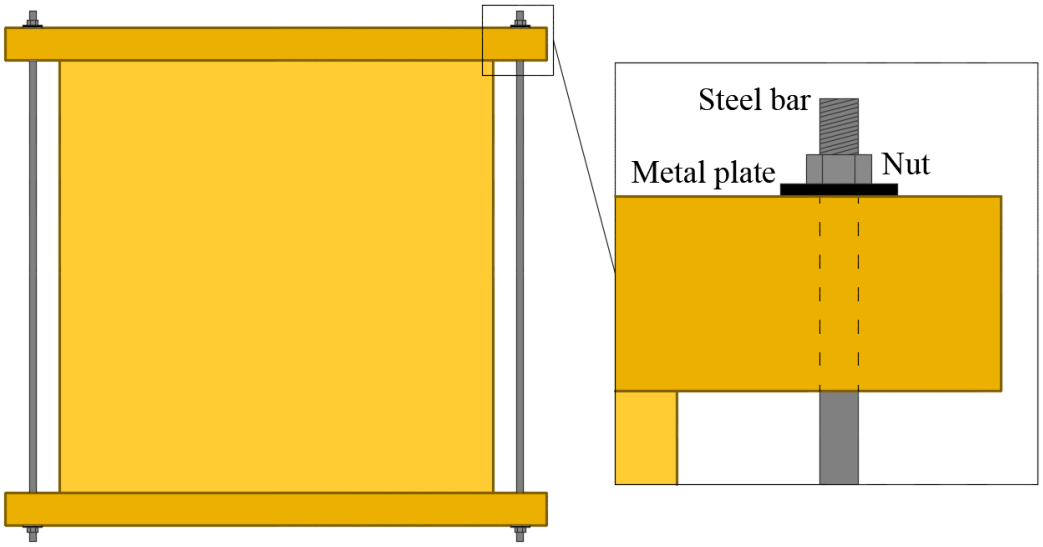

Figure 2.2.8 – Detail of the ATS steel rod connection.

2.2.2.2. X-Rad

The X-Rad connection combines a higher prefabrication, a higher speed of assembly at the construction site and an easier design. The connection is pre-installed to the panels at the plant and consist in metal plates screwed in each corner of the panel (generally four per panel). The high precision prefabrication allows matching each part on-site and to connect them together through bolts and purposely created metal plates. Connections can also be used to lift the panels, without any need of cutting holes in it for the purpose.

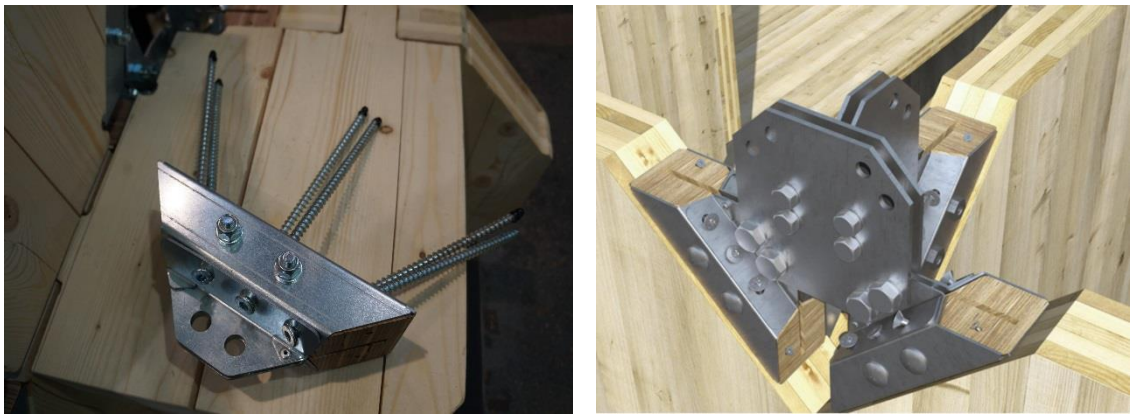

Figure 2.2.9 – The X-Rad connection with all its parts exposed (a) and an assembly of three connections (b) [53][54].

Structural performances of this connection have been tested in all the direction of loading, making, possible to derive a resistant domain and designing rules. Performances of panels and composed walls have been tested too and compared to those of a typically connected wall, giving almost the same results in terms of strength, stiffness and ductility.

2.2.2.3. Post-tensioning

In CLT structure, the recentring of the structure after a major earthquake could be a problematic issue due to residual slip. Studies have highlighted that, depending on the displacement referred to the size of the structure, it is sometimes more economically efficient to demolish the old building to erect a new one.

Efforts have been made in order to achieve a self-recentring system, and one of the most known method is the use of post-tensioned shear walls [38][47].

This solution applies mainly to balloon type structures. Shear walls in the structure are coupled to steel rods, which are anchored at the top of the wall through metal plates and at the foundation level. These rods have threaded parts, at least at both ends, in which nuts are screwed. Screwing in these nuts pushing on the metal plates, the rods are tensioned to a fixed value of stress, depending on the load they are designed to born. When the shear wall rocks because of an external lateral load, the rods operate in the opposite direction of motion, forcing the wall to go back to its starting position. This mechanism prevents slip favoring rocking and, most importantly, recentring.

2.2.2.4. Resilient Slip Friction Joint – RSFJ

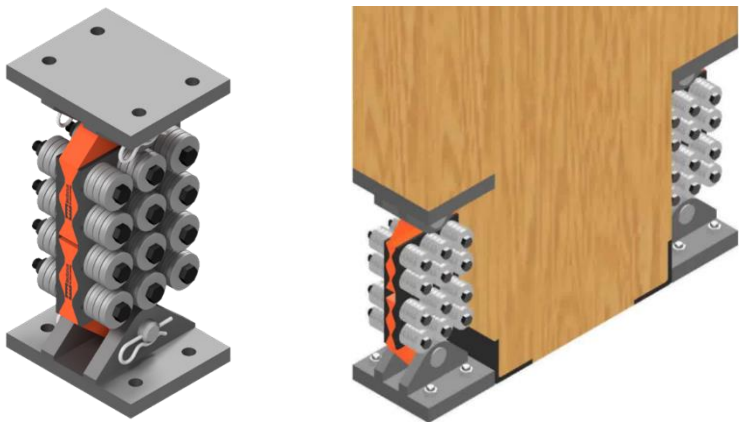

(a) (b)

Figure 2.2.10 – Example of RSFJ connection (a) and its placement in a shear wall (b) [79].

This connection can be used in many structural systems (wood, steel, concrete). For what concerns CLT structures, it can be used as bottom connection of shear walls [79].

It is composed by two inner slotted plates, one linked to each member jointed by the connection, and two outer cap plates clamping the two inner plates through high strength bolts.

All the plates are grooved. When the load overcomes the frictional resistance between the surfaces, the inner plate starts to slide inside the outer plates, dissipating energy. The design of such connections is quite easy and the system is completely self-recentring. Furthermore, the modelling of this connection have already been done in previous studies and guidelines are provided by the producer.

2.3. Modelling approaches

Numerical modelling is an essential tool for the design of any construction, when specific problems arise, and an analytical procedure is not sufficient, or in case of lack of regulation for the specific structural type. In Europe, the Eurocodes 5 and 8, regulating timber structures design and general structures seismic design, respectively, do not provide the designer with specific rule for CLT structures, who is forced to follow generic rules and opt for standard geometries, in order to be able to us analytical approaches. Unlike steel or concrete structures, however, structures made in CLT have not a well-established set of rules for modelling, being a relatively new construction material and due to higher uncertainties related to almost all timber structures (e.g. cyclic behavior of connections, impairment of strength and stiffness).

From an academic point of view, CLT modelling has been used to try to reproduce lab tests, investigating connections, assemblies and entire structures, to better evaluate the behavior of each component, to enlarge the number of analyzed cases and to give designers hints on how to perform a numerical analysis of this type of structures.

As previously mentioned, a unique and comprehensive method to model CLT structures is still missing. In this thesis, the component approach developed by Rinaldin et al. [60] is used for different purposes (see chapter 1 and chapter 4). In this chapter, after a brief introduction on numerical modelling in CLT structures, the approach is presented, together with all the phases of the modelling procedure followed.

2.3.1. Background in CLT modelling

As previously stated, connections are the elements dissipating energy, so their behavior needs to be calibrated with more accuracy than the one of panels.

The main challenge, dealing with connection modelling, is to describe all the different characteristics a joint presents when subjected to cyclic loads (e.g. pinching, degradation of stiffness and strength, etc). Through the years, several have been the attempts to model CLT connections, but many of those were not able to depict accurately the hysteretic behavior.

The behavior of connections is typically defined according one of the following method:

- Connections resist only in their primary direction: hold-downs in tension and angle brackets in shear [10][57][78];

- Connections are modelled through a biaxial behavior, resisting both shear and tension forces independently [30][39][66][69];
- Connections are modelled through a biaxial behavior and an interaction domain is considered [58][60].

As for other structural materials, the use of assemblies of non-linear springs have been considered for CLT connections [56]. A major disadvantage of using this technique is that impairment of strength and softening cannot be accounted. Another method is to use hysteretic laws already implemented in FE modelling software, like SAP2000 [15], calibrating the parameters of the springs to match the behavior of connections [30][31][70]. This approach is limited by the hysteretic behaviors implemented in the FE software and how they are able to accurately represent the behavior of the connection. Finally, the use of purposely-developed springs has been considered. The method uses external subroutines and specific FE solvers that permit their implementation. This last procedure represents the best option when hysteretic laws implemented in a FE solver are not able to depict accurately the desired behavior and all its characteristics, as it permits to fully tune all the parameters and to purposely-create a hysteretic behavior. On the other hand, coding could be demanding and many parameters needs to be defined.

The last method presented is the one used in most of the numerical analyses presented in this thesis. Its principles are described in chapter 2.3.3.

2.3.2. Creating the mesh: X-lam Wall Mesher

The first step in the conception of every model is the definition of the geometry. To do so, the purposely-developed software X-lam Wall Mesher, created by G. Rinaldin, gives the user the possibility to define the geometry of the assembly or of the structure and the position of the various connections. The software is organized in four sheets: Walls, Springs, Loading and Solver. The software allowed the user to export models for several FE solvers: SAP2000, Abaqus, OpenSees, Midas GEN and OOFEM.

2.3.2.1. Walls

In this sheet, the panels are created. The user defines the position of the bottom left corner of the panel (x, y and z), the height, the length and thickness, the number of divisions to be performed in the mesh, the working plane (x-y, x-z or y-z) and the identification number of the wall. Openings can be created too, specifying the origin, within the mesh of the selected panel, and the size, measured in mesh division or giving the desired size, which is then compared to the actual size of the mesh.

The main advantage of this tool is that panels can be replicated, using the *drawing*

controls, moving up, down, left or right from the original panel position and creating there an equal sized panel. In structures, where panel arrangements are the same at each level, this tool speed up the modelling process.

2.3.2.2. Springs

After having defined a set of connections (Tools → Spring declarations...), the user can place them within the various panels defined in the previous sheet. Once a panel is selected, the user can choose a point specifying the edge (i.e. top, left, bottom or right) and the position of the point to be connected within the mesh. A graphical representation of the wall ease the process.

Basing on the mutual position of the panels (i.e. in-plane or orthogonal), the software suggests the point belonging to another panel to be connected to the chosen one. Where needed, the user can specify the points to be connected. Single connections or set of connections can then be duplicated automatically in other points of the same panel or different panels.

2.3.2.3. Loading

In this sheet, loads are assigned to the panels created. Loads can be applied as distributed, specifying the value per unit area, or as point load, specifying the value and the points where the load will be placed. The mass is applied here too, together with the mass damping. User have also to select the direction in which the load acts

2.3.2.4. Solver

Here the user can select which type of analysis will be performed, set the properties of the springs, set the properties of the material composing the panels, etc.

2.3.2.5. Additional features

2.3.2.5.1 Additional nodes

This comes useful when nodes not belonging to the mesh have to be placed. For example, when it is necessary to add restrained points to which the model is linked (e.g. foundation level).

Here nodes are specified matching the position of existing points of the mesh, selecting the active panel, the side (i.e. top, left, bottom or right) and the place within the divisions of that specific edge.

2.3.2.5.2 Gmsh

This powerful tool permits graphically to see in a 3-dimensional space the model created, in order to check its accuracy. This external software, developed by Geuzaine and Remacle, is present in the X-lam Wall Mesher package by default.

2.3.3. Component approach

This method has been developed by Rinaldin et al. [60][63] and has been used in many numerical studies, showing good accuracy [41][62][75].

The approach consider nonlinear springs characterized by linear branches in the force-displacement domain. The springs work with several input parameters, which can be set to describe not only wood connections, but also force-displacement behavior of other materials. Springs can be calibrated through results of cyclic tests or through simplified models based on analytical approaches. The model considers stiffness and strength degradation.

In following, working principles of this method, together with the parameters to be defined, are presented.

2.3.3.1. Shear hysteresis law

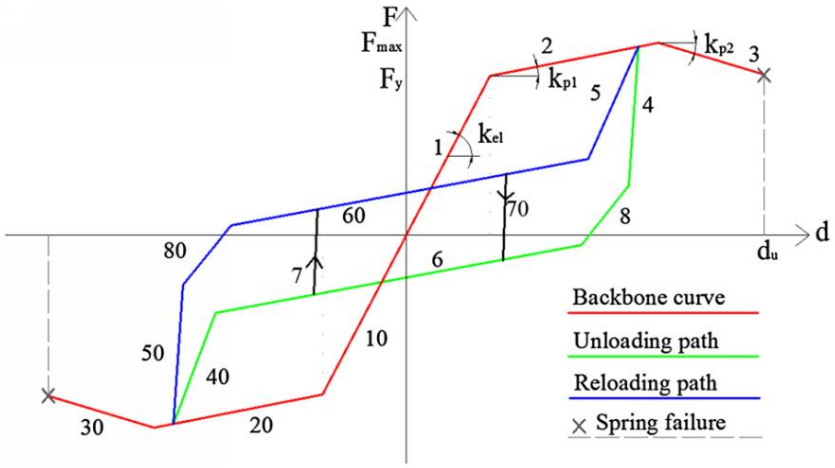

Figure 2.3.1 - Piecewise-linear law of shear spring component [60].

Figure 2.3.1 shows the general force-displacement piecewise-linear law implemented in the model. The parameters defining the entire behavior are:

k_{el} Elastic stiffness;

F_y Yielding force;

k_{p1} First inelastic stiffness (Hardening);

F_{max} Maximum strength;

k_{p2} Second inelastic stiffness (Softening);

K_{SC} Unloading stiffness of branches #4 and #50 are obtained multiplying this factor by k_{el};

R_C Lower limit of branches #5 and #40 are obtained multiplying this factor by the value of the force F attained before entering the unloading path;

S_C Lower limit of branches #4 and #50 are obtained by multiplying this factor by the value of the force F attained before entering the unloading path;

d_u Ultimate displacement;

c_5 Stiffness of branch #5 is obtained multiplying this factor by k_{el};

d_{kf} Stiffness degradation parameter.

When the ultimate displacement is reached, a brittle failure occurs. The stiffness degradation parameter d_{kf} controls the linear degradation of the unloading stiffness once entered in the plastic range (see chapter 2.3.3.3)

2.3.3.2. Axial Hysteresis law

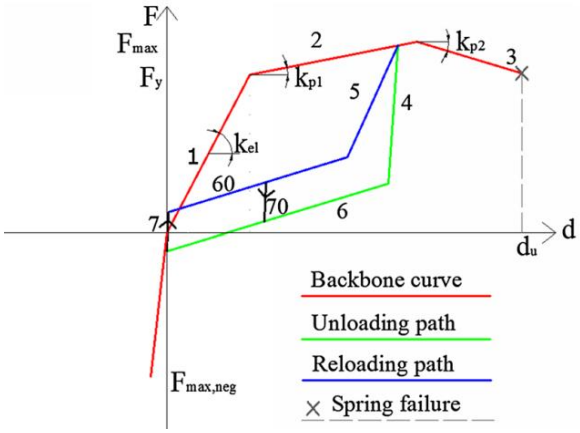

Figure 2.3.2 - Piecewise-linear law of axial spring component [60].

Figure 2.3.2 shows the general force-displacement piecewise-linear law implemented in the model. The parameters defining the entire behavior are the same listed for the shear law, with the addiction of the following three parameters:

c_{10} The stiffness of the compression branches #10 and #20 are obtained multiplying this factor by k_{el};

F_6 The force value at the end of branch #6 is obtained multiplying this factor (percentage) by F_y;

F_{60} The force value at the beginning of branch #60 is obtained multiplying this factor (percentage) by F_y.

2.3.3.3. Stiffness and strength degradation

The stiffness degradation is proportional to the maximum displacement attained during the load history for the last unloading branches #4 and #50:

$$k_{deg} = k_{el}\left[1 - \frac{d_{max}}{d_{ult}}\left(1 - d_{kf}\right)\right] \qquad [2.3.1]$$

where

k_{deg} Degraded stiffness;

k_{el} Elastic stiffness;

d_{max} Maximum displacement attained during the load history;

d_{ult} Ultimate displacement;

d_{kf} Stiffness degradation parameter.

The strength degradation is function of both the maximum displacement attained during the load history and the energy dissipated:

$$\Delta d = \gamma d_y \left(\frac{E_{dis} - E_{dis(A)}}{E_{dis}} \right)^{\alpha} \left(\frac{d_{max}}{d_{ult}} \right)^{\beta} \quad [2.3.2]$$

where

Δd Additional displacement at reloading because of the strength degradation;

γ Linear parameter;

d_y Displacement at yielding force;

α Exponential energy degradation parameter;

E_{dis} Dissipated energy;

$E_{dis(A)}$ Dissipated energy at the beginning of unloading path;

d_{max} Maximum displacement attained during the load history;

d_{ult} Ultimate displacement;

β Exponential displacement degradation parameter.

2.3.3.4. Strength domain and static friction contribution

An axial-shear load domain formulation taken from a European Technical Approval document for CLT connections is considered (ETA 06/0106).

$$\left(\frac{F_N}{R_N} \right)^2 + \left(\frac{F_V}{R_V} \right)^2 \leq 1 \quad [2.3.3]$$

where

F_N Axial force at the previous analysis step;

R_N Yielding axial strength of the connector;

F_V Shear force at the previous analysis step;

R_V Yielding shear strength of the connector.

Friction at the interface between panels has a significant contribution to the global response of a CLT structure [19][68]. The contribution of static friction is taken into account within the method:

$$F_f = k_f F_N \quad [2.3.4]$$

where

F_f Static friction force;

k_f Static friction coefficient;

F_N Axial force at the current analysis step.

A value equal to 0,4 has been chosen for the coefficient k_f as suggested by Dujič et al.

[18].

2.3.3.5. Springs calibration with software So.Ph.I

The parameters of the springs used throughout this thesis have been taken from the results of the tests on metal plate and screwed connections carried out by Gavrić et al. [35][36] (for more information, see chapter 4).

To calibrate the springs using these results, the purposely-developed software So.Ph.I (SOftware for PHenomenological Implementations) [59] has been used. The software allows the user to import a set of parameters, obtained from cyclic tests or analytically calculated, giving as output the parameters describing the spring, usable, with the purposely-developed subroutine, to perform FE analyses using the component approach described earlier in this chapter.

The software permits to calibrate springs not only from a set of given parameters, but to attain the same result also analyzing an image of a force-displacement plot.

2.3.4. SAP2000 modelling

SAP2000 [15] is one of the most utilized software for FE analysis and calculations in structural design worldwide. One of the aims of this thesis is to give suggestions for CLT structures modelling. For this reason, this software has been considered due to its popularity.

While FE solvers like Abaqus [17] or OpenSees [42] allow users to implement external subroutines to integrate the already present features of the software, SAP2000 does not. As mentioned earlier (chapter 2.3.1), approaches that use internal features of a software to perform non-linear cyclic analyses are limited by the limited number of the already present hysteretic laws within the software and how they are able to correctly simulate the behavior needed.

In SAP2000, three are the hysteretic laws implemented for *Multilinear plastic* links: Kinematic, Takeda and Pivot. For wood connections, the Pivot model appears to be the more suitable.

Using this model, it is possible to set the values of the points of the backbone once they are available, from lab tests or analytical calculations. In this thesis, as previously mentioned, results of cyclic tests on typical connections have been used. They were taken and processed with the So.Ph.I software (chapter 2.3.3.5) to draw the backbone of each connection.

During Master Degree thesis studies [70], this approach was followed to model and perform numerical analyses of a 3-story building tested within the SOFIE Project [10][11][40]. The analyses highlighted several problems when connections passed from the hardening branch to the softening one of their force-displacement behavior. After various attempts trying to modify the backbone in order to avoid convergence problems, the final solution was to change the softening branch slope to a stiffness equal to 1/10 of the elastic one. This was made because the software does not work fine with changes in stiffness sign (in this case, from positive

stiffness to negative stiffness) when the second branch is too steep. This approach overestimates maximum displacements and misrepresent the global behavior of the structure when near-collapse loads are considered.

For this reason, SAP2000 has not been used for non-linear analyses within this thesis, but it has only been used for monotonic load analyses (see chapter 6).

2.3.5. Damping in FE analyses

2.3.5.1. Rayleigh damping

This approach defines the damping matrix as proportional to the mass and stiffness matrices:

$$C = \alpha M + \beta K \qquad [2.3.5]$$

where

C Damping matrix

K Stiffness matrix

M Mass matrix

α *M*ass-proportional damping coefficient

β Stiffness-proportional damping coefficient

Using the orthogonality properties of the mass and stiffness matrices, the critical damping ratio can be written as follows:

$$\xi_n = \frac{1}{2\omega_n}\alpha + \frac{\omega_n}{2}\beta \qquad [2.3.6]$$

where

ξ_n Critical damping ratio

ω_n Natural frequency of the system

The constants α and β can be chosen basing on a specific value of critical damping and two given modes of the system:

$$\alpha = 4\pi\xi_n \frac{1}{T_i + T_j} \qquad \beta = \frac{\xi_n}{\pi}\frac{T_i T_j}{T_i + T_j} \qquad [2.3.7]$$

where T_i and T_j are two periods with $T_i > T_j$.

The damping matrix *C* can be defined, if more favorable, as proportional only to either the mass matrix *M* or the stiffness matrix *K*, depending on the type of model analyzed (e.g. geometry, force-displacement/stress-strain relationships, etc)

2.3.5.2. Caughey damping

This approach is based on the Rayleigh method. In this case, a number (greater than two)

of damping ratios are available.

$$C = \sum_{p=1}^{n_1} a_{l_p} K_{l_p} \qquad [2.3.8]$$

where l_p is an arbitrary selected integer, a_{lp} is an arbitrary coefficient and K_{lp} is a matrix that fulfills the following orthogonality property:

$$S^T K_l S = \left(km^{-1}\right)^l m \qquad l = 0, \pm 1, \pm 2, ... \qquad [2.3.9]$$

where

S Modal matrix

k Modal stiffness matrix

m Modal mass matrix

The Rayleigh model is obtained for n_1 equal to 2 and for the indices l_1 and l_2 equal to 0 and 1, respectively.

$$\begin{aligned} l_1 = 0 \quad &\Rightarrow \quad K_0 = M \\ l_2 = 1 \quad &\Rightarrow \quad K_1 = \left(KM^{-1}\right)M = K \end{aligned} \qquad [2.3.10]$$

From the modal matrix c diagonal components, the selected number j of damping ratios can be determined:

$$c_j = 2\xi_j \omega_j m_j = \sum_{p=1}^{n_1} a_{l_p} \omega_j^{2l_p} m_j \quad \Rightarrow \quad \xi_j = \frac{1}{2} \sum_{p=1}^{n_1} a_{l_p} \omega_j^{2l_p - 1} \qquad j = 1, 2, ..., n \qquad [2.3.11]$$

If the damping ratio ξ_j and the frequency ω_j are known for all the coefficient j from 1 to n_1, then the coefficient a_{lp} of Equation [2.3.8] can be directly calculated from Equation [2.3.11] for an arbitrary selection of indices l_1,….,l_{n1}.

With this method, the representation of the damping ratios for the first n_1 modes is correct. For higher modes, the damping ratios are calculated using Equation [2.3.11].

A NOVEL METHOD FOR NON-LINEAR DESIGN OF CLT WALL SYSTEMS

SHORT SUMMARY

In this chapter, a non-linear procedure for the seismic design of metal connections in cross-laminated timber (CLT) walls subjected to bending and axial force is presented. Timber is conservatively modelled as an elasto-brittle material, whereas metal connections (hold-downs and angle brackets) are modelled with an elasto-plastic behavior. The reaction force in each connection is iteratively calculated by varying the position of the neutral axis at the base of the wall using a simple algorithm that was implemented first in a purposely developed spreadsheet, and then into a purposely developed software. This method is based on the evaluation of five different failure mechanisms at ultimate limit state, starting from the fully tensioned wall to the fully compressed one, similarly to reinforced concrete (RC) section design. By setting the mechanical properties of timber and metal connections and the geometry of the CLT panel, the algorithm calculates, for every axial load value, the ultimate resisting moment of the entire wall and the position of the neutral axis. The procedure mainly applies to platform-type structures with hold-downs and angle brackets connections at the base of the wall and rocking mechanism as the prevalent way of dissipation. This method allows the designer to have information on the rocking capacity of the system and on the failure mechanism for a given distribution of external loads. The proposed method was validated on the results of FE analyses using SAP2000 and ABAQUS showing acceptable accuracy.

3.1. Introduction

Cross-laminated timber (CLT) panels have become a common prefabricated structural element used for multi-story timber and hybrid buildings.

In normal practice, CLT structures are made using panels connected with various type of metal connections [32]. Walls are usually connected to the foundation or floor slabs using two types of metal plates: hold-downs (Figure 3.1.1.a) and angle brackets (Figure 3.1.1.b). These plates are connected to the walls using nails (Figure 3.1.1.c) and to the foundation or floor slab using screws (Figure 3.1.1.d) or bolts (Figure 3.1.1.e). To construct wider floor slabs or walls, different panels are commonly linked together through nails, or screws when a stiffer joint is needed, whereas perpendicular walls are usually connected with screws.

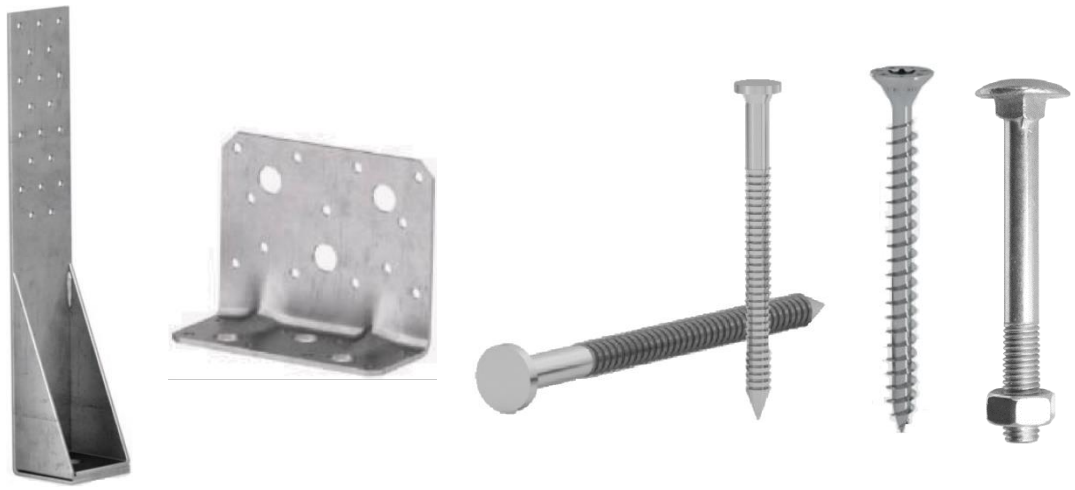

(a) (b) (c) (d) (e)

Figure 3.1.1 - Typical hold-down (a), angle bracket (b), nail (c), screw (d) and bolt (e) used in CLT structures (from Rothoblaas catalogs).

Two types of CLT structures can be built: platform-type, where floor diaphragms bear directly on wall panels that interrupt at each level, and balloon-type, where walls continue for several stories and floors are attached to them. Among platform type construction, two types of structure can be constructed: box type structures (Figure 3.1.2.a) and shear wall type structures (Figure 3.1.2.b). The two types differ for the presence or the lack, respectively, of connections between walls at the corners of the building.

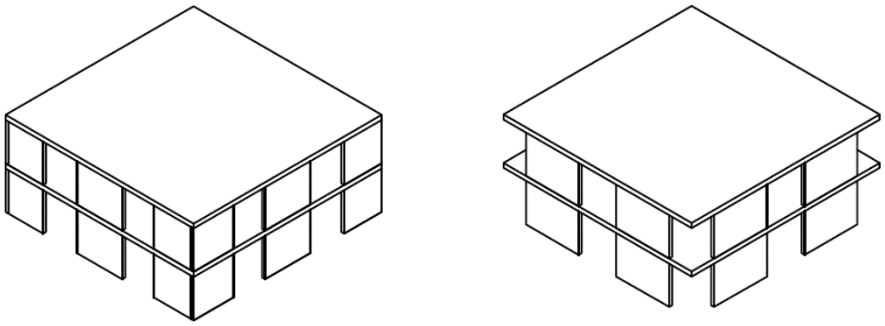

(a) (b)

Figure 3.1.2 - Example of a box type CLT structure (a) and a shear type CLT structure (b).

Although the CLT construction system is relatively new, it is being used extensively in Europe and overseas. Nevertheless, comprehensive regulations are still missing. A clear and widely accepted design procedure under seismic actions has not been defined yet, even though research is in progress [26][33][34][49].

Currently, specific rules for the design of CLT structures are given in few standards around the world [14], though various design method have been proposed during the last years [34]. A simple straightforward way to calculate the reaction force in each metal connection at the base of a CLT wall is still needed [23][24]. Nowadays, designers deal with this problem through a simplified approach and treat hold-downs and angle brackets in two different ways.

Hold-downs are assumed to resist only tension loads due to up-lift of the wall. Their capacity is calculated through a simple rotational equilibrium around one base corner of the wall, see Equation [2.3.12], considering only the opposite hold-down as resisting the tensile force due to the overturning moment, as shown in Figure 3.1.3.b.

$$F_{HD}l = \frac{Nl}{2} - Vh - M = 0 \quad \Rightarrow \quad F_{Rd,HD} \geq F_{HD} = \frac{Vh}{l} - \frac{N}{2} + \frac{M}{l} \qquad [2.3.12]$$

where

F_{HD} Reaction force in the hold-down due to the load condition

$F_{Rd,HD}$ Design resistance of the hold-down

M Bending moment

N Axial force

V Shear force

h Height of the wall

l Length of the wall

Angle brackets are assumed to resist only lateral loads and prevent lateral motion. Their minimum shear capacity is given by Equation [2.3.13]. The described failure mechanism is shown in Figure 3.1.3.c.

$$F_{AB}\, n_{AB} = V \quad \Rightarrow \quad F_{Rd,AB} \geq F_{AB} = \frac{V}{n_{AB}} \qquad [2.3.13]$$

where

F_{AB} Reaction force in each angle bracket due to the load condition

$F_{Rd,AB}$ Design resistance of the angle brackets

n_{AB} Number of angle brackets

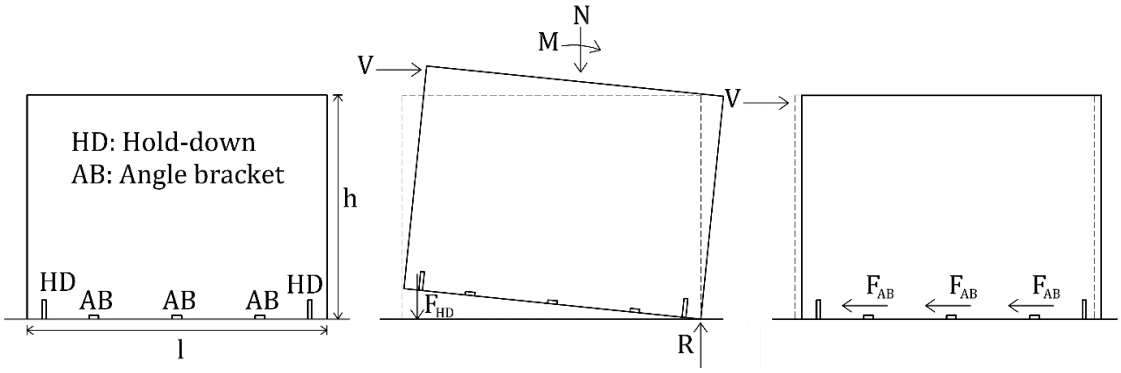

Figure 3.1.3 - Typical CLT wall panel connected to the foundation with hold-downs and angle brackets (a), failure mechanisms considered for hold-down design (b) and angle bracket design (c).

It is easy to foresee that these simplifications lead to a too conservative design. Furthermore, as pointed out by different authors [35][37], the tensile resistance and stiffness of angle brackets are not negligible, leading to significantly different load distributions, if

compared to those obtained using the aforementioned method.

In this chapter, a more realistic and less conservative method for the calculation of tensile force in the metal connectors at the base of a CLT wall is proposed considering the tensile resistance and stiffness of both hold-downs and angle brackets. The shear reaction forces of hold-downs have not been considered because their shear resistance and stiffness are significantly lower than the ones offered by angle brackets [35][37]. Usually, only two hold-downs are used per wall and, during the first part of a lateral motion, they rotate rigidly, acting mostly like a truss element. Furthermore, in order to allow recentring of the structure after a seismic event, lateral displacements should be kept in the elastic range. Plasticization should occur in vertical joints, such as connections between wall panels, and tension resisting connections, such as hold-downs and angle brackets in tension, rather than horizontal shear resisting elements, such as angle brackets in shear. For these reasons, since only angle brackets resist lateral loads and they should remain elastic, the simplified approach mentioned before could be used (see Figure 3.1.3.c and Equation [2.3.13]).

The proposed method is based on the analogy between the design of rectangular reinforced concrete sections and the design of the base of a CLT wall with metal connections (hold-downs and angle brackets). A similar subdivision into sub-domains was made by setting different well-defined failure mechanisms [22]. With this method, the load distribution in the connections can be calculated for a certain load condition, and the most probable collapse mechanism is identified. The procedure mainly applies to platform frame structures with hold-downs and angle brackets connections at the base of the wall and rocking mechanism as prevalent way of dissipation.

3.2. Method derivation

The proposed method, compared to the usual practice, considers the tensile strength of angle brackets. It is based on the assumption that a design, in order to allow the recentring of the structure after a later load, due to wind loads or earthquake, should favor rocking over slip, and so favor the plasticization of tension resisting connections, such as hold-downs and angle brackets in vertical direction, rather than the plasticization of shear resisting connections, such as angle brackets in horizontal direction, which should remain in their elastic domain.

For these reasons, only tension is considered

3.2.1. Hypotheses

In order to derive a simplified method, some assumptions were made:

- Wood is modelled with a conservative elasto-brittle behavior (see Figure 3.2.1), characterized by the Young modulus E and the ultimate compressive stress f_c. Such a

behavior has been chosen as in a typical design wood members are regarded as rigid and ductility is concentrated in the connections. A triangular stress-block in compression is assumed;

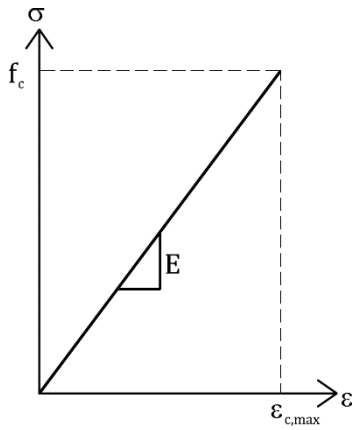

Figure 3.2.1 - Stress-strain relationship of wood in compression at the wall-foundation interface.

- Only compression stresses are assumed to be transferred by the wood of the wall to the floor/foundation interface. Tensile forces are only transferred by metal connections.
- As wall panels are in direct contact with the surface underneath, whether it is the foundation or a floor slab, the contribution of hold-downs and angle brackets to the compression resistance of the system is negligible. As a consequence, both connections are modelled as only resisting in tension through elasto-plastic behaviors with limited ductility (see Figure 3.2.2), characterized by the yielding force F_y, the elastic stiffness k_s and the ultimate displacement U_{ult};

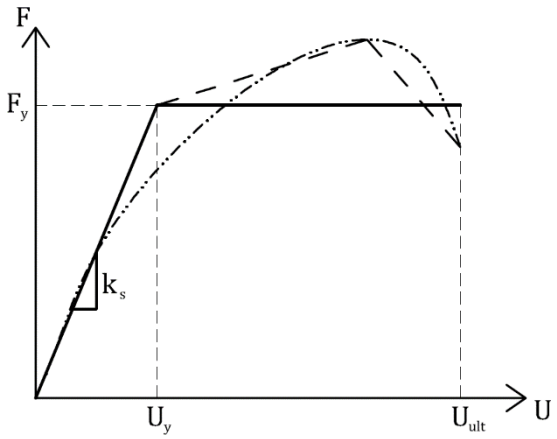

Figure 3.2.2 - Experimental force-displacement relationship (line with dashes and dots), tri-linear approximation of the test result (dashed line) and elasto-plastic approximation of the test results (solid line) for connections.

- CLT wall panels are regarded as rigid bodies. For this reason, the compressive stress at the bottom corner of the wall σ_c is related to a fictitious displacement u_c underneath the foundation surface and a coefficient k (see chapter 3.3.1.1 and Equation [2.5.1]) of compressive stress distribution along the height of the panel h through Equation [2.4.1]:

$$\sigma_c = \frac{u_c E}{k h} \quad \Rightarrow \quad u_{c,max} = \frac{f_c k h}{E} \qquad [2.4.1]$$

Figure 3.2.3 depict the rocking mechanism and the forces considered.

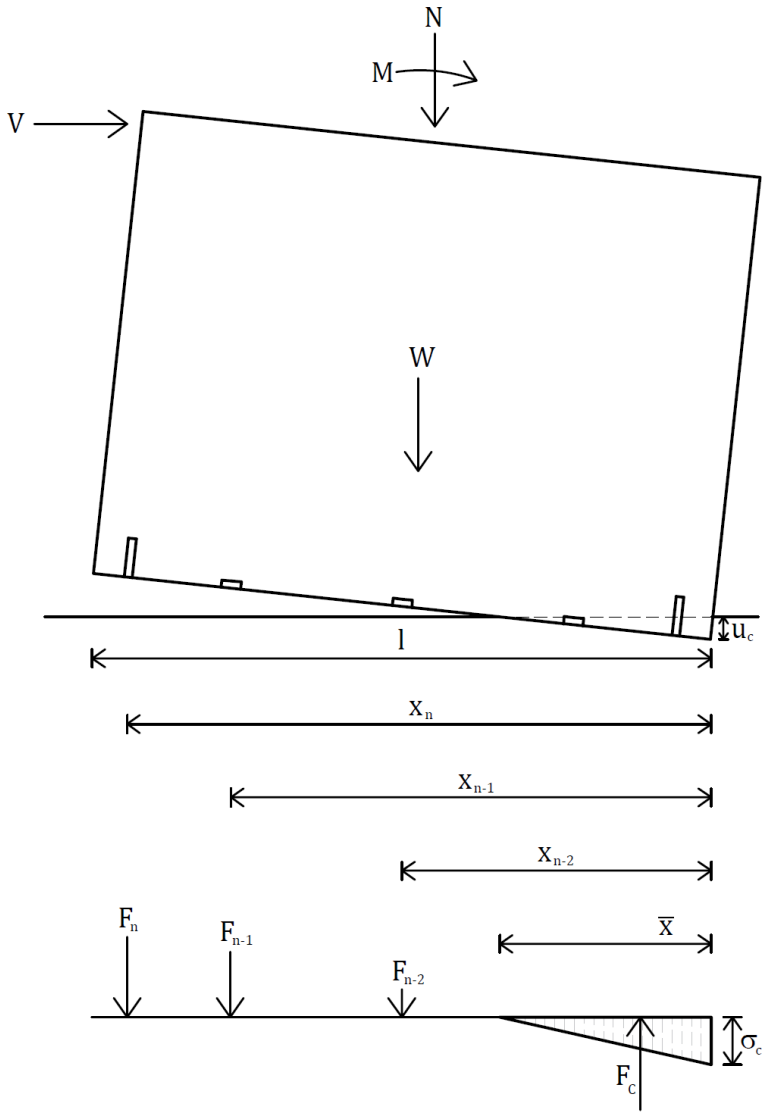

Figure 3.2.3 - Rotational mechanism and forces involved.

With reference to Figure 3.2.3

F_c Value of the reaction force in compression in the contact zone between panel and supporting surface

F_i Value of the reaction force in the i^{th} connection

W Self-weight of the panel

k Compressive stress distribution coefficient

n Number of connections

u_c Fictitious displacement underneath the foundation surface

$\bar{x}$ Distance of the neutral axis from the bottom right corner

x_i Distance of the i^{th} connection from the compressed panel corner

σ_c Compressive stress at the bottom corner of the wall

The reference point for the position of the neutral axis is the bottom right corner of the panel if the lateral force at the top of the wall is directed rightward, the bottom left corner of the panel if the lateral force at the top of the wall is directed leftward. All forces are regarded as positive if they are oriented like those indicated in Figure 3.2.3. The axial force *N* is therefore considered positive if the wall is compressed.

3.2.2. Limit States definition

As previously mentioned, the proposed method is developed by analogy with the design of RC cross-sections.

According to the assumptions made, five failure sub-domains were defined to consider the occurrence of all the possible ultimate limit states at the wall-support interface. The case discussed herein is for lateral load at the top of the panel directed rightward:

1. Pure tension: At least one connection attains its ultimate displacement U_{ult}. Timber is not compressed;
2. At least one connection attains its ultimate displacement U_{ult}. The bottom right corner of the panel is compressed with a stress lower than f_c;
3. At least one connection is subjected to tension. The bottom right corner of the panel attains the compression resistance f_c;
4. No connection is in tension. The bottom left corner of the panel is not compressed;
5. The whole base of the panel is compressed. None of the connections is in tension.

The subdivision detailed herein is displayed in Figure 3.2.4.

Referring to Figure 3.2.4

s.s. Supporting surface

Limit in tension, starting configuration of the domain

Interface between sub-domains 1 and 2

Interface between sub-domains 2 and 3

Interface between sub-domains 3 and 4

Interface between sub-domains 4 and 5

Limit in compression, ending configuration of the domain.

It can be noticed that in sub-domains 1, 2 and 3 the connections are loaded in tension, and therefore an iterative solutions will have to be computed as the force-displacement relationship is elasto-plastic with limited ductility.

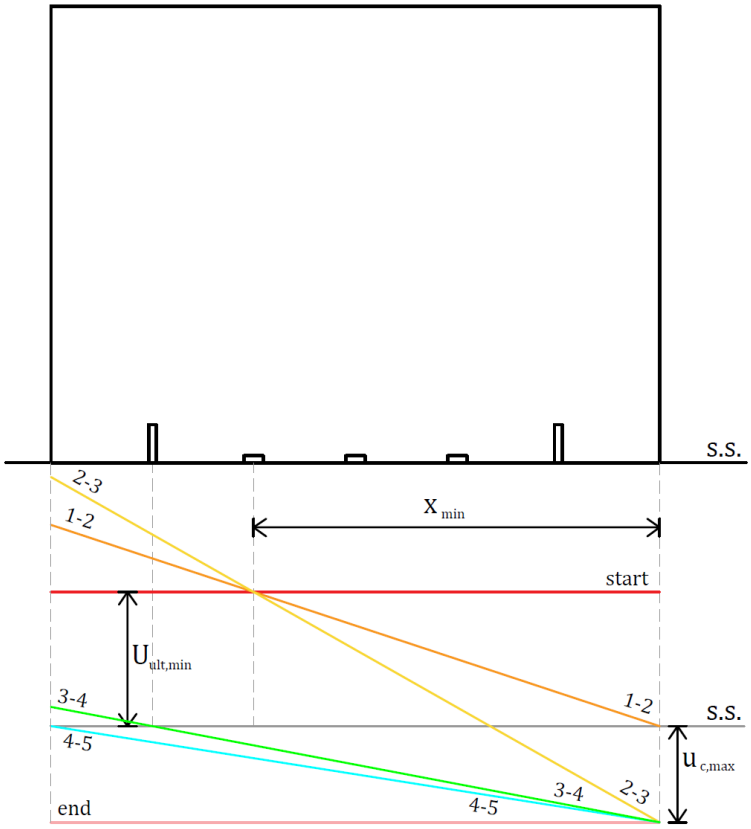

Figure 3.2.4 - Schematic representation of the considered sub-domains.

On the other hand, sub-domains 4 and 5 do not depend on anything but the timber compressive stress. The choice of an elasto-brittle relationship leads to closed form solutions for these last two cases.

From Figure 3.2.4 it can be noted that the position of the neutral axis at the boundaries of each sub-domain is a mere geometrical problem since it can be deduced from the values U_{ult} and $u_{c.max}$. Consequently, the possible range of axial forces leading to the attainment of a particular ultimate limit state condition can be immediately assessed: by knowing the geometry of the wall, the location of the connections, the stress-strain and force-displacement relationships of wall and metal connections, respectively, the minimum and maximum value of axial force allowed in the system and all the four values of axial force at the boundary between sub-domains can be immediately derived. Once the value of the axial load is known, the failure mechanism occurring first and the corresponding sub-domain can be determined.

In Figure 3.2.4, the notation $U_{ult,min}$ is used since two different types of connection are generally used, each one with its own force-displacement behavior, and therefore a different ultimate displacement, so that $U_{ult,min}$ is the minimum ultimate elongation, among the two available connections, and $U_{ult,max}$ is the largest one. Usually, in a structure, at least in the same wall, all the hold-downs have the same mechanical properties and all the angle brackets have the same mechanical properties. Having two different ultimate displacements leads to two possible rotation points of the wall in order to fulfill the ultimate state conditions of sub-domains 1 and

2. In the example shown in Figure 3.2.4, the lower ultimate displacement is the angle brackets one. For a connection arrangement similar to that depicted in Figure 3.2.4, the rotation point used to trace sub-domains 1 and 2 is (x_{min};$U_{ult,min}$), where x_{min} signifies the distance of the farthest connection, characterized by an ultimate displacement $U_{ult,min}$, from the right wall corner. However, the possibility for the base of the wall to reach the point (x_{max};$U_{ult,max}$) should be considered (Figure 3.2.5.b), where x_{max} is the distance of the last connection, having $U_{ult,max}$ as ultimate displacement, from the right wall corner. If this condition occurs, two connections attain the ultimate displacement, leading to the shift of the rotation point from (x_{min};$U_{ult,min}$) to (x_{max};$U_{ult,max}$), in order not to overcome the ultimate elongation of the more flexible connection, as shown in Figure 3.2.5.c.

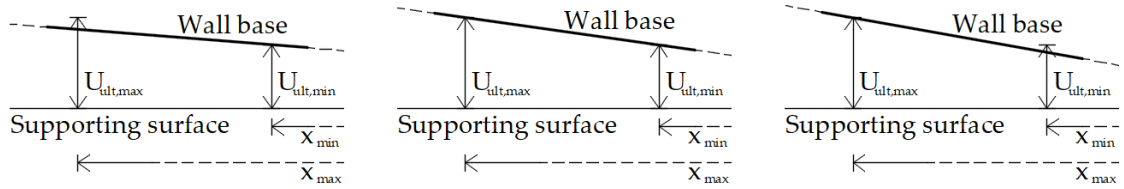

Figure 3.2.5 - Starting condition for the definition of subdomains 1 and 2 (a), attainment of the ultimate condition in two different connections (b) and change in the point of rotation of the system (c).

This shift cannot take place in sub-domains 3, 4 or 5, since the rotation point is always (0;$u_{c,max}$) (see Equation [2.4.1] and Figure 3.2.4). The position of the neutral axis where this shift occurs is defined as $\bar{x}_p$ and its value can be calculated by a proportion of similar triangles, as shown in Equation [2.4.2]:

$$\bar{x}_p = \frac{U_{ult,max} x_{min} - U_{ult,min} x_{max}}{U_{ult,max} - U_{ult,min}} \qquad [2.4.2]$$

The value of $\bar{x}_p$ has to be limited to the position of the neutral axis between sub-domains 2 and 3. This restriction results in the condition given by Equation [2.4.3]:

$$\bar{x}_p \leq \frac{x_{min} u_{c,max}}{U_{ult,min} + u_{c,max}} \qquad [2.4.3]$$

Once the value of $\bar{x}_p$ is known, sub-domains 1 and 2 can be easily defined.

Table 3.2.1 - Position of the neutral axis at the lower and upper limit for each sub-domain.

Sub-domain	1		2		3		4		5
$\bar{x}$	-∞	0	$\bar{x} = \frac{x_{min} u_{c,max}}{U_{ult,min} + u_{c,max}}$ if $\nexists \bar{x}_p$ $\bar{x} = \frac{x_{max} u_{c,max}}{U_{ult,max} + u_{c,max}}$ if $\exists \bar{x}_p$	[2.4.4]	x_n		l		+∞

Referring to Table 3.2.1, x_n signifies the distance of the leftmost connection from the right

base corner, as this corner is taken as reference point to measure distances and positions, and *l* is the length of the wall.

The definition of sub-domains 1, 2 and 3 needs an iterative process to be made. The first quantity to assess is the elongation of each connection. A simple proportion between similar triangles is used. The value of $\bar{x}_p$ is crucial, for sub-domains 1 and 2, because it sets whether this proportion has to be made using $U_{ult,min}$ or $U_{ult,max}$, as shown in Equation [2.4.5]:

$$u_i = \begin{cases} \dfrac{U_{ult,min}(x_i - \bar{x})}{x_{min} - \bar{x}} & \text{when} \quad \bar{x} \le \bar{x}_P \\ \dfrac{U_{ult,max}(x_i - \bar{x})}{x_{max} - \bar{x}} & \text{when} \quad \bar{x} > \bar{x}_P \end{cases} \qquad [2.4.5]$$

In sub-domain 3, where the elongation of the connections still plays a role, the proportion is made using $u_{c,max}$, as the rotation point for this sub-domain becomes the bottom right corner:

$$u_i = \frac{u_{c,max}(x_i - \bar{x})}{\bar{x}} \qquad [2.4.6]$$

Knowing the value of vertical displacement in each connection allows calculation of the corresponding reaction force:

$$F_i = \begin{cases} F_{y,i} & \text{when} \quad u_i > U_{y,i} \\ k_i u_i & \text{when} \quad 0 < u_i \le U_{y,i} \end{cases} \qquad [2.4.7]$$

The last unknown to be calculated is the contact reaction force in wood F_c. This value depends on the position of the neutral axis $\bar{x}$ and the stress value at the right base corner. The compressive stress can be calculated using Equation [2.4.1] as seen in chapter 3.2.1 for sub-domain 2. For sub-domain 3 this value is constant and equal to f_c. The contact force F_C is given by Equation [2.4.8] for sub-domain 2 and by Equation [2.4.9] for sub-domains 3 and 4:

$$F_c = \frac{\sigma_c s \bar{x}}{2} \qquad [2.4.8]$$

$$F_c = \frac{f_c s \bar{x}}{2} \qquad [2.4.9]$$

s signifies the thickness of the panel.

All the previously derived quantities depend upon the value of $\bar{x}$. The value of $\bar{x}$ can be determined with some iterations by solving the equilibrium of the vertical forces (Equation [2.4.10]):

$$N = F_c(\bar{x}) - \sum_1^n F_i(\bar{x}) - W \qquad [2.4.10]$$

If the value of the axial force *N* is greater than the value at the limit between sub-domain 3 and 4, a closed form solution can be employed. In this case, the summation term in Equation [2.4.10] disappears, leading to a solution that only depends on the compressive force F_c, which

is a linear function of the neutral axis position $\bar{x}$.

In sub-domain 4, which is a particular case of sub-domain 3 where the summation term is equal to zero, the value of the neutral axis position is given by Equation [2.4.11]:

$$F_c = \frac{f_c s \bar{x}}{2} \quad \Rightarrow \quad N = \frac{f_c s \bar{x}}{2} - W \quad \Rightarrow \quad \bar{x} = \frac{2(N+W)}{f_c s} \qquad [2.4.11]$$

For sub-domain 5, an additional consideration has to be made in order to find the correct value of the contact force F_c. Here the neutral axis lays outside the base of the wall, meaning that the stress block has a trapezoidal shape, and therefore the stress at the left base corner σ_d is needed. This value is calculated again via a simple proportion between similar triangles, as shown in Equation [2.4.12]:

$$\frac{\sigma_d}{\bar{x} - l} = \frac{f_c}{\bar{x}} \quad \Rightarrow \quad \sigma_d = \frac{f_c(\bar{x} - l)}{\bar{x}} = f_c\left(1 - \frac{l}{\bar{x}}\right) \qquad [2.4.12]$$

Having found the value of σ_d, the value of F_c can then be calculated according to Equation [2.4.13]:

$$F_c = \frac{(f_c + \sigma_d) s l}{2} = \frac{\left[f_c + f_c\left(1 - \frac{l}{\bar{x}}\right)\right] s l}{2} = f_c s l \frac{2 - \frac{l}{\bar{x}}}{2} = f_c s l \left(1 - \frac{l}{2\bar{x}}\right) \qquad [2.4.13]$$

The position of the neutral axis can then be calculated using the equilibrium equation:

$$N = f_c s l\left(1 - \frac{l}{2\bar{x}}\right) - W \Rightarrow 1 - \frac{l}{2\bar{x}} = \frac{N+W}{f_c s l} \Rightarrow \frac{2\bar{x}}{l} = \frac{f_c s l}{f_c s l - N - W} \Rightarrow \bar{x} = \frac{f_c s l^2}{2(f_c s l - N - W)} \qquad [2.4.14]$$

Once the position of the neutral axis $\bar{x}$ and all the reacting forces at the ultimate limit state are known, the resisting bending moment of the system M_{Rd} can be calculated. This is made through a simple rotational equilibrium around the midpoint of the wall base:

$$M_{Rd} = F_C\left(\frac{l}{2} - \frac{\bar{x}}{3}\right) - \sum_1^n F_i\left(\frac{l}{2} - x_i\right) \qquad [2.4.15]$$

Equation [2.4.15] is valid for sub-domains 1 to 4, recalling that the reaction contact force F_c is equal to zero for sub-domain 1 and so is the summation term for sub-domain 4.

In sub-domain 5, having a trapezoidal stress block, a different equation to calculate M_{Rd} is needed:

$$M_{Rd} = F_C\left[\frac{l}{2} - \frac{l}{3}\frac{2\sigma_d + f_c}{\sigma_d + f_c}\right] \qquad [2.4.16]$$

The procedure displayed above is valid for a lateral force applied at the top of the wall directed rightward. When the lateral force is directed leftward, the reference point has to be moved from the bottom right corner to the bottom left corner. The distances of the connections x_i should be changed in accordance to Equation [2.4.17]:

$$x_{i,sx} = l - x_{i,dx} \quad [2.4.17]$$

where $x_{i,sx}$ and $x_{i,dx}$ signify the distances of the i^{th} connection from the bottom left and the bottom right corner, respectively.

By using these new values, the problem is equivalent to the one for lateral load directed rightward.

By varying the position of the neutral axis from -∞ to +∞ for both cases of lateral force directed rightward and leftward, all the possible couples (N;M_{Rd}) can be calculated, and an axial force-bending moment resisting domain can be drawn. An example is displayed in Figure 3.2.6.

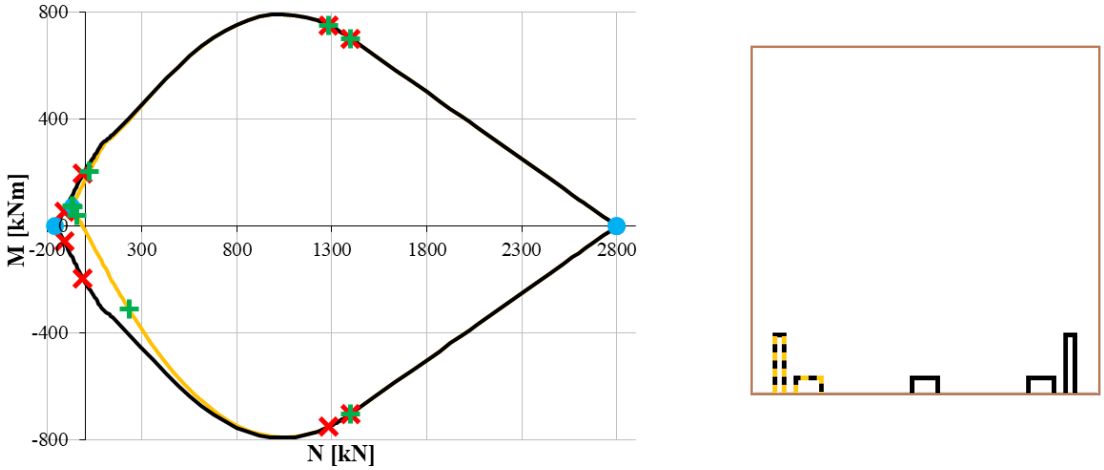

(a) (b)

Figure 3.2.6 - Examples of axial force-bending moment resisting domain for a symmetrical (black line (a) and black connections (b)) and non-symmetrical (orange line (a) and orange connections (b)) arrangement of connections. In the second configuration, only the two connections on the left are present with respect to the symmetrical one (b). X and + marks denote the passage from a sub-domain to another for symmetrical and non-symmetrical arrangement of connections, respectively. Circles denote the starting (left, sub-domain 1) and end (right, sub-domain 5) points of the domains.

Initially, the procedure was implemented into a spreadsheet, and then in a Windows application. This software, written in VB.NET and available both in Italian and English, allows the user, once the needed parameters have been set, to calculate the resisting domain. It draws the positions of the neutral axis at the intersection of the various sub-domains for the analyzed wall. Furthermore, the sub-domain where the ultimate limit state takes place for the given value of axial force N can be determined.

3.3. Method validation

This section investigates the values of the stress distribution coefficient k and validates the proposed method using two different numerical approaches. The first approach is based on the use of SAP2000 [15] and derives values of k for walls on a rigid support. The second approach uses ABAQUS [17] and derives values of k for both rigid foundation and CLT support. All numerical models used within this chapter were validated in previous papers and

studies [62][70].

3.3.1. SAP2000 analyses

3.3.1.1. Investigation of the stress distribution coefficient *k*

The proposed method converts the strain of the wall panel at the interface with the supporting foundation/floor panel into an equivalent fictitious displacement of the panel underneath the support surface, so that the loss of height of the panel due to the compression of CLT is equal to the fictitious displacement underneath the supporting surface. This permits to regard the panel as rigid, easing the computation. The change is made through a coefficient of stress distribution *k*. This coefficient depends upon the stress distribution along the CLT panel above the rocking corner, and can be calculated according to Equation [2.5.1]:

$$k = \frac{\int_0^h \sigma_c(z)\,dz}{f_c h} \qquad [2.5.1]$$

In order to find a proper value for this coefficient, several numerical analyses using the software SAP2000 [15] were carried out. Two CLT panels 3 m long and 85 mm thick with different heights, 3 m and 1,75 m, were analyzed. The unit weight of wood and the Young modulus were assumed 4,2 kN/m3 and 5,7 GPa, respectively [7][62][70]. The geometric characteristics of the panels have been taken from the panels tested within the SOFIE Project [10][11][40], while the choice of a single MOE was made because the method takes into account only compression stiffness of CLT and the analyses have been carried out by modelling the panels via isotropic shell elements. The value is an average between perpendicular and parallel to the grain MOEs accounting for number and orientation of layers within the panel [62].

The two panels were linked with three different types of connections to the foundation surface. The tension force-displacement relationships of the connections are described in the following (Figure 3.3.1):

1. Hold-down
   - Elastic phase with a stiffness of 4,82 kN/mm and a yielding force of 40,31 kN;
   - Hardening phase with a slope of 0,37 kN/mm and a peak strength of 48,33 kN;
   - Quasi-vertical failure;
   - Residual horizontal strength at 5% of the peak strength.
2. Angle bracket
   - Elastic phase with a stiffness of 2,7 kN/mm and a yielding force of 19,27 kN;

- Hardening phase with a slope of 0,25 kN/mm and a peak strength of 23,47 kN;
- Quasi-vertical failure;
- Residual horizontal strength at 5% of the peak strength.

3. Contact spring
   - In order to simulate the contact between wall and foundation, all the nodes at the base of the panel were linked to the ground with a connection having loose behavior in tension (force/displacement ratio of 1/1000).

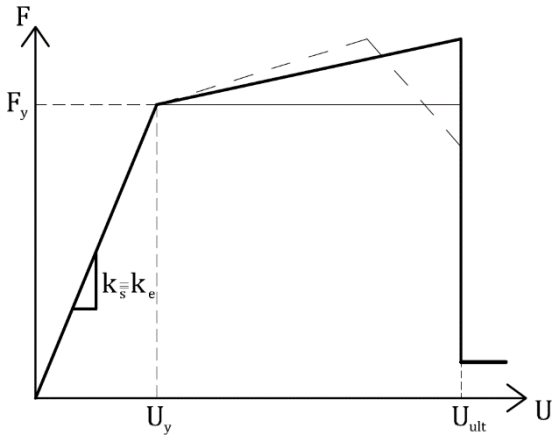

Figure 3.3.1 - Comparison between SAP2000 connections force-displacement relationship (bold solid line), trilinear force-displacement relationship (dashed line) and elasto-plastic force-displacement relationship (solid line).

The set of parameters chosen for hold-down and angle bracket links are the same of the connections used within the SOFIE Project [10][11][37][40] in terms of elastic branches, ultimate displacements and peak strengths. The hardening slope was set as a function of the known values of ultimate strength and displacement.

In compression, for the three links, a conventional stiffness was used for the force-displacement relationship to obtain a rigid behavior [60]. A rigid behavior has also been considered for in-plane shear.

Two hold−downs were placed, at 250 and 2750 mm, three angle brackets were placed, at 750, 1500 and 2250 mm, and in the other points contact links were placed.

The two panels were subjected to pushover analyses by increasing the lateral load, directed rightward, applied at the top of the panel. These analyses were executed for different values of axial load (12, 24, 36 and 48 kN). The resulting compression stress distributions were computed at the step of the analysis corresponding to a stress value at the bottom right corner equal to the compression limit for CLT (≈13MPa). Then, Equation [2.5.1] was applied, providing a range of *k* from 0,29 to 0,43. For this first validation, an average *k* value equal to 0,36 was chosen.

3.3.1.2. Analyses description

In order to validate the proposed simplified method, some pushover analyses were performed on different systems using SAP2000, comparing the results obtained through the numerical analyses with those obtained with the proposed method. The investigated systems are:

1. Two 2-dimensional models:
   - A single-panel CLT wall;
   - A 3-panel CLT wall.
2. A 3-dimensional model of a 3-story building.

The single panel was modelled in the same way as described in chapter 3.3.1.1 for an aspect ratio of 1. The 3-panel wall was modelled by linking together the panels using springs simulating screws in a half-lap joint. Multilinear plastic joints with a conventional stiffness of 100 kN/mm in the two in-plane directions were used. A semi-rigid connection was chosen here because the method does not account yet for loose connections between panels.

The 3-story building model schematizes a building tested within the SOFIE Project [10][11][62][70] and numerically investigated through SAP2000 [15]. To ease the convergence in non-linear analyses, the quasi-vertical failure branch was replaced by a softening branch with a slope of one-tenth of the elastic slope. In these analyses, in fact, this software proved to be unstable using steep descending gradients in the softening branch of the force-displacement relationship [70].

3.3.1.3. Validation through a 2-D model

Both 2D validations were carried out through several displacement-controlled pushover analyses. Using the spreadsheet, four different values of axial forces at the interface of the five sub-domains were calculated. Such values were used to run the analyses in SAP2000.

For each case, the ultimate limit state which occurred first was investigated and, at that step, the position of the neutral axis was assessed. These results were compared to those obtained using the spreadsheet. A summary of the comparison for the single panel and the 3-panel wall is presented in Table 3.3.1 and Table 3.3.2, respectively.

Table 3.3.1 - Comparison between numerical and analytical results - single panel wall.

N [kN]	Neutral axis position [mm]		Difference [mm]	Error related to the wall length [%]
	Algorithm	SAP2000		
462	3000	3050	50	1,7
423	2750	2800	50	1,7
-101	63	138	75	2,5
-114	0	-83	83	2,8

Table 3.3.2 - Comparison between numerical and analytical results - 3-panel wall.

N [kN]	Neutral axis position [mm]		Difference [mm]	Error related to the wall length [%]
	Algorithm	SAP2000		
1386	9000	8750	250	2,8
1347	8750	8733	17	0,2
-112	525	370	155	1,7
-154	0	36	36	0,4

In the first case, the error is always lower than 10 cm (3% of the wall length). Even in the second case, the evaluation of the neutral axis using the method is good, leading to an error of less than 3% of the wall length in this case too.

3.3.1.4. Validation through a 3-D model

In the 3D validation, the comparison was made for a wall of the ground floor.

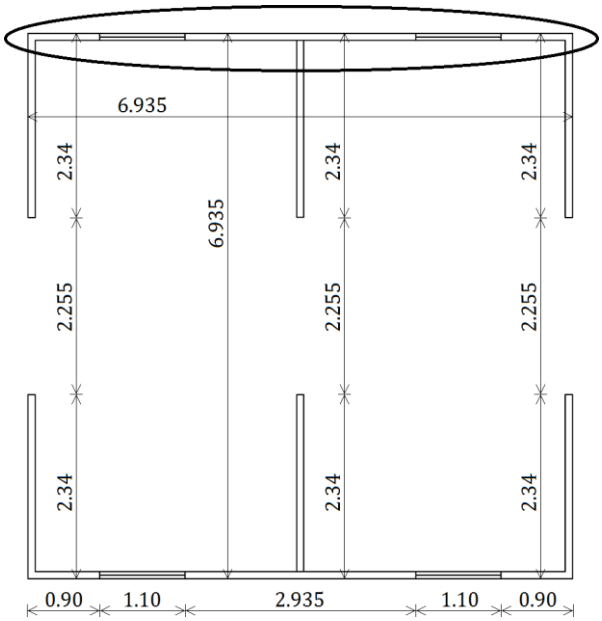

Figure 3.3.2 - Plan of the ground floor of the case study building with the investigated wall highlighted.

Contact springs were placed in each node of the wall base where neither hold-downs nor angle brackets are applied. Such springs are placed at the base of the various walls in the same way as for the single panel wall and for the 3-panel wall (see chapter 3.3.1.1). The axial force applied on the wall used for the analytical calculation was obtained by summing the axial reaction forces in the connections and in the contact links of the SAP2000 FE model after the application of the permanent loads. The numerical investigation was carried out by searching for the step of the analysis where an ultimate condition occurred and evaluating the position of the neutral axis there. The resulting position of the neutral axis was 2500 mm from the compressed edge, with an ultimate limit state characterized by crushing of CLT. The method predicted the same ultimate limit state, but a neutral axis at 1304 mm. This difference (1196 mm), if compared to the wall length, gives an error of 17,7%.

Further analyses were performed by making some changes in the model. All the following cases are additional, and so, for instance, the third case brings the alterations of the first and the second case too:

1. The central wall perpendicular to the one investigated and all its connections were removed;
2. The out-of-plane shear stiffness of the connections linking the walls perpendicular to the one investigated were set to a very low value, in order to neglect their contribution;
3. The tension stiffnesses of the connections mentioned at step 2 were set as very loose too.

The results are summarized in Table 3.3.3.

Table 3.3.3 - 3-story building verification in the different cases.

Analysis	Distance from the compressed corner [mm]	Difference [mm]	Error related to the wall length [%]
Model	2500	1196	17,7
1st case	2350	1046	15,5
2nd case	2350	1046	15,5
3rd case	2050	746	11

It can be noticed that, by introducing the modifications in the model, the error drops to 11%, as the stiffening effect due to the presence of perpendicular walls is, at the moment, neglected in the proposed simplified method.

3.3.2. Abaqus analyses

To improve the FE model and to compute the more realistic force-displacement relationships for connections characterized by a softening branch displayed in Figure 3.2.2 [60], the general FE solver ABAQUS was used [17].

3.3.2.1. Model description

Three different wall panels were tested. These three panels, having the same mechanical properties and thickness shown in chapter 3.3.1.1, differ for their height to length ratio, which were set equal to 1, 1,5 and 3 respectively, considering the same height of 3 m. Each panel has two hold-downs at the ends of the base and angle brackets spaced at 1m c/c, leading to a total of 3, 2 and 1 angle brackets respectively. The mechanical properties of these two connections are shown in Table 3.3.4. These properties are the same as those considered within the SAP2000 analyses. The advantage of using ABAQUS was no convergence problems during the analyses unlike with SAP2000, allowing consideration of hardening and softening.

These connections were modelled with loose behavior in compression.

To include more cases of technical interest, the three panels were placed on two different

types of support: rigid foundation and CLT floor panel support. In order to simulate such conditions, various contact connections were placed at the base of the CLT walls. These contact springs were modelled depending on whether a rigid or a CLT support was investigated. For both of them, a loose behavior in tension was set. For the rigid support case, the same value of stiffness was considered for the three panels. A linear elastic behavior was introduced in this case. In the case of the CLT wall panel supported by a CLT floor panel, a possible plasticization of timber of the CLT floor panel in the direction perpendicular to the grain may occur. Since the contact links cannot plasticize in compression, new elasto-plastic springs were introduced. The compressive stiffness and strength were derived by multiplying the mean values of the modulus of elasticity and compression strength perpendicular to the grain of the CLT floor panel by a tributary area. The mechanical properties were taken from the compression tests carried out on CLT specimens at Växjö University [1]. The tributary area was calculated by considering a 45° diffusion angle within the CLT floor panel from the bearing area of the CLT wall panel. As consequence, each type of panel resulted to have a different value of compressive strength of its contact links due to different ratios of tributary surface over base area.

Table 3.3.4 - Tensile behavior of hold-downs and angle brackets.

	Hold-downs	Angle brackets
Branch	Stiffness [kN/mm]	Stiffness [kN/mm]
Elastic	4,8	2,7
Hardening	0,69	0,4
Softening	-0,38	-0,81
Characteristic	Value	Value
F_y	40,31 kN	19,27 kN
F_{max}	48,33 kN	23,47 kN
U_{ult}	35 mm	24 mm

3.3.2.2. Investigation of the stress distribution coefficient *k*

Numerical analyses were performed for the three panels in five different conditions of load applied on the top of them:

1. Only compressive axial load;
2. Only horizontal shear load;
3. Only bending moment;
4. Axial compressive and horizontal shear loads;
5. Bending moment and horizontal shear load.

The values of the *k* coefficient were assessed using the results of these analyses. Cases 4 and 5 were investigated for different values of the shear-axial load ratio *V*/*N* and *Vh*/*M* ratio, where *Vh* signifies the overturning moment due to the horizontal shear force and M denotes the

bending moment applied on top of the panel. All loads were modelled through a distribution of concentrated forces applied in all the nodes at the top of the wall. The following loading conditions were taken into consideration:

- Axial load: unitary vertical forces directed downward;
- Shear load: unitary horizontal forces directed rightward;
- Moment loads: forces varying linearly from a unitary value directed downward on the right top corner to a unitary value directed upward on the left top corner, to form a bi-triangular distribution of forces (Figure 3.3.3).

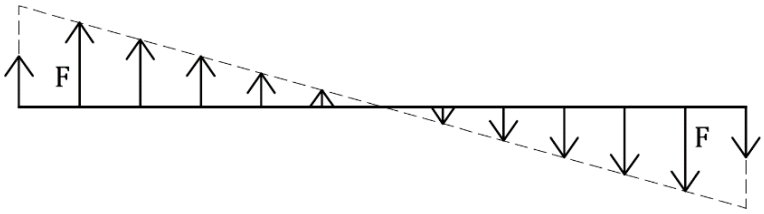

Figure 3.3.3 - Force distribution on top of the wall for the case with bending moment.

In order to avoid singularities in the model, forces in the left and right corners were assumed equal to half the unitary value in all the configurations. A non-linear monotonic analysis was carried out for all cases by increasing the forces up to the attainment of either the compressive strength in the bottom right corner of the panel, or the ultimate displacement in the metal connections, whichever occurs first. The stress distribution and, consequently, the coefficient *k* were computed at this last step of analysis.

The first three configurations were investigated to define the limits for *k* at the ultimate state of compression in the CLT panel. The results of these analyses are presented in Table 3.3.5.

Table 3.3.5 - Values of *k* for rigid and CLT support for different loads and h/l ratios.

Loading condition	Rigid support			CLT support		
	h/l			h/l		
	1	1,5	3	1	1,5	3
Axial force	0,984	0,969	0,974	0,976	0,951	0,954
Shear force	0,184	0,151	0,138	0,298	0,288	0,201
Bending moment	0,271	0,227	0,219	0,419	0,428	0,344

In Figure 3.3.4 the results for the last two configurations (case 4 and 5) are displayed for rigid (foundation) and flexible (CLT floor panel) support conditions.

The variation of *k* is larger for the axial-shear load condition (case 4) as bending moment and shear load lead to a stress concentration on the base corner.

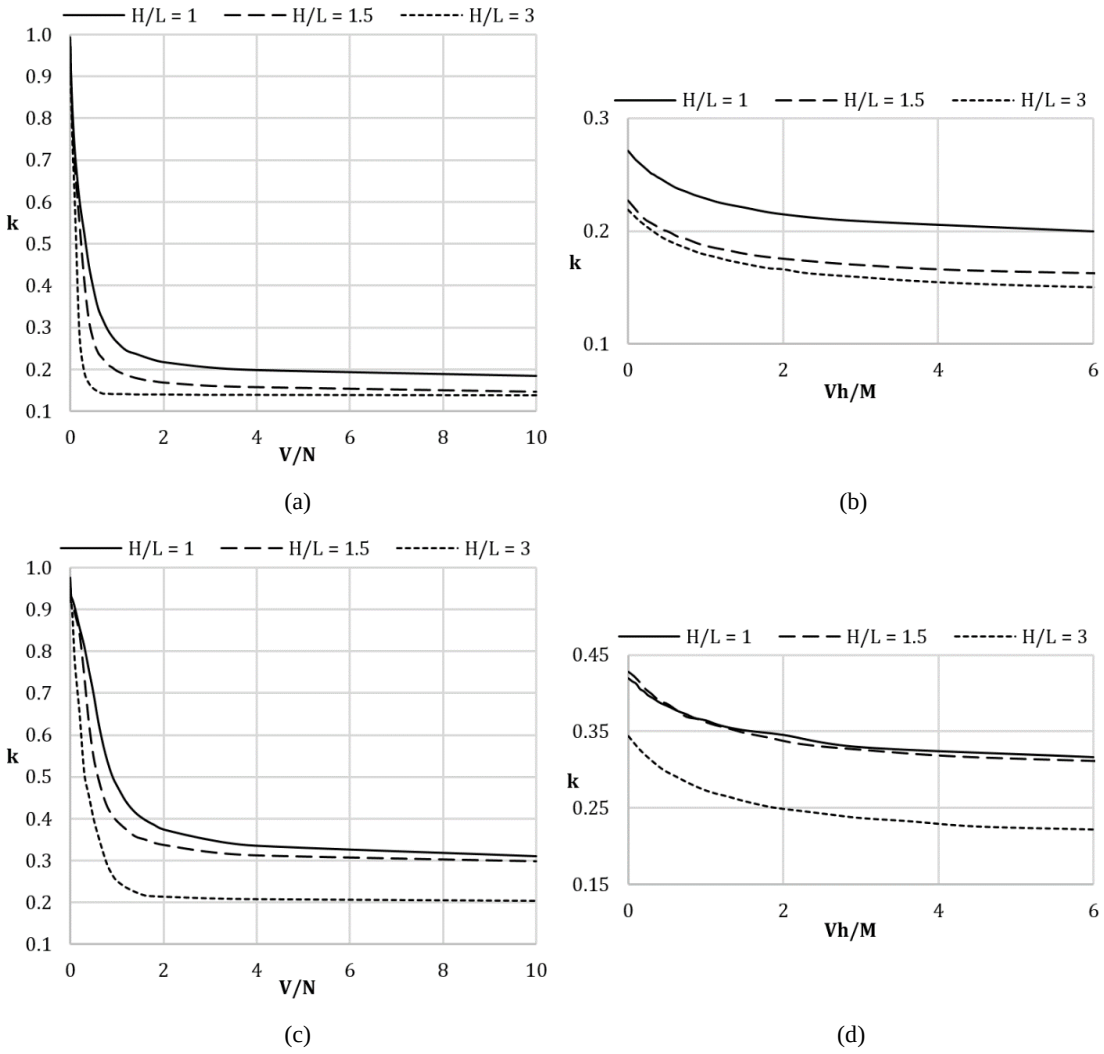

Figure 3.3.4 - Values of the distribution coefficient *k* for (a) axial-horizontal load condition (case 4) and (b) bending moment-horizontal load condition (case 5) for rigid support and for (c) axial-horizontal load condition (case 4) and (d) bending moment-horizontal load condition (case 5) for CLT support.

However, the values of *k* of technical interest are those for *V*/*N* ratios greater than 2 as shear in CLT structures is, for the conventional design approach, resisted only by walls parallel to the seismic forces whereas axial loads are resisted by all the walls, and therefore the *V*/*N* ratio usually exceeds the value of 2 in Damage and Near Collapse limit states.

For this reason, the coefficient *k* was chosen as an average value for *V*/*N* greater than 2, resulting in a value of 0,23 and 0,33 for rigid and CLT support, respectively. It is important to highlight that these values strongly depend on the compressive resistance of the wall. Lower values of f_c lead to higher values of *k* [70].

For example, for a timber stress value equal to the compressive strength perpendicular to the grain (≈ 3 MPa) and a *V*/*N* ratio of 2, a value of *k* around 0,29 is obtained for panels with an h/l ratio equal to 1 on a rigid support. In this investigation, a timber stress of 11 MPa, which can be regarded as an average value between parallel and perpendicular to the grain compressive resistance, was considered, leading, for the same kind of panel, to a *k* value of 0,22. However,

the variation of *k* within a suitable range does not significantly affect the results of the proposed method (see Figure 3.3.5).

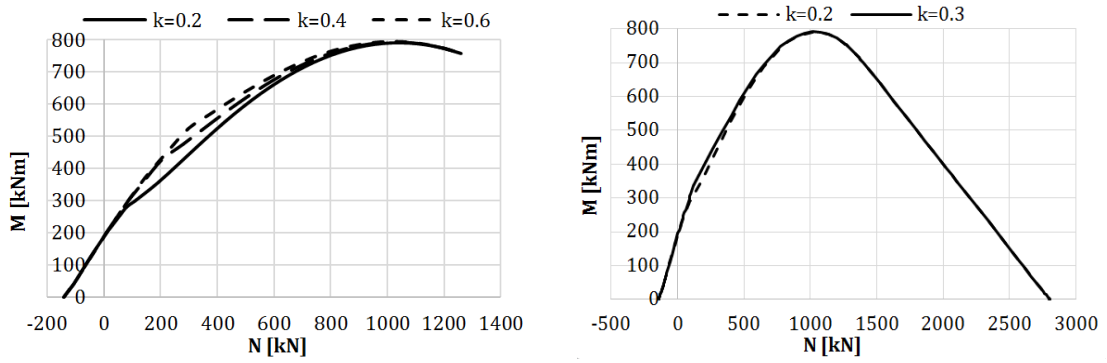

(a) (b)

Figure 3.3.5 - Dependency of (a) the first part of the M-N domain on the *k* value and (b) M-N domain for different *k* values (0,2 and 0,3).

3.3.2.3. Analyses description

To validate the proposed simplified method, sixteen analyses, differing for load and supporting conditions, were performed on the 3×3 m panel used for the *k* coefficient investigation (see chapter 3.3.2.2). The load conditions correspond to the axial load and bending moment values at the limit between the various sub-domains as calculated using the proposed algorithm. The bending moment was applied in two different ways:

- As an equivalent distribution of concentrated forces applied at the top of the wall;
- Through a corresponding value of horizontal shear load applied at the top of the wall.

In this way, four cases with bending moment and four cases with shear load were considered. In this second approach, the analyses were carried out for both rigid concrete foundation and flexible (CLT) support, using *k* values of 0,23 and 0,33, respectively.

3.3.2.4. Validation through a 2-D model

The position of the neutral axis obtained from the FE analysis was compared with the one predicted by the proposed simplified algorithm.

The first investigation was performed to check whether the given external loads lead to the attainment of the ultimate conditions, that are (i) the compression strength of the CLT panel f_c for the boundaries between sub-domains characterized by crushing of timber panel and/or (ii) the ultimate displacement in at least one connection for the boundaries between sub-domains characterized by failure of at least one connection. For all failure mechanisms between sub-domains 3 and 4 and between sub-domains 4 and 5, this verification was satisfied with a negligible error of 3% on average. However, the verification was not satisfied for the failure mechanism between sub-domains 1 and 2 and between sub-domains 2 and 3. In these cases, a

second investigation was carried-out, where the values of the imposed loads were increased and their proportions was not changed until either the ultimate displacement of a connection or the compressive strength of timber was attained.

In Table 3.3.6 and Table 3.3.7, the results of both investigations are presented for rigid and flexible support, respectively. In these tables, the "Shear" column lists the results for the configurations with axial and shear loads as external loads, while the "Bending moment" column reports the results for the load conditions with axial and flexural loads.

Table 3.3.6 - Comparison between neutral axis position prediction using the proposed algorithm and the FE model case with bottom rigid support.

N [kN]	M [kNm]	Neutral Axis Prediction [mm]			Error related to the wall length [%]	
		Proposed Algorithm	FE-Shear	FE-Bending moment	FE-Shear	FE-Bend. mom.
-108,69	38,09	0	-156	-153	5,2	5,1
-38,75	137,19	131,4	110	140	0,7	0,3
1259,19	757,35	2700	2590	2632	3,7	2,3
1399,44	701,25	3000	3200	3080	6,7	2,7

Table 3.3.7 - Comparison between neutral axis position prediction using the proposed algorithm and the FE model case with bottom CLT support.

N [kN]	M [kNm]	Neutral Axis Prediction [mm]			Error related to the wall length [%]	
		Proposed Algorithm	FE-Shear	FE-Bending moment	FE-Shear	FE-Bend. mom.
-108,69	38,09	0	-156	-153	5,2	5,1
-38,75	175,87	184,3	288	290	3,5	3,5
1259,19	757,35	2700	2100	2594	20	3,5
1399,44	701,25	3000	2226	2886	25,8	3,8

If the rigid support case is considered, load cases with shear load and bending moment give similar results in terms of neutral axis position.

Furthermore, even when the numerical values of load to achieve the ultimate condition are higher than the ones predicted using the proposed algorithm, the neutral axis position calculated with the proposed method is close to the numerically predicted one in most of the cases.

It should also be pointed out that the collected differences in loads leading to collapse between FE analyses and proposed method are mainly due to the fact that hardening and softening in connections were conservatively neglected in the proposed method.

3.4. Concluding remarks

In this chapter, a simplified non-linear procedure for seismic design of CLT wall systems has been proposed. This method assumes the wall as rigid with an elasto-brittle behavior in compression, and metal connections with an elasto-plastic force-elongation relationship. A

triangular compressive stress distribution at the wall-support interface is considered. The forces in the connections are calculated by considering the base section of a CLT wall as a reinforced concrete section. The position of the neutral axis is found with an iterative procedure. The method mainly applies to platform-type structures with hold-downs and angle brackets connections at the base of the wall and rocking mechanism as prevalent way of dissipation.

The proposed method was validated against different numerical results carried out using SAP2000 and ABAQUS software packages.

In the analyses carried out using SAP2000, acceptable accuracy was obtained in 2-dimensional numerical simulations, whereas larger errors were detected in 3-dimensional simulations due to the box effect of the CLT structure investigated. The box effect has a stiffening influence on the actual in-plane response of the wall, decreasing the actual sliding and rocking deformations and leading to larger differences if compared to the simplified method.

Further analyses were performed using ABAQUS in order to improve the evaluation of the stress distribution coefficient k for both cases of rigid and flexible support. In addition, the effect of using a more realistic trilinear force-displacement relationship for the angle bracket connections in shear was investigated. The proposed method was found to provide acceptable results, as the neutral axis position was predicted with good accuracy in most of the cases analyzed. The safety factor, calculated as ratio between the loads leading to the ultimate condition and the predicted ones, was found to be in the range from 1 to 1,85.

The proposed approach is intended to be a starting point for further studies aimed to find simplified rules for CLT seismic design. While the proposed method is now limited to single monolithic CLT walls subjected to in-plane load, it will be developed further in order to consider more cases of technical interest such as, for example, the stiffness contribution of perpendicular walls, with the final aim to have a complete design tool for CLT designers. In addition to that, the method could also be used to evaluate the axial force-bending moment resistant domain or the lateral displacement of the top corner of the wall due to rocking for inter-story drift calculations.

ROCKING OF A TWO-PANEL CLT WALL: BEHAVIOR PREDICTION AND INFLUENCE OF FLOOR DIAPHRAGM

SHORT SUMMARY

In the design of CLT buildings in earthquake-prone areas, a crucial role in energy dissipation is played by the panel-to-panel joint. Such linkage, theoretically, could be designed for three different types of behavior: coupled and uncoupled behaviors, providing a certain amount of energy dissipation, and monolithic behavior, without any dissipation. Currently, no specific design rules to attain such conditions are provided in any code.

In this chapter, a formula for the design of wall-to-floor and wall-to-wall connections is proposed. Giving the external loads (axial load and shear load on the wall), the geometry of the wall assembly and the characteristics of the connections involved, the proposed method allows the designer to evaluate the stiffness of the connections between adjacent panels in order to obtain a monolithic or a coupled behavior. This formula has been validated based on the results of experimental tests and numerical analyses.

Furthermore, no information on the dependency of the panel-to-panel behavior upon other variables such as the out-of-plane stiffness of the floor slabs and the stiffness of other metal connections, such as hold-downs and angle brackets, can be found in literature.

In an attempt to fill in this gap, this chapter presents the results of numerical analyses carried out using the Abaqus FE software package. In these analyses, the influence of the upper floor diaphragms on the rocking behavior of a two-panel wall assembly is investigated. Fully reversed displacement-controlled cyclic tests are simulated by varying the geometrical properties (aspect ratio of the wall panels), mechanical properties (types and number of connectors used for the panel-to-panel, wall-to-foundation and wall-to-upper floor connections, out-of-plane stiffness of the floor panels) and gravity load applied on top of the walls. The rocking capacity of the walls is investigated, together with displacements and global behavior of the assembly. Obtained results highlight the important role played by the stiffness of wall-to-floor diaphragm joint, whereas the out-of-plane stiffness of the slab has a negligible effect on the overall response of the assembly.

4.1. Introduction

Different research projects carried out around the world, such as the SOFIE [10][11][40], the SERIES [52] and the NHERI TallWood Research [6][8][51][76], have highlighted that CLT structures can perform satisfactorily in earthquake-prone areas.

Many tests have been performed and studies undertaken over the years to investigate the structural behavior of components and assemblies made of CLT. In particular, great effort has been devoted to experimentally assess the capacity and behavior of typical connections under monotonic and cyclic loads (Gavric et al. [35][36] and Tomasi [74]), as well as to investigate innovative connections. Zarnani et al. [79] tested a new Resilient Slip Friction Joint (RSFJ) for seismic damage avoidance design of structures, Polastri et al. [53][54] tested a new connection system for CLT structures aimed to speed up the erection without losing performance compared to traditional connection systems, D'Arenzo et al. [16] tested a new type of angle bracket with similar behavior in both tension and compression to be able to build typical CLT structures using only one type of connection for wall-to-diaphragm joints.

The capacity and the behavior of CLT wall assemblies was investigated via experimental cyclic tests carried out in order to assess the rocking behavior and performances (Gavric et al. [37], Popovski and Gavrić [55]). The most proper value of the seismic behavior factor was investigated by Amini et al. [4] for the seismic design of CLT structures, and by Follesa and Fragiacomo [28] for hybrid CLT and light-frame buildings. A proposal of revision of the current version of the timber chapter of the Eurocode 8 [24] is given by Follesa et al. [29], which includes specific provisions for capacity-based design and the behavior factor of CLT buildings. A worked example of application of such rules for the design of a six-story building is presented in the paper by Vassallo et al. [77].

Furthermore, several numerical investigations have been carried out to extend the experimental results to other cases of technical interest. As CLT panels are designed to behave elastically, careful consideration was given to an accurate modelling of connectors, which are the only component able to deform plastically and to dissipate energy. Rinaldin et al. [60] proposed a phenomenological model that, through the definition of a set of parameters, allows the user to properly reproduce the cyclic behavior of single connections, including the energy dissipation, the pinching behavior, and the strength degradation.

Numerical models have been also used to reproduce two-dimensional and three-dimensional full scale tests, like the one published by Rinaldin and Fragiacomo [62] where the 3- and 7-story buildings tested within the SOFIE Project [10][11][40] are reproduced.

Reliable designing rules, however, are still needed. Only basic rules are available for designers. Specific rules for CLT structures are still missing, including the design of panels and connections or the consideration of all the different scenarios (e.g. failure mechanisms, load

patterns) this structural system could undergo during its lifetime.

In CLT structures, like in almost all timber structures, connections play a crucial role in terms of energy dissipation if a dynamic action such as earthquake is considered. The panel-to-panel vertical joint is an important way to increase ductility and dissipated energy, and can give a very different response depending on the way they are design. In the case of a wall assembly made of two adjacent panels linked with a vertical joint, three different rocking behaviors can be observed depending on the stiffness of the panel-to-panel connection:

- Coupled: the panels rock separately, rotating around one of their base corners;
- Uncoupled: the link is stiff enough to prevent the contact along the base of one panel, but not enough to entail a monolithic behavior;
- Monolithic: the entire wall rotates monolithically around one of the two edge base corners acting like a single panel.

While the first two situations are realistic, the third one would be realistic only in the event of infinite stiffness, namely only if glue was used, which is usually not the case.

Several tests have been carried out to assess the behavior of CLT wall assemblies subjected to lateral loads, highlighting the importance of the vertical panel-to-panel joints. The different behavior (i.e. stiffness) of such connections influences the amount of sliding and rocking displacements contribution to the total lateral movement of top of the assembly. Furthermore, this joint influences the energy dissipation and structural capacity of the assembly, as it provides the wall with higher energy dissipation and ductility when a coupled behavior is obtained, compared to an uncoupled behavior or a monolithic wall [37]. Some attempts have been made to give analytical predictions of their behavior and design with respect to the other connections involved in the rocking mechanism [9].

The main issue is to move from the assembly behavior to the complete structure response. In a building, the walls at a certain level are restrained, in- and out-of-plane, by the floor slabs. In laboratory tests, wall assemblies are usually linked to the foundation via usual connectors, such as angle brackets or hold-downs, but may have different types of constraints at the top, depending on the testing equipment and on the nature of the test itself.

In this chapter, results from nonlinear displacement-controlled fully reversed cyclic analyses performed on two-panel wall assemblies are presented. Such analyses have been carried out to assess the influence of a CLT floor diaphragm on the top of the two-panel CLT wall in terms of rocking behavior. Among all the parameters analyzed, different sets of connections linking wall and slab together with different types of floor diaphragms have been considered.

4.2. Formula derivation

In order to find a formula to design the joint between wall panels and able to predict the global rocking behavior of the wall, it is crucial to investigate how the different elements composing the assembly and the external forces interact within the rocking mechanism due to a lateral force applied at the top of the assembly itself.

To this purpose, the starting point has been the analysis of the simplest case, which is a wall composed of only two panels of equal length. This case is also the one of the full-scale tests whose results have been utilized in the first step of the validation (see chapter 4.3.1).

4.2.1. Two panels of equal length

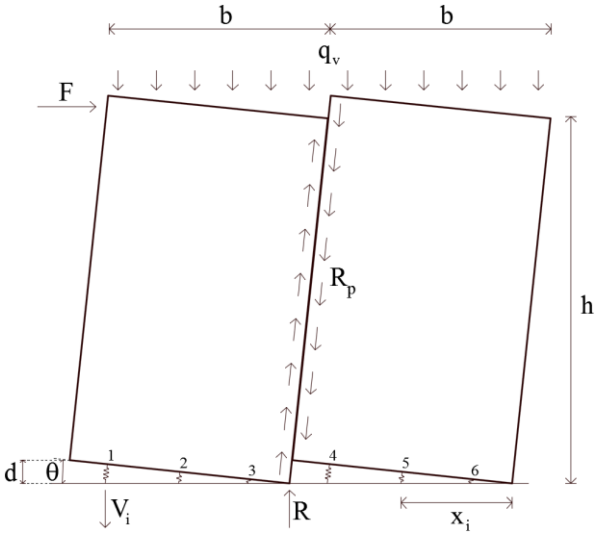

Figure 4.2.1 – Analyzed scheme.

Figure 4.2.1 depict the scheme analyzed for the case of wall with two panels of equal length. Referring to the figure

F Lateral force applied at the top of the wall

R Compressive reaction force at the interface between the first panel and the supporting surface during the rocking mechanism

R_p Reaction force at the interface between panels during the rocking mechanism

V_i Reaction force in the i^{th} connection during the rocking mechanism

b Length of the panel

d Uplift of the uncompressed edge of the panel

h Height of the wall

q_v Axial load per linear meter applied to the assembly

x_i Distance of the i^{th} connection from the compressed panel corner

θ Angle between the panel and the supporting surface during the rocking mechanism

The value of the axial load q_v should consider the self-weight of the panels per linear

meter, as it contributes to the stabilizing forces in the analyzed scheme. However, its value is generally low if compared to the axial forces considered during the design (e.g. weight of upper floors).

The aim of this method is to be able to predict the behavior of a panel-to-panel joint in order to achieve a coupled behavior, which is characterized by a higher energy dissipation and provides the system with higher ductility, if compared to the other possible behaviors [37].

The first step is the imposition of the equilibrium for the vertical forces in the first panel.

$$R + R_p - q_v b - \sum_1^3 V_i = 0 \qquad [3.2.1]$$

The necessary condition to obtain a coupled behavior is that the compressive reaction force at the interface between the first panel and the supporting surface R is equal to or greater than zero. Imposing this condition corresponds to:

$$R \geq 0 \quad \Rightarrow \quad q_v b + \sum_1^3 V_i - R_p \geq 0 \qquad [3.2.2]$$

From Equation [3.2.2], the condition on the joint between panels is obtained.

$$q_v b + \sum_1^3 V_i \geq R_p \qquad [3.2.3]$$

The unknowns V_i and R_p needs to be evaluated. The reaction force at the interface between panels R_p depends upon the shear stiffness of the single connection k_p, the number of connections between wall panels n_p and the mutual shear displacement of the two panels, which could be, for little values of the angle θ, be set equal to uplift d.

$$R_p = n_p k_p d \qquad [3.2.4]$$

The uplift of the uncompressed edge of the panel d con be expressed as a function of the length of the panel b and the angle between the panel and the supporting surface θ.

$$d = b\theta \qquad [3.2.5]$$

By substituting Equation [3.2.5] in Equation [3.2.4], an equation depending on θ is obtained.

$$R_p = n_p k_p b\theta \qquad [3.2.6]$$

The reaction force in the i^{th} connection V_i is function of the vertical stiffness k_i and the vertical displacement u_i of the connection itself.

$$V_i = k_i u_i \qquad [3.2.7]$$

The vertical elongation u_i can be expressed as a function of distance of the connection from the compressed panel corner x_i and the angle between the panel and the supporting surface θ.

$$u_i = \theta x_i \qquad [3.2.8]$$

By substituting Equation [3.2.8] in Equation [3.2.7], an expression with the only unknown θ is obtained.

$$V_i = k_i \theta x_i \quad [3.2.9]$$

By substituting Equation [3.2.6] and Equation [3.2.9] in Equation [3.2.3], a new equation with the only unknown θ can be written.

$$q_v b + \sum_1^3 k_i \theta x_i \geq n_p k_p b \theta \quad [3.2.10]$$

The value of the angle θ is obtained by imposing the equilibrium to the rotation of the entire assembly around the compressed corner of the second panel.

$$Fh - q_v 2b^2 + Rb - \sum_1^3 V_i (x_i + b) + \sum_4^6 V_i x_i = 0 \quad [3.2.11]$$

By substituting the values of R (Equation [3.2.1]), V_i (Equaiton [3.2.9]) and R_p (Equation [3.2.6]) in Equation [3.2.11], a new equation with the angle θ as only unknown is obtained.

$$Fh - q_v 2b^2 + \left(q_v b + \sum_1^3 k_i \theta x_i - n_p k_p b \theta \right) b - \sum_1^3 k_i \theta x_i (x_i + b) + \sum_4^6 k_i \theta x_i x_i = 0 \quad [3.2.12]$$

From Equation [3.2.12], the value of θ is derived.

$$\theta = \frac{Fh - q_v b^2}{\sum_1^6 k_i x_i^{\,2} + n_p k_p b^2} \quad [3.2.13]$$

By substituting [3.2.13] in Equation [3.2.10]:

$$q_v b \geq \frac{\left(n_p k_p b - \sum_1^3 k_i x_i \right) \left(Fh - q_v b^2 \right)}{\sum_1^6 k_i x_i^{\,2} + n_p k_p b^2} \quad [3.2.14]$$

By isolating the $n_p k_p$ term, the condition sought is obtained:

$$n_p k_p \leq \frac{\left(\frac{Fh}{b} - q_v b \right) \sum_1^3 k_i x_i + q_v \sum_1^6 k_i x_i^{\,2}}{Fh - 2 q_v b^2} \quad [3.2.15]$$

4.2.2. Two panels of different length

The length of the first and second panel are named b_1 and b_2, respectively. In this case, the vertical slip between the two panels is equal to the uplift of the second panel, namely d_2. Equation [3.2.5] is consequently modified as follows.

$$d_2 = b_2 \theta \quad [3.2.16]$$

The new equilibrium equation of the vertical forces in the first panel, and consequently the value of the compressive reaction force R, is given by Equation [3.2.17].

$$R = q_v b_1 + \sum_1^3 k_i \theta x_i - n_p k_p b_2 \theta \qquad [3.2.17]$$

Accordingly, a new rotational equilibrium, defined by Equation [3.2.18], and a consequent new value of the angle θ, defined by Equation [3.2.19], are obtained.

$$Fh - q_v (b_1 + b_2) \frac{(b_1 + b_2)}{2} + \left(q_v b_1 + \sum_1^3 k_i \theta x_i - n_p k_p b_2 \theta \right) b_2 - \\ - \sum_1^3 k_i \theta x_i (x_i + b_2) + \sum_4^6 k_i \theta x_i x_i = 0 \qquad [3.2.18]$$

$$\theta = \frac{Fh - \frac{q_v}{2}\left(b_1^2 + b_2^2\right)}{\sum_1^6 k_i {x_i}^2 + n_p k_p b_2^2} \qquad [3.2.19]$$

By imposing the second member of Equation [3.2.17] to be greater than zero and by substituting the value of θ obtained through Equation [3.2.19], the condition for the coupled behavior of a wall composed of two panels of different length is obtained.

$$n_p k_p \le \frac{\left(Fh - \frac{q_v}{2} \sum_1^2 b_i^2 \right) \sum_1^3 k_i x_i + q_v b_1 \sum_1^6 k_i {x_i}^2}{\left[Fh - \frac{q_v}{2} \left(\sum_1^2 b_i \right)^2 \right] b_2} \qquad [3.2.20]$$

It is worth nothing to say that if b_1 and b_2 were equal, Equation [3.2.20] and Equation [3.2.15] would be the same.

4.3. Validation of the proposed formulation

4.3.1. Validation through full-scale experimental tests results

In order to validate the proposed formulation, the method has been applied to predict the behavior of several wall assemblies tested at IVALSA Trees and Timber Institute, whose connection characteristics, geometry and rocking behavior observed, namely coupled, uncoupled or monolithic, are reported in literature.

4.3.1.1. Experimental program

The data used are the results of tests on screwed connections [36], nailed metal plate connections, namely hold-downs and angle brackets [35], and CLT wall assemblies [37].

4.3.1.1.1 Tests on screwed connections

In this test campaign, several screwed joints between CLT panels were tested, mainly under cyclic shear loads.

The tests of interest for this validation are the tests assessing the vertical shear performance of spline joints and half-lapped joints, named test #1 and test #2 [36]. Both type of connections were used in the test on wall assemblies [37] described in chapter 4.3.1.1.3.

For the panel-to-panel connection, the elastic stiffness against a shear load along the joint line of a single screw, for the half-lapped joint, and of two screws, for the spline joint, is considered. The values obtained 1,24 and 0,84 kN/mm, respectively.

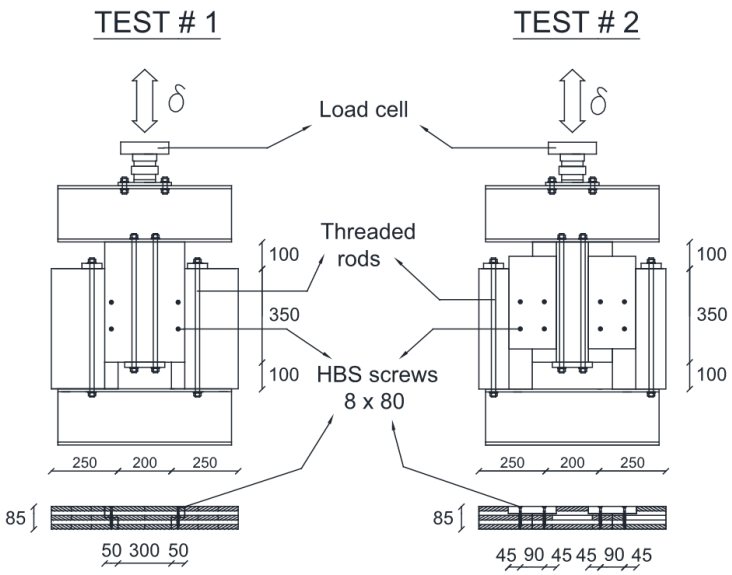

Figure 4.3.1 - Test setups #1 and #2 (measures in mm) [36].

4.3.1.1.2 Tests on metal plates connections

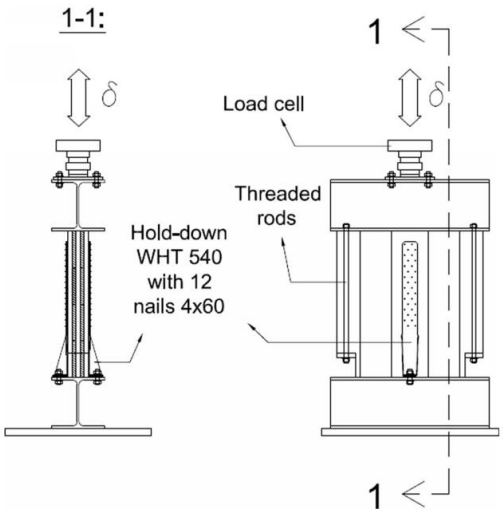

Figure 4.3.2 - Elevation (right) and cross-section (left) of test setup used for wall-foundation hold-down connection loaded in tension (Test configuration #1) [35].

As for the screwed connections described previously, these connections were used within the tests described in chapter 4.3.1.1.3. In this test campaign, angle bracket and hold-down connections were tested against cyclic loads of both tension and shear. For the purpose of the validation, the tests of interest are the ones evaluating the tension performance of hold-down

and angle bracket connections on rigid support against tension loads. These tests have been named #1 and #5 in the reference paper, respectively [35].

As for the previous case, the characteristic of interest is the elastic stiffness, that was evaluated equal to 4,51 kN/mm for hold-down and equal to 2,65 kN/mm for the angle bracket.

4.3.1.1.3 Tests on CLT walls

In this test program, the rocking capacity of several CLT wall assemblies was evaluated with fully reversed displacement-controlled cyclic tests. The different assemblies were divided in three groups:

- Monolithic walls (test I);
- Walls composed of two panels vertically jointed through a half-lapped joint (test II);
- Walls composed of two panels vertically jointed through a spline joint (test III).

Tests of groups II and III have been considered for the validation. In the reference paper [37], the type of deformation observed is reported for all the tests conducted. With this information, using the geometrical parameters (see Figure 4.3.3) and the mechanical properties presented in the previous sections, the inequality [3.2.15] has been used to compare the analytical previsions with the behaviors experimentally observed

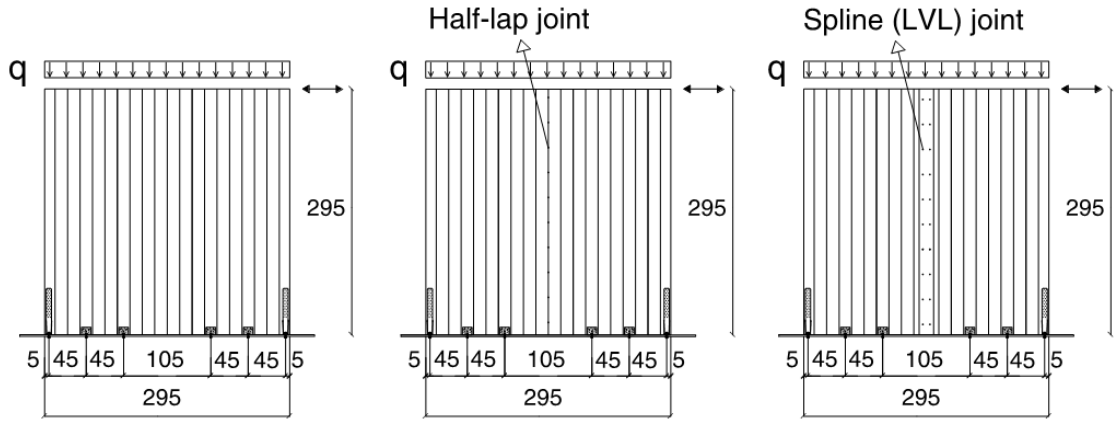

Figure 4.3.3 - Wall panel test configurations: (a) configuration I - single walls; (b) configuration II - coupled walls with half-lap joint; (c) configuration III - coupled walls with spline (LVL) joint (measures in cm) [37].

4.3.1.2. Comparison between experimental and analytical results

As mentioned in chapter 4.3.1.1.3, the data necessary for the comparison are:

- Geometrical properties of the system;
- Stiffness of the connections in the analyzed direction;
- External forces, namely the lateral force at the top of the system and the axial load.

The information on the geometry is given in the reference paper [37] (see Figure 4.3.3).

Panels have the same length of 1475 mm. Table 4.3.1 show the number of connections used in each test. The properties of interest, which have already been discussed in chapters 4.3.1.1.1 and 4.3.1.1.2, are summarized in Table 4.3.2.

Table 4.3.1 - Test configuration.

Test ID	num. HD	num. AB	num. Screws
II.1	2	4	20
II.2	2	4	20
II.3	2	4	10
II.4	4	4	5
III.1	2	4	2x20
III.2	2	4	2x10
III.3	4	4	2x5
III.4	2	4	2x10
III.5	2	4	2x10
III.6	2	4	2x10
III.7	2	4	2x10
III.8	2	4	2x10

Table 4.3.2 - Stiffnesses considered.

Connection	Stiffness [kN/mm]
Half-lap joint	1,24
Spline joint	0,84
Hold-down	4,51
Angle bracket	2,65

The forces considered in the proposed method are the lateral force applied at the top of the wall F and the axial load per linear meter applied to the assembly q_v. The axial load is an input data of the test, whereas the lateral force, being an unknown, has been set equal to the yielding force (F_y) and maximum force (F_{max}), both at the first cycle, obtained during the same test. The values of these forces are given in Table 4.3.3.

Table 4.3.3 - Forces considered for each test.

Test ID	q_v [kN/m]	F_y [kN]	F_{max} [kN]
II.1	18,5	69,2	97,2
II.2	18,5	65,5	92,3
II.3	18,5	65,4	84,4
II.4	18,5	69,2	93,1
III.1	18,5	72,1	102,5
III.2	18,5	67,6	91,8
III.3	18,5	80,4	102,9
III.4	18,5	61,7	82,4
III.5	18,5	68,1	86,4
III.6	0	46,5	63,4
III.7	18,5	60,0	84,6
III.8	18,5	64,9	79,3

Through a purposely-developed spreadsheet, the goodness of the proposed method has

been assessed. The results obtained for the comparison between analytically predicted, through Equation [3.2.15], and experimentally observed rocking behavior are summarized in Table 4.3.4.

As it can be observed, the analytical method correctly predicted the behavior for almost all the cases (83,3%).

Table 4.3.4 - Comparison between analytically predicted and experimentally observed rocking behavior.

Test ID	Right member of the inequality [kN/mm]		$n_s k_s$	Behavior	Verification	
	with F_y	with F_{max}			with F_y	with F_{max}
II.1	11,46	9,64	24,8	Single-Coupled	YES	YES
II.2	11,90	9,85	24,8	Single-Coupled	YES	YES
II.3	11,91	10,25	12,4	Coupled	NO	NO
II.4	13,09	10,94	6,2	Coupled	YES	YES
III.1	11,17	9,45	16,8	Single-Coupled	YES	YES
III.2	11,64	9,87	8,4	Coupled	YES	YES
III.3	11,84	10,45	4,2	Coupled	YES	YES
III.4	12,45	10,37	8,4	Coupled	YES	YES
III.5	11,58	10,14	8,4	Coupled	YES	YES
III.6	6,93	6,93	8,4	Coupled	NO	NO
III.7	12,73	10,24	8,4	Coupled	YES	YES
III.8	11,98	10,58	8,4	Coupled	YES	YES

4.3.1.3. Parametric studies

The proposed inequality could be rewritten highlighting ratios between forces and dimensions involved. In particular, the inequality could be rewritten as function of the ratio between lateral force and axial load ($F/q_v 2b$) and the ratio between the height and the length of the panel (h/b). In this way, Equation [3.2.15] turns into Equation [3.3.1].

$$n_p k_p \leq \frac{\left(\frac{F}{V}\frac{h}{b}-\frac{1}{2}\right)\sum_1^3 k_i x_i + \frac{1}{2b}\sum_1^6 k_i x_i^2}{\frac{F}{V}h - b} \qquad [3.3.1]$$

It is possible to evaluate the incidence of these ratios on the formula itself. Figure 4.3.4.a and b depict the variation of the term $n_p k_p$ to fulfil Equation [3.3.1] varying the value of the ratio $F/q_v 2b$ and the ratio h/b, respectively. It is important to highlight that, in both cases, the left limit of the curve is given by the condition of denominator different from zero. For the first curve, the limit is set by the b/h ratio. For lower values of this ratio, Equation [3.3.1] gives negatives values of the panel-to-panel joint stiffness. For the second curve, the limit is set by the ratio $q_v 2b/F$.

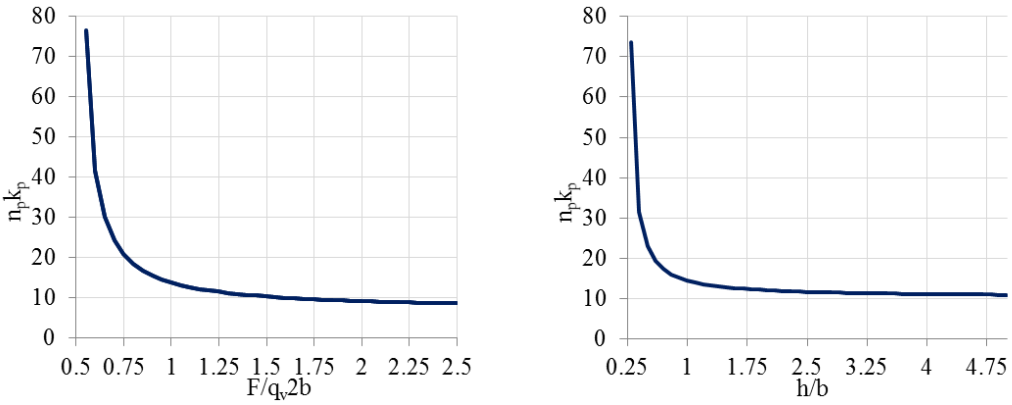

(a) (b)

Figure 4.3.4 – Variation of the panel-to-panel stiffness varying the $F/q_v 2b$ ratio (a) and the h/b ratio (b).

Within a parametric study, the variation range of the ratio $F/q_v 2b$ must be considered. For the validation of the proposed method, the yielding force and the maximum force as obtained through the test have been taken into account. Designing a wall, unless of a too much over resisting design, these are the forces considered. It is then reasonable to assume the range of validity of the aforementioned forces has to be determined based on the design condition. In fact, when the axial force varies, so does the capacity of the system. In the examples analyzed, disregarding the case of no axial force applied, the ratio is always included between 1,08 and 1,86. These values belong to the part of the curve (Figure 4.3.4.a) where, even with great variation of the ratio, there is not a high difference in the resulting panel-to-panel stiffness.

Same considerations must be made on the aspect ratio h/b. The aspect ratio of the panel plays a crucial role in the determination of the rocking capacity of the assembly.

It is necessary to carry out tests investigating different schemes in order to obtain reliable results describing the relationships among the different terms of the proposed formula and giving more information on the goodness of the output.

4.3.2. Validation through FE analyses results

In order to extend the validation to further cases, several FE analyses using the Abaqus software have been performed [17].

In these analyses, a cyclic displacement time-history was applied in the model at the top points of the assembly.

The non-linear springs used in the model to describe the connections behavior are those discussed in [60], which have been successfully used in [62] and other publications.

4.3.2.1. Model description

The FE models have been created through the purposely-developed software X-lam Wall Mesher [62], which allows the user to build the geometry of 4-node shell models for different

FE solver, including Abaqus [17], which has been used for these analyses.

The characteristics of the connections have been taken from the tests analyzed in [35], [36] and [37]. The values of the mechanical properties of the connections in shear and tension are listed in Table 4.3.5 and Table 4.3.6, respectively.

Table 4.3.5 - Mechanical properties of the connections used in the model – shear.

Mechanical property	Connection		
	Spline joint	Angle Bracket	Hold-down
k_{el} [kN/mm]	0,84	1,96	3,2
k_{pl} [kN/mm]	0,1	0,23	0,28
F_y [kN]	4,85	22,98	3,61
v_y [mm]	5,7	11,74	1,13
F_{max} [kN]	7,33	26,85	10,0
v_{max} [mm]	34,37	28,51	23,95
F_u [kN]	5,86	21,48	12,2
v_u [mm]	37,66	31,86	48,42

Table 4.3.6 - Mechanical properties of the connections used in the model – tension.

Mechanical property	Connection		
	Spline joint	Angle Bracket	Hold-down
k_{el} [kN/mm]	0,94	2,65	4,51
k_{pl} [kN/mm]	0,16	0,41	0,75
F_y [kN]	3,23	19,22	40,46
v_y [mm]	3,13	7,26	8,81
F_{max} [kN]	6,4	23,47	48,33
v_{max} [mm]	39,4	17,69	20,3
F_u [kN]	5,12	18,74	38,79
v_u [mm]	50,52	23,19	23,75

Referring to Table 4.3.5 and Table 4.3.6: k_{el} and k_{pl} signify the elastic and hardening stiffness of the backbone, respectively, F_y and v_y signify the yielding force and yielding displacement, respectively, F_{max} and v_{max} signify the maximum force and the corresponding displacement, respectively, and v_u and F_u signify the ultimate displacement and the corresponding force, respectively.

The tension properties for the spline joint refer to the shear strength of the screws for in-plane panel separation.

Compression has been set as rigid for every connection. Connections Additional connections simulating wall-to-supporting foundation and wall-to-diaphragm contact have been considered in the nodes of the base and top of the assembly where no metal connection was placed. Out-of-plane stiffness of the connections has been disregarded since the wall panels were loaded in-plane.

The connections have been modeled through an Abaqus sub-routine created by Rinaldin et al. [60]. The model, which was already used in [62], has been validated against results of full-scale cyclic load tests on CLT wall assemblies, whose description is found in [37].

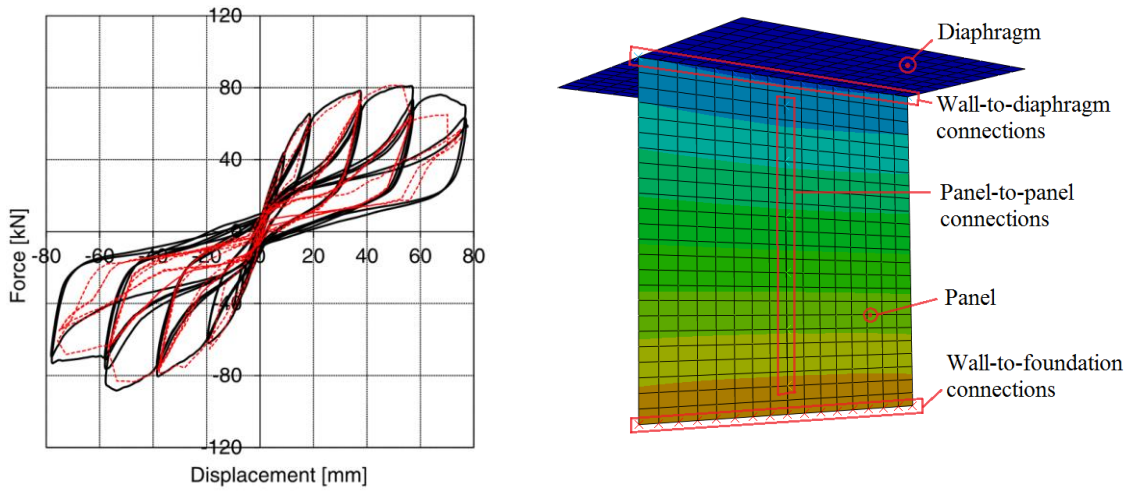

(a) (b)

Figure 4.3.5 - Validation of the model (dashed red line) against test results (solid black line) (force-displacement graph taken from [37]) (a) and an example of undeformed shape of a FE model described in this chapter (b).

A comparison between test results and FE model results for the same displacement pattern and an example of the numerical model tested within these analyses are shown in Figure 4.3.5.

To be consistent in every analysis, the same cyclic displacement pattern has been used for all the analyses (Figure 4.3.6). This history of displacements has been imposed to the top nodes of the assembly for the basic configurations, namely the assemblies without diaphragm, whereas it has been imposed to the nodes of the diaphragm for the other configurations. In these last cases, the nodes of the diaphragm have been constrained to not rotate around the longitudinal axis (X-axis) due to the symmetry of the model.

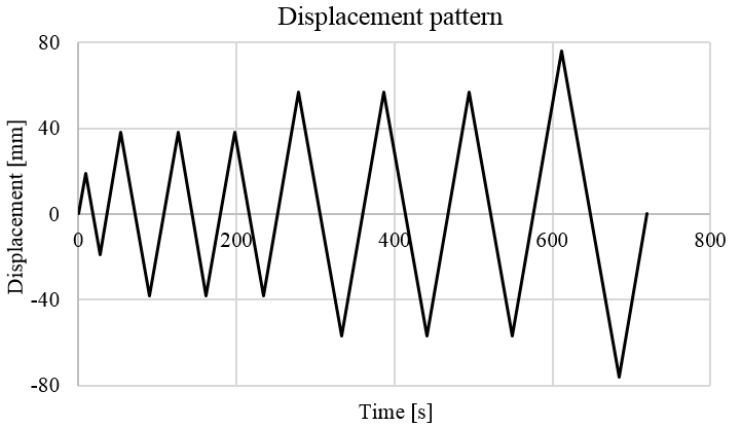

Figure 4.3.6 - Imposed cyclic displacement for the FE analyses.

4.3.2.2. Analyzed cases

Four different parameters have been varied in the analyses:

- Height-to-length ratio of panels;
- Axial load applied at the top of the specimen;

- Number and position of connections at the base of the assemblies;
- Number of screws at the interface between panels.

Three different h/b aspect ratio has been used: 2, 3 and 4. The height of the panels have been set always equal to 3 m.

Seven different axial loads have been considered, starting from 0 kN/m to 24 kN/m with a 4 kN/m step.

Five different configurations of base connections have been used. The different setups are shown in Figure 3. Referring to the figure, the spacing represents the mesh in the model, so the position of the connections in each scenario is scaled when moving from an aspect ratio to another.

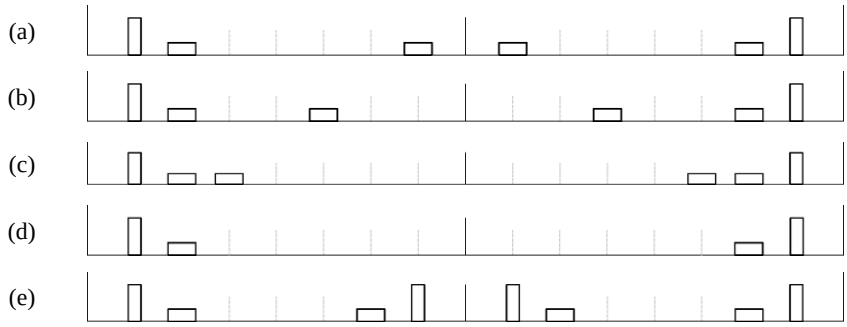

Figure 4.3.7 - Different configurations of base connection used in the FE analyses.

For what concerns the connections between panels, three different numbers of screws have been chosen: (i) 6 screws, calculated with the proposed analytical method so as to ensure a coupled behavior for every other set of parameters; (ii) 23 screws, calculated with the proposed analytical method so as to ensure a single-coupled behavior for every other set of parameters; and (iii) 12 screws, in order to achieve a different type of behavior depending on the set of parameter chosen.

To summarize, 315 different analyses have been run (3 aspect ratios × 7 axial loads × 5 configurations of connections at the base × 3 numbers of screws between panels = 315 analyses).

4.3.2.3. Comparison between numerical and analytical results

As expected, the two control analyses (case (i) and (ii)) have given all coupled and single-couple behaviors, respectively, so the proposed analytical method have provided good previsions for these extreme situations. For what concerns the target analyses, the observed behaviors are summarized in Table 4.3.7.

In Table 4.3.8, the previsions made with the proposed analytical method are summarized. The cases where the analytical prevision was right/wrong are indicated in green/red, respectively.

Table 4.3.7 - Rocking behavior of the walls in the analyses (S-C: single-coupled: C: coupled).

q_v [kN/m]	h/b	A	B	C	D	E
0	2	S-C	S-C	S-C	S-C	S-C
	3	S-C	S-C	S-C	S-C	S-C
	4	S-C	S-C	S-C	S-C	C
4	2	S-C	S-C	S-C	S-C	S-C
	3	S-C	S-C	S-C	S-C	S-C
	4	S-C	S-C	S-C	S-C	C
8	2	S-C	S-C	S-C	S-C	S-C
	3	S-C	S-C	C	S-C	C
	4	S-C	S-C	C	S-C	C
12	2	S-C	C	C	S-C	C
	3	S-C	C	C	S-C	C
	4	S-C	C	C	S-C	C
16	2	C	C	C	S-C	C
	3	C	C	C	C	C
	4	C	C	C	S-C	C
20	2	C	C	C	C	C
	3	C	C	C	C	C
	4	C	C	C	C	C
24	2	C	C	C	C	C
	3	C	C	C	C	C
	4	C	C	C	C	C

Table 4.3.8 - Rocking behavior prediction of the walls using the proposed analytical method and comparison with the results of the FE analyses.

q_v [kN/m]	h/b	A	B	C	D	E
0	2	S-C	S-C	S-C	S-C	S-C
	3	S-C	S-C	S-C	S-C	S-C
	4	S-C	S-C	S-C	S-C	S-C
4	2	S-C	S-C	S-C	S-C	S-C
	3	S-C	S-C	S-C	S-C	S-C
	4	S-C	S-C	S-C	S-C	S-C
8	2	S-C	S-C	S-C	S-C	S-C
	3	S-C	S-C	S-C	S-C	S-C
	4	S-C	S-C	S-C	S-C	S-C
12	2	S-C	S-C	S-C	S-C	S-C
	3	S-C	S-C	S-C	S-C	S-C
	4	S-C	S-C	S-C	S-C	S-C
16	2	S-C	S-C	C	S-C	S-C
	3	S-C	S-C	S-C	S-C	S-C
	4	S-C	S-C	S-C	S-C	S-C
20	2	S-C	C	C	S-C	C
	3	S-C	S-C	C	S-C	S-C
	4	S-C	S-C	S-C	S-C	S-C
24	2	C	C	C	C	C
	3	S-C	S-C	C	S-C	S-C
	4	S-C	S-C	S-C	S-C	S-C

As can be seen, the analytical method leads to right predictions for the majority of the cases (55%).

Looking at the results, it can be noticed that configurations with a lower aspect ratio of panels are more prone to rock with a coupled behavior than the ones with a higher aspect ratio. Nevertheless, the analytical method foresee a coupled behavior for higher aspect ratios. For this reason, a corrective coefficient equal to $(h/b)^{\alpha}$ multiplying the right member of Equation [3.2.15] has been introduced.

If the term $\Sigma k_i x_i$ is calculated alone, it can be noticed that configuration C presents higher values of this quantity than configuration E, which is the one resulting in the highest number of coupled behaviors. For this reason, this member have been adjusted as shown in Equation [3.3.2]:

$$\sum_{1}^{3} k_i x_i \quad \Rightarrow \quad \sum_{1}^{3} k_i x_i + \beta \sum_{4}^{6} k_i x_i \qquad [3.3.2]$$

The coefficients α and β have been calibrated in order to find the best match with the FE analyses.

The values found are 0.1 and 0.35 for α and β respectively. The adjusted analytical relationship correctly predicts 91.4% of the cases. The new results and comparison are summarized in Table 4.3.9.

Table 4.3.9 - Rocking behavior prediction of the walls using with the adjusted analytical method and comparison with the results of the FE analyses.

q_v [kN/m]	h/b	A	B	C	D	E
0	2	S-C	S-C	S-C	S-C	S-C
	3	S-C	S-C	S-C	S-C	S-C
	4	S-C	S-C	S-C	S-C	C
4	2	S-C	S-C	S-C	S-C	C
	3	S-C	S-C	S-C	S-C	C
	4	S-C	S-C	S-C	S-C	C
8	2	S-C	S-C	C	S-C	C
	3	S-C	S-C	C	S-C	C
	4	S-C	S-C	C	S-C	C
12	2	C	C	C	S-C	C
	3	S-C	C	C	S-C	C
	4	S-C	C	C	S-C	C
16	2	C	C	C	S-C	C
	3	C	C	C	S-C	C
	4	C	C	C	S-C	C
20	2	C	C	C	C	C
	3	C	C	C	S-C	C
	4	C	C	C	S-C	C
24	2	C	C	C	C	C
	3	C	C	C	C	C
	4	C	C	C	S-C	C

For the two control configurations, the predictions remain unchanged.

The new analytical formulation has the following expression:

$$R_p \leq \left[\frac{\left(\frac{Fh}{b} - q_v b\right)\left(\sum_1^3 k_i x_i + 0.35\sum_4^6 k_i x_i\right) + q_v \sum_1^6 k_i x_i^2}{Fh - 2q_v b^2} \right] \left(\frac{h}{b}\right)^{0.1} \quad [3.3.3]$$

Comparing the different behavior basing on the base connection arrangements, it can be noted the stronger the base connection is, the higher the number of coupled behavior cases is (conf. D vs conf. E).

4.4. Lateral force estimation

In the presented methodology, the top lateral force to be applied to the wall, present in Equation [3.3.3], is unknown. This force can be assumed as the lateral load capacity of the assembly. In this section, the method proposed in chapter 3 is used to find this force. As the method applies to single-panel walls, it has been used accordingly to hypotheses discussed in each sub-section, depending on the predicted rocking behavior.

4.4.1. 6-screw assemblies

The control configuration characterized by the presence of 6 screws connecting the two panels exhibits a coupled behavior. For this reason, the method to calculate the rocking capacity of the assembly has been used by calculating separately the capacity of the two panels and summing them up. Then, a comparison with the maximum forces obtained through the FE analyses has been made.

Table 4.4.1 - Analytical-numerical comparison – 6-screws case.

F_{met}/F_{FE}	
Mean value	0,666
Maximum value	0,802
Minimum value	0,528
Standard deviation	0,061

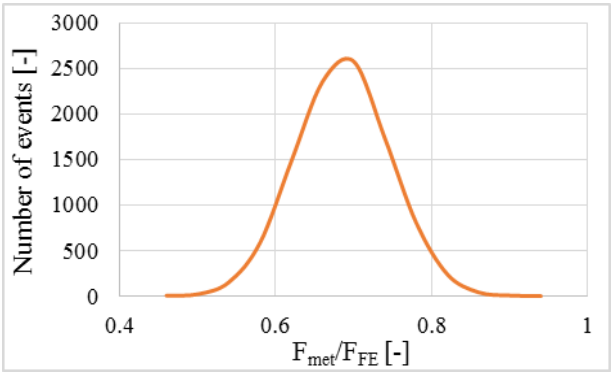

Figure 4.4.1 - Normal distribution for the 6-screw case.

Table 4.4.1 summarizes this comparison. F_{met} and F_{FE} signifies the force obtained from the application of the proposed method and the FE analysis, respectively. Using the mean value and the standard deviation, a normal distribution of 10000 random numbers has been created. In Figure 4.4.1 the aforementioned distribution is shown.

This distribution has been used to assess the proper coefficient used to divide the F_{met} value and find an estimated capacity of the assembly. According to the rules governing the European codes, the coefficient was chosen so that the 5% of the resulting values are greater than 1, that is only 5% of the capacities are overestimated. The resulting number is 0,76.

$$F_{FE} = \frac{F_{met}}{0,76} \qquad \left(F_{FE} = 1,32F_{met}\right) \qquad [3.4.1]$$

4.4.2. 23-screw assemblies

The control configuration characterized by the presence of 23 screws connecting the two panels has always shown a single-coupled behavior. For this reason, the method to calculate the rocking capacity of the assembly has been used as the assembly was a single-panel wall. Table 4.4.2 provides the results of this comparison.

Table 4.4.2 - Analytical-numerical comparison – 23-screw case.

F_{met}/F_{FE}	
Mean value	1,023
Maximum value	1,268
Minimum value	0,789
Standard deviation	0,100

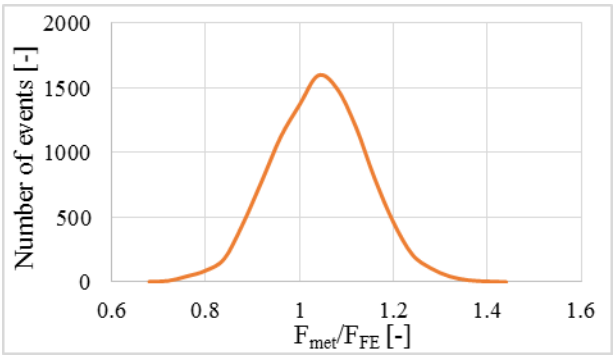

Figure 4.4.2 - Normal distribution for the 23-screw case.

Using the mean value and the standard deviation, a normal distribution of 10000 random numbers has been created. In Figure 4.4.2, the aforementioned distribution is shown.

Using the same considerations made for the 6-screw case, a coefficient equal to 1,19 has been found.

$$F_{FE} = \frac{F_{met}}{1,19} \qquad \left(F_{FE} = 0,84F_{met}\right) \qquad [3.4.2]$$

4.4.3. 12-screw assemblies

The target configuration characterized by the presence of 12 screws connecting the two panels is the one showing both a single-coupled and a coupled behavior.

To compare the capacities calculated using the proposed method and the ones resulting from the FE analyses, the following steps have been followed:

- Equation [3.3.3] has been used to evaluate if the given assembly would show a coupled or a single-coupled behavior;
- When predicting a coupled behavior, the capacity is calculated using the approach described in chapter 4.4.1 and divided by the coefficient given in the same chapter (0,76). When predicting a single-coupled behavior, the capacity is calculated using the approach described in chapter 4.4.2 and divided by the coefficient given in the same chapter (1,19);
- The calculated capacity is then divided by the capacity estimated via FE analysis in order to calculate a safety factor.

In Table 4.4.3 the characteristic values of this comparison are listed.

Table 4.4.3 - Analytical-numerical comparison – 12-screw case.

F_{met}/F_{FE}	
Mean value	0,799
Maximum value	1,114
Minimum value	0,557
Standard deviation	0,130

Only 4 ratios exceed 1, that is more than 95% of the cases are in the safe zone. Furthermore, all these 4 cases are single-coupled behaviors, meaning that the coefficient dividing the capacity for the coupled cases could be lowered (in the analyzed cases till 0,71) without increasing the unsafe cases.

4.5. Influence of the floor diaphragm

In this section, the analyses and results assessing the dependency of the rocking behavior of a two-panel wall assembly upon the presence of a diaphragm above are described and discussed. The FE model utilized is the same depicted at chapter 4.3.2.1.

4.5.1. Analyzed cases

In order to assess the dependency of the rocking behavior of a two-panel wall with an upper floor diaphragm on various parameters, many non-linear displacement-controlled cyclic analyses have been carried out using the FE software Abaqus [17]. The variables investigated are the following:

- Different aspect ratio of panels (3 ratios);
- Different arrangements of wall-to-foundation connections (2 sets);
- Different position and type of connectors linking the wall to the slab (3 sets);
- Different number of screws linking the two panels vertically (2 sets);
- Different thickness of the floor diaphragm (4 values, as specified in the following);
- Different value of the gravity load applied on the wall per linear meter (3 values).

The total amount of analyses, adding the basic analyses without the diaphragm, is 468.

For what concerns the aspect ratio *h/b*, to be consistent with the previous analyses, the chosen values are 2, 3 and 4.

The two sets of connections linking the wall to the foundation are shown in Figure 4.5.1. It has been decided to choose sets representing something similar to a typical distribution of connectors rather than less realistic cases.

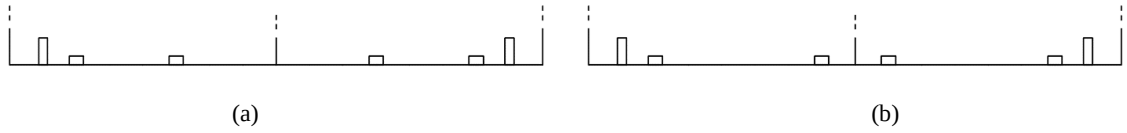

Figure 4.5.1 - Arrangements of bottom connections implemented in the FE model.

The patterns of connections linking the panels to the overlapping diaphragm are the same as the ones on the bottom side, plus a set of stiffer links simulating 45° inclined screws (Figure 4.5.2).

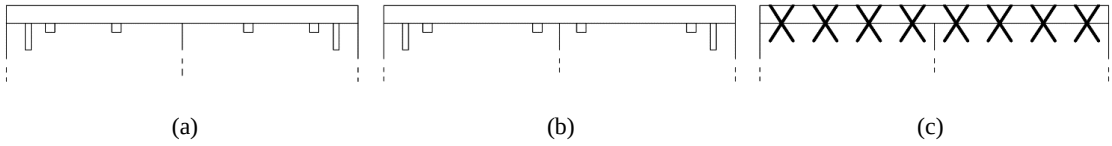

Figure 4.5.2 - Configurations of wall-to-diaphragm connections implemented in the FE model.

For the vertical joint, 6 and 12 screws have been considered.

In order to account for different scenarios, four floor diaphragms have been investigated. Their cross-sections are depicted in Figure 4.5.3. Floor slabs have been modelled through an isotropic material and their stiffness has been calculated considering a C24 wood through the Blaβ-Fellmoser composition factors [7] for the out-of-plane load/bending stiffness. Floor slabs are only loaded in one direction (one-way systems), so their Young modulus has been calculated using the Blaβ-Fellmoser's constant k_1. The values obtained for the elastic modulus are 10,61 GPa, 9,05 GPa, 10,51 GPa, 10,25 GPa for diaphragm (1), (2), (3) and (4) (Figure 4.5.3), respectively. All the configurations present a diaphragm 3 m long in the out-of-plane direction and as long as the wall in the in-plane direction.

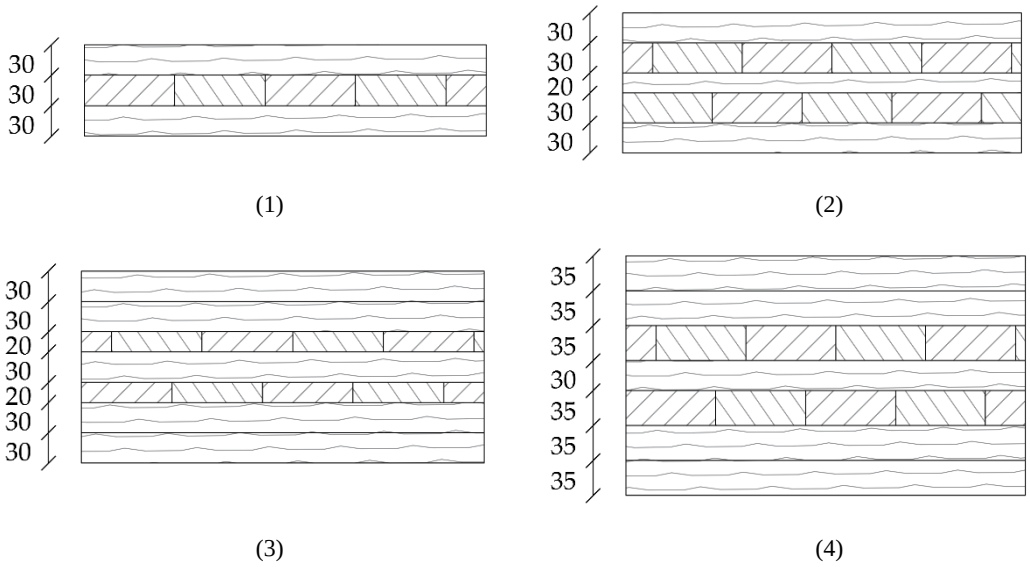

Figure 4.5.3 - Layout of the four diaphragms analyzed (measures in mm).

The values chosen for the gravity load on the walls are 12 kN/m, 20 kN/m and 28 kN/m. Loads have been applied as point loads at the top of the panels in the base configurations and on every point of the diaphragm in the others.

4.5.2. Analyses results

The main issues investigated have been the effect of the out-of-plane stiffness of the floor slab and the effect of the wall-to-diaphragm joint on the rocking behavior of the system compared to the configuration without floor diaphragm, and the comparison between schemes differing for either slab stiffness or wall-to-diaphragm connections stiffness, or both.

Collected results include: (i) the reaction forces in the displacement direction for the base joints; (ii) the percentage, for the displacement of the top of the assembly, of horizontal slip displacement or displacement due to rocking, calculated as shown in Equation [3.5.1]; (iii) the uplift at the center of the wall assembly, calculated as the minimum uplift between the bottom right corner of the left panel and the bottom left corner of the right panel.

$$d_{rock} = \frac{d_{top} - d_{bottom}}{d_{top}} \qquad d_{slip} = 1 - d_{rock} \qquad [3.5.1]$$

where d_{top} is the lateral displacement of the top corner of the assembly, which is applied during the simulation of the cyclic test, while d_{bottom} is the lateral displacement of the bottom corner of the assembly.

The rocking deformation, as calculated with Equation [3.5.1], has a contribution given by the shear and bending deformation of the wall. This amount, according to [37], is usually lower than 3% of the total top displacement.

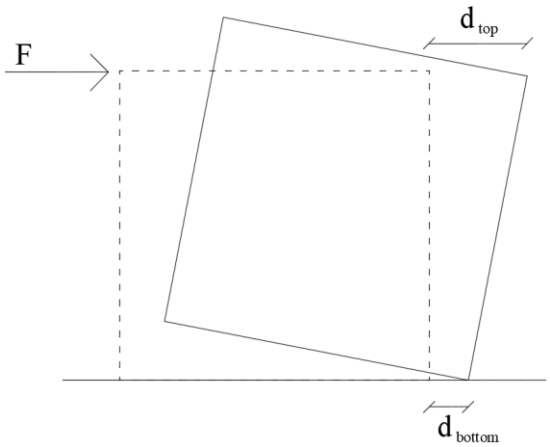

Figure 4.5.4 – Graphical explanation of the terms d_{top} and d_{bottom}. The dashed line depicts the initial position of the wall while the solid line shows the deformed shape of the same wall due to a lateral load applied at the top of the wall itself.

The results of the analyses of all the models with the same base configuration without floor diaphragms have been collected, and the minimum, maximum and average value of reaction force, slip displacement, rocking displacement and central uplift have been calculated for each analysis. Four diagrams have been created: reaction force vs. top displacement, slip vs. time, rocking vs. time and central uplift vs. time.

It is worth nothing that the maximum and minimum values are not very significant when the slip displacement and the rocking displacement are considered, as the value of d_{top}, which is at the denominator in the d_{rock} formula, goes to zero every half cycle, making the value of d_{rock}, and d_{slip} consequently, to infinite. For this reason, the average value is more interesting. On the other hand, for what concerns the reaction force, no information can be extrapolated from the average value; the maximum and minimum values together with the force-displacement graph provide more useful information.

The first important remark is that the out-of-plane stiffness of the slab has almost no influence on any value of the output variables analyzed. No specific trend has been recognized when this parameter is varied alone within the same configuration (see Figure 4.5.5). What really influences the behavior of the models is the stiffness of the connections between the floor diaphragm and the wall. This result seems quite reasonable if the rocking mechanism in this specific scheme (single wall alone with an upper diaphragm) is considered: a loose wall-to-floor slab linkage makes the wall detach from the diaphragm, so that its stiffness does not play a role on the global behavior of the assembly. On the other hand, if a stiff bond is used, the assembly behaves as a single rigid body, removing the potential contribution of the slab stiffness on the global behavior of the assembly. In this case, the assembly behavior is governed by the bottom connections, which are less resistant. An example of what discussed above is depicted in Figure 4.5.5a and b, which display the results for the specimens with the set of top connectors named (a) in Figure 4.5.2, whereas Figure 4.5.5c and d display the set of top joints named (c) in Figure

4.5.2. Figure 4.5.5a and c refer to the specimens with the diaphragm named (a) in Figure 4.5.3, whereas Figure 4.5.5b and d refer to the specimens with the diaphragm named (d) in Figure 4.5.3. The other parameters are the same for all the configurations shown.

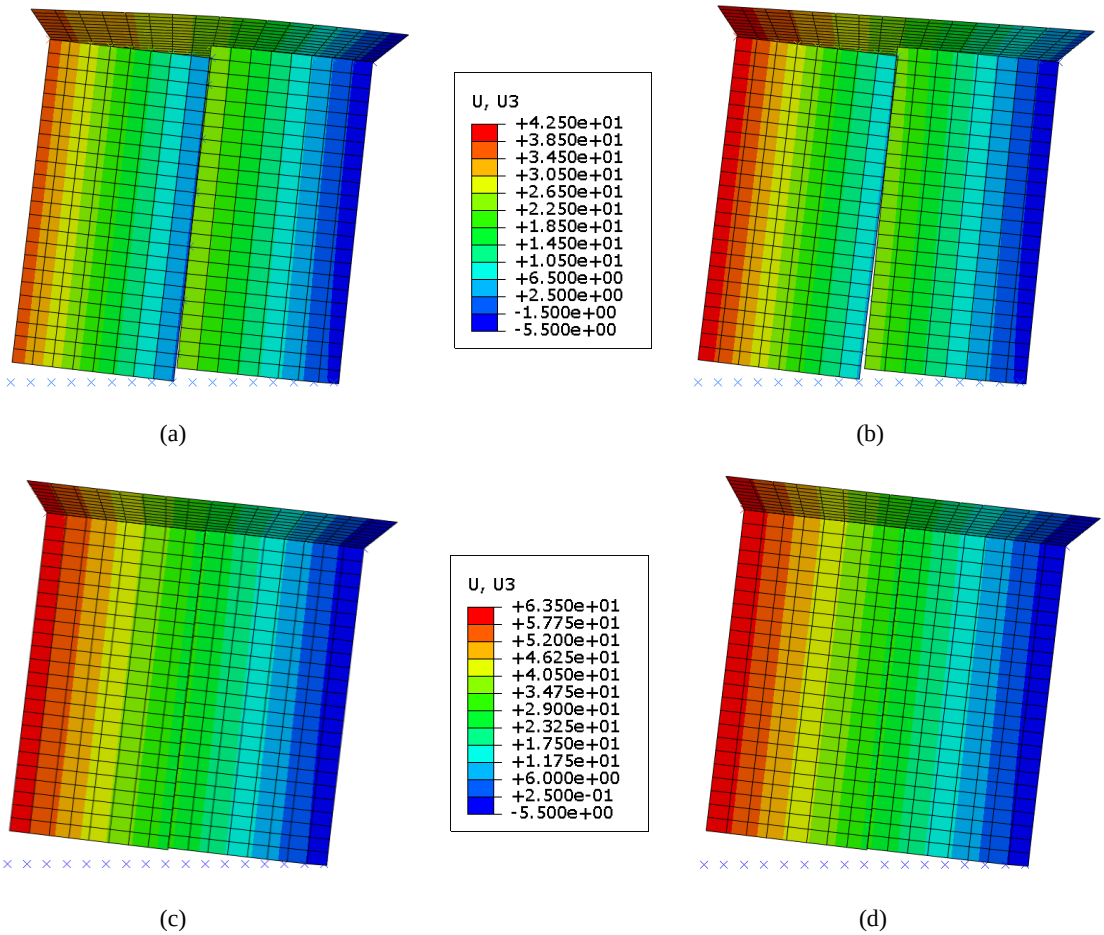

Figure 4.5.5 - Deformed shapes for different combinations of thin/thick diaphragm and loose/stiff wall-to-floor diaphragm connections: thin diaphragm-loose connections (a), thick diaphragm-loose connections (b), thin diaphragm-stiff connections (c), thick diaphragm-stiff connections (d). Measures in mm. Deformation scale factor equal to 5 for all figures.

As it can be seen, different floor slabs with the same joint exhibit similar behavior ((a) vs. (b) and (c) vs. (d)). Conversely, the stiffness of the connections changes significantly the assembly behavior ((a) vs. (c) and (b) vs. (d)).

The out-of-plane stiffness of the floor diaphragm might play a role in the global capacity and behavior of more complex assemblies. However, no significant difference has been found within these analyses.

As only the connections between floor diaphragm and wall panels contribute to the differences encountered during the analysis of the results, the schemes differing only for the stiffness of the floor slab have been averaged and are presented together.

Considering wall-to-floor diaphragm joint, arrangements A and B (Figure 4.5.2) did not present any significant difference for any of the parameters analyzed. For this reason, the corresponding results are averaged and presented as a unique case.

As mentioned in the introduction, the motivation for this study was to investigate the rocking behavior of simple wall assemblies and the validation of an empirical formulation to predict the interaction between panels. Bearing this in mind, it was first assessed whether the wall assembly behavior, such as coupled or uncoupled, is affected by the presence of the slab.

In configurations A and B of the wall-to-floor diaphragm connections, the six-screw panel-to-panel joint do not show any significant variation in behavior, which is always coupled. For the twelve-screw models, in general, the amount of uplift was found to increase due to the presence of the floor diaphragm, and the tendency to have an uncoupled behavior is greater too. However, no clear trend in relation to the various parameters have been detected.

With an arrangement C of the wall-to-floor slab connections, the behavior has been uncoupled for both the six- and twelve-screw cases, proving that the stiffness of this joint play an important role in the rocking behavior of the assembly.

As discussed previously, a coupled behavior ensures, in most cases, a higher level of energy dissipation and a more ductile behavior of the assembly [37]. A coupled behavior is characterized by the prevalence of rocking displacement among the different contribution to the total lateral top displacement, with a consequent lower amount of base slip displacement. Since the floor diaphragm stiffens the assembly, it may cause a different amount of slip deformation. For this reason, this aspect has been investigated in details.

As expected, since the C configuration assemblies always showed an uncoupled behavior, their difference in slip displacement from the reference scheme is generally larger than the A and B arrangements assemblies. The schemes with an aspect ratio *h/b* of the panels equal to 2 have significantly larger differences compared to the 3 and 4 aspect ratios for all A, B and C patterns, as shown in Figure 4.5.6. No substantial difference can be noticed when six-screw and twelve-screw models are analyzed individually.

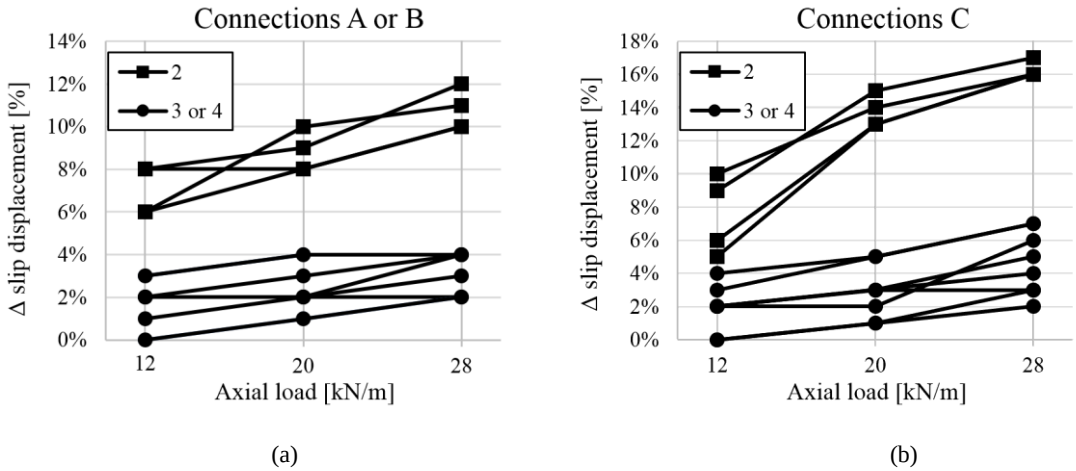

(a) (b)

Figure 4.5.6 - Percentage of difference in slip displacement in the panel-to-panel connection from the reference analyses for connections arrangements A and B (a) and C (b) between wall and floors diaphragm. Squared markers are for assemblies with aspect ratio equal to 2, circles for aspect ratios equal to 3 or 4.

The differences in rocking capacity between the reference scheme and the configurations with the floor diaphragm have been also investigated.

The higher the axial load, the greater the difference between the rocking capacity of the analyzed assembly and the rocking capacity of the reference assembly without diaphragm subjected to the same axial load. The differences are larger for the six-screw model than for the twelve-screw case. Last, arrangements A and B present a lower difference than pattern C.

As no trend has been found when varying either the aspect ratio or the layout of the connectors at the base of the wall, the results of this comparison, presented in Figure 4.5.7, have been averaged among all the ratios and base connections.

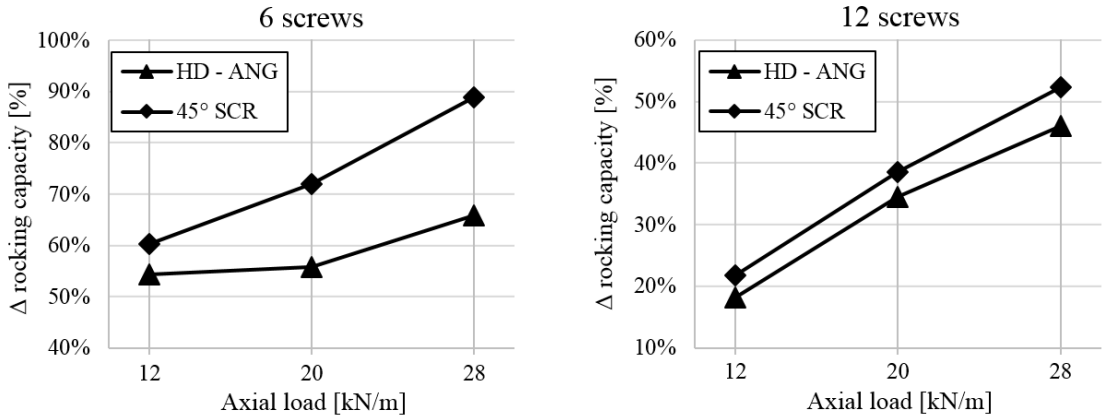

Figure 4.5.7 - Percentage of difference in rocking capacity from the reference analyses for assemblies with 6 (a) and 12 screws (b).

4.6. Concluding remarks

In the first part of this chapter, a method to predict the rocking behavior of a two CLT panel wall assembly is proposed. The method is validated using real scale cyclic test results and, furthermore, several FE analyses carried out in Abaqus to extend the number of considered cases. The method have been derived from equilibrium equations using connections' stiffnesses and external loads.

In the first part of the validation, the method have provided good results for the analyzed cases (83.3% of correct predictions).

Being the variability of tested cases relatively poor, three different set of 105 FE analyses each have been carried out based on the data used in the previous validation. Here the method proved not to be so reliable for the target group (12 connections between panels), giving a good prediction for only the 55.2% of the cases.

Some changes have therefore been made to the original formulation by introducing two new coefficients (α and β). With this modification, the number of right previsions have

increased to 91.4%.

In addition to that, a previously developed method to calculate the structural capacity of a CLT wall has been used for the three group of analyzed walls separately. Being such a method derived for a single panel wall, some considerations have been made and two coefficients have been calculated to extend the formulation to a two-panels CLT wall assemblies and the corresponding rocking behaviors.

In the second part of this chapter, the influence of floor slab out-of-plane stiffness and wall-to-floor diaphragm joints on the rocking behavior of two-panel CLT wall assemblies are investigated. The investigation have been conducted via FE analyses using the Abaqus software package. The influence of different parameters, including height-to-length ratio of the panels, gravity load, base and wall-to-floor diaphragm connections pattern, number of panel-to-panel connections and out-of-plane stiffness of the diaphragm, have been assessed. The assembly behavior has been analyzed for a displacement-controlled cyclic analysis. The reference model has been validated through the results of full-scale experimental tests.

The main result is that the bending stiffness of the floor slab has no influence on any of the collected results for these specific analyses, different configurations, such as different geometries, number of panels or connections (newer connections are stiffer and stronger), could lead to a different influence of the overlapping floor diaphragm. On the other hand, the stiffness of the wall-to-floor diaphragm connections has a strong influence. Rocking capacity, lateral displacement contributions (rocking and slip) and rocking behavior (coupled or uncoupled) have been investigated by comparing configurations with different out-of-plane floor diaphragm stiffness and top wall-to-floor slab linkage with the same assembly without floor diaphragm, and differences have been highlighted, reporting the general trends.

Stiff connections between wall and floor diaphragm always lead to an uncoupled behavior, regardless the other variables. A general increase in wall-foundation slip displacements, as contribution to the total lateral displacement of the assembly, has been noted for all the cases analyzed and it has been found to be greater for an aspect ratio *h/b* equal to 2. The difference in rocking capacity between assemblies with and without floor slab has been found to be larger when:

- A higher axial load is applied;
- A looser joint between wall panels is used;
- A stiffer wall-to-floor diaphragm connection is used.

As no result from full-scale test involving walls with diaphragm have been available, and thus no comparison with real specimens have been made, these numerical tests are meant as a preliminary study to the topic and could be taken as a base for future full-scale tests.

Further analyses could be performed to explore the influence of the position of the joints between panels composing the floor diaphragm, the influence of the upper floors, the effect of the orthogonal walls and number of wall panels on floor slab and wall behavior.

EXPERIMENTAL SEISMIC BEHAVIOR OF A TWO-STORY CLT PLATFORM BUILDING

SHORT SUMMARY

In the US, the growth of the CLT adoption is inhibited by the lack of codified design provisions for CLT in high seismic regions. This led to a multi-year study conducted by Colorado State University to investigate suitable seismic design parameters of CLT shear wall systems. This chapter presents the results from a series of shake-table tests featuring a full-scale two-story mass-timber building utilizing CLT Seismic Force Resisting Systems (SFRS). The building was designed using an R- factor equal to 4.0 under the equivalent lateral force procedure specifications of the ASCE 7-16 Standard. The test program included three phases with different wall configurations, reflecting different wall panel aspect ratios and the existence of transverse CLT walls. Test results indicate that the code-level life safety objective was achieved in all test configurations. The addition of transverse walls did not affect the ability of the panels to rock, and improved the performance of the building structural system.

5.1. Introduction

In the United States of America (US), Cross-laminated Timber (CLT) has only been introduced into the construction market recently, but it has been used in Europe since the 1990s. The use of CLT in the US has largely been limited to regions of low seismicity primarily due to the lack of code and standards allowing the use of CLT as a seismic force resisting system (SFRS). Existing design using CLT in these regions has to either adopted a different lateral system (steel or concrete) or used the alternate design means and methods available within American Society of Civil of Engineers Standard 7 (ASCE 7). The additional cost associated with the alternate design pathway makes the CLT lateral solutions less competitive economically. As the interest in directly using CLT as a SFRS has been growing in North America, there is an immediate need for further research into CLT as a code- recognized SFRS in the US.

Research into CLT as a SFRS has been a globally notable trend for over a decade [50]. One of the first studies investigating CLT as a SFRS was performed at the University of Ljubljana, Slovenia [18]. That study involved subjecting fifteen CLT panels with various anchorages and vertical loads to reversed cyclic lateral loading. From these experiments, it was

determined that the type of anchorage and the vertical load both have a significant effect on performance, and that failure was most likely to occur from connector/anchorage failure, or from localized failures in the wood material. Although these conclusions may seem obvious at present, they were quite novel at the time setting a stage for numerical modeling approaches. The SOFIE Project, an international study funded by the Trento Province in Italy, was an influential comprehensive study on the feasibility of CLT as a SFRS in mid-rise buildings. The objectives of the project were extensive and included investigations into material behavior, fire durability, earthquake behavior, and culminated in three-story and seven-story full-building tests in Japan. Gavric et al. [37] summarizes the essential information for the design of seismic connections for CLT, specifically connections that remain undamaged after seismic excitation. The experimental components of that project included CLT shear wall tests, connection testing, and several other full-scale tests cumulating in a shake table test of a full-scale seven-story CLT building at Japan's E-Defense Shake Table. A full summary of the results from this test can be found in Ceccotti et al. [11]. The SOFIE project demonstrated the capability and suitability of CLT structures for use in high seismic regions and interest soon spread to other areas of the globe. Okabe et al. [45] investigated the structural performance of CLT manufactured with Sugi softwood (Japanese cedar) under seismic and wind loading. The testing was separated into two methods, both utilizing cyclic lateral loading, but with differing boundary conditions introducing shear and rocking responses. The main results demonstrated that rocking was the main deformation mode for the CLT panels with the corners of the panel determining the strength and deformation of the shear wall and the inter-panel LVL connectors were shown to be vulnerable to splitting failures during the testing. The study also reinforced earlier findings that increased vertical loading improved the lateral performance of the shear walls. In North America, Popovski et al. [55] conducted a quasi-static test program of a two-story CLT house with varying wall configurations throughout the structure subjected to monotonic and cyclic loading. The results of the testing demonstrated that rocking and sliding motions are caused by failures in the brackets and are responsible for most of the deformation and displacement of CLT structures, reinforcing earlier work by other researchers. It was also observed that the CLT wall panels exhibit rigid body motion (such as rocking) and that the floors acted as rigid diaphragms. The study also stressed the need for further research into the effects of different panel aspect ratios on the performance of CLT walls. In the U.S., the FEMA P-695 [25] methodology is being applied by a research team led by Colorado State University (CSU) to enable the use of CLT in high seismic areas without the need of alternative means and methods in ASCE 7 [5].

In this chapter, the results of a two-story shake-table test program is presented, which sought to (1) demonstrate the effectiveness of CLT shear-walls as a SFRS to provide life-safety; (2) provide insight into the aspect ratios where CLT panels might transition from rocking to

sliding behavior for platform style construction; and (3) suggest design provisions of shear walls using the equivalent lateral force procedure.

5.2. Test building layout and configuration

The two-story test building constructed in this study utilized CLT panel shear walls in a platform construction configuration. The CLT shear walls were connected by generic shear connectors at the base and ceiling to a CLT floor/roof diaphragm. The overturning was resisted by continuous hold down rods typically used in stacked shear walls in light-frame wood construction (see chapter 2.2.2.1). The gravity frame of the test building was designed to facilitate the needs of two previous stages of testing [8][51] that investigated CLT rocking wall systems. This chapter focuses exclusively on the third stage of testing and its three sub-phases: Phase 3.1, Phase 3.2, and Phase 3.3. Phase 3.1 and Phase 3.2 investigate the effects of different CLT panel aspect ratios on the performance of the stacked shear walls, while Phase 3.3 investigates the effects of adding transverse walls to either end of each shear wall stack. The test structure was a two-story mass-timber building with glulam (vertical loads bearing system and beams) and CLT panel (lateral load bearing system and floor diaphragms) components, as can be seen in Figure 5.2.1, which was constructed over several days by professional contractors experienced in CLT construction.. The dimension of the building is shown in the figure with a height, width, and length of 6.7 m (22 ft.), 6.1 m (20 ft.), and 17.7 m (58 ft.), respectively. Structurally, the building can be divided into three sub-systems, namely the gravity frame, the floor/roof diaphragms, and the CLT shear wall seismic force resisting system (SRFS).

Figure 5.2.1.a shows the gravity frame, which consists of the glulam beams and columns that support the dead load (gravity) loads of the structure, which can be split into the first and second story. The column system on the first story consists of 12 columns, all grade L2, with four (4) columns being continuous to the second story and roof level. The first floor level consists of four grade 24F-V8 longitudinal beams spanning the N-S direction, nine (9) grade 24F-V4 transverse beams spanning the E-W direction, and with beams and columns connected using commercial connectors [50]. The second story of the structure has a similar column layout to the first story with 12 total columns, also grade L2, with the four (4) continuous columns terminating at the roof level, and eight (8) discontinuous columns located above their respective first story counterparts. The roof level beam system was significantly different than the first floor level since it had only beams in the longitudinal directions. There were a total of six (6) beams, four (4) grade 24F-V8, and two (2) grade 24F-V4 which are also connected using similar hardware to the first floor level.

Similar to the gravity frame, the diaphragms for the first floor level and the roof floor level were different with the objective of investigating two design configurations in one test [6].

The floor diaphragm (first floor) level panels were all 3-ply grade V1 CLT panels, although the size of the panels varied. The roof diaphragm was a composite system consisting of CLT panels with a concrete topping slab. The CLT panels were 1.5 m x 6 m (5 ft x 20 ft), with the exception of two 1.2 m x 6 m (4 ft x 20 ft) panels, 5-ply grade V1 panels spanning the E-W direction, as seen in Figure 5.2.1.a. The concrete layer was a 57.2 mm (2.25 inch) concrete topping on the CLT panels with composite action being achieved with 45-degree anchors installed into the CLT panels.

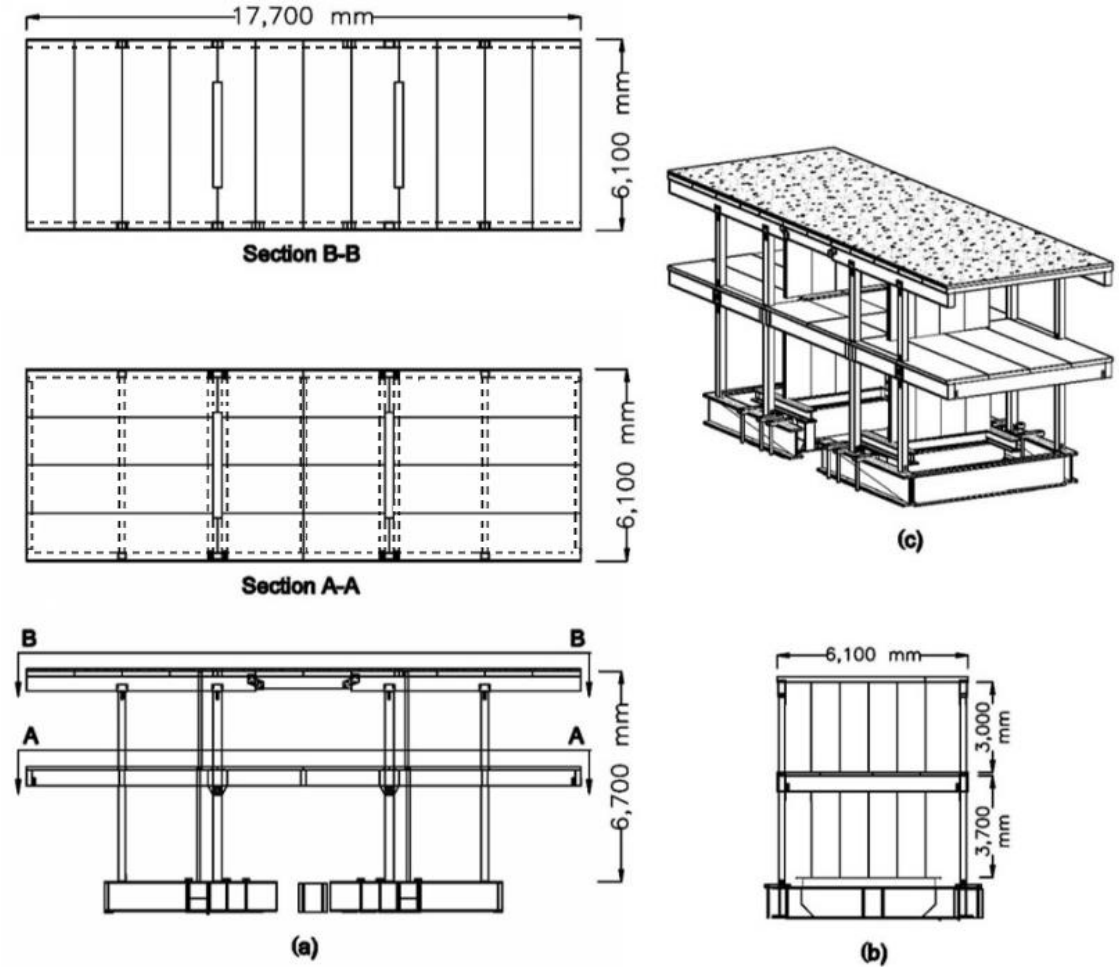

Figure 5.2.1 - Test Building: (a) Front elevation and plan view (solid lines for CLT panels, dashed lines for the beam system underneath); (b) Side elevation view; (c) Isometric view.

The SFRS system used for the testing varied for each phase, but were all consisted of CLT panels connected with metal hardware to form a wall at each story. There are two parallel shear wall lines as it is shown in Figure 5.2.2. The two-story stacked wall system was designed against overturning by two continuous steel tie-down rods while the shear demand was designed to be resisted by inter-panel connectors and generic angle brackets (both fastened using 16D sinker nails) [3]. The assumption of decoupled shear and overturning force transfer using different components is a common design assumption that leads to conservative designs, and is the main assumption consistent with the design approach for platform CLT construction

standards developed in the US. The design method being proposed for CLT platform construction in the U.S. assumes the brackets only take shear forces and the continuous steel rod hold downs take only uplift, both of which are not exactly correct since the wall does try to rock. However, the phi factor for capacity reduction was adjusted within the design method to account for this during calibration of the proposed design procedure. The loading used in the design was derived using the Equivalent Lateral Force (ELF) method as described in ASCE 7 [5], with design spectral values of 1.5g for SDS and 1.0g for SD1 for a site near San Francisco, California. An R-factor of 4.0 was used for the design of the lateral resisting system and the diaphragm was assumed to be rigid. The number and spacing of the shear connectors for each phase were such to maintain a constant design shear story capacity of 174 kN (39 kips) and 120 kN (27 kips) per wall line for the first and second stories respectively. The linear per foot design capacity varied between the phases however, and for Phase 3.1 and Phase 3.3, the shear connectors had a capacity of 4.7 kN/m (3.4 kips/ft) and 3.4 kN/m (2.5 kips/ft) for the first and second stories respectively, while in Phase 3.2 the connectors had a capacity of 5.4 kN/m (4 kips/ft) and 4.2 kN/m (3 kips/ft) for the first and second stories. The steel tie-down rods resisting the overturning moment in Phase 3.1 and Phase 3.3 had a design capacity of 124.5 kN (28 kips) and 320 kN (72 kips) per wall for the first and second stories respectively, while the tie-down rods in Phase 3.2 had a design capacity of 138 kN (31 kips) and 351 kN (79 kips) for the first and second stories.

The NHERI@UCSD Shake-Table is a 7.6m x 12.2 m (25 ft x 40 ft) uniaxial table equipped with two actuators with a total maximum payload of 20,000 kN (4,496 kips). This location has been used for many previous tests, and the full details of the shake-table can be found in Ozcelik et al. [46]. The footprint of the test structure was larger than the table in the N-S, which is the direction perpendicular to the actuator movements that apply shaking in the E-W direction, so large steel outrigging beams were used as a way to extend the table to the appropriate dimensions. To ensure safety, two steel towers were installed in front of the control building to the south of the building specimen. A third tower was installed on the east side of the structure with safety straps wrapping around the center of the structure, with the straps remaining slack unless the structure became unstable and began to collapse. Figure 5.2.2 shows the orientation of the structure on the shake-table and the location of the safety towers.

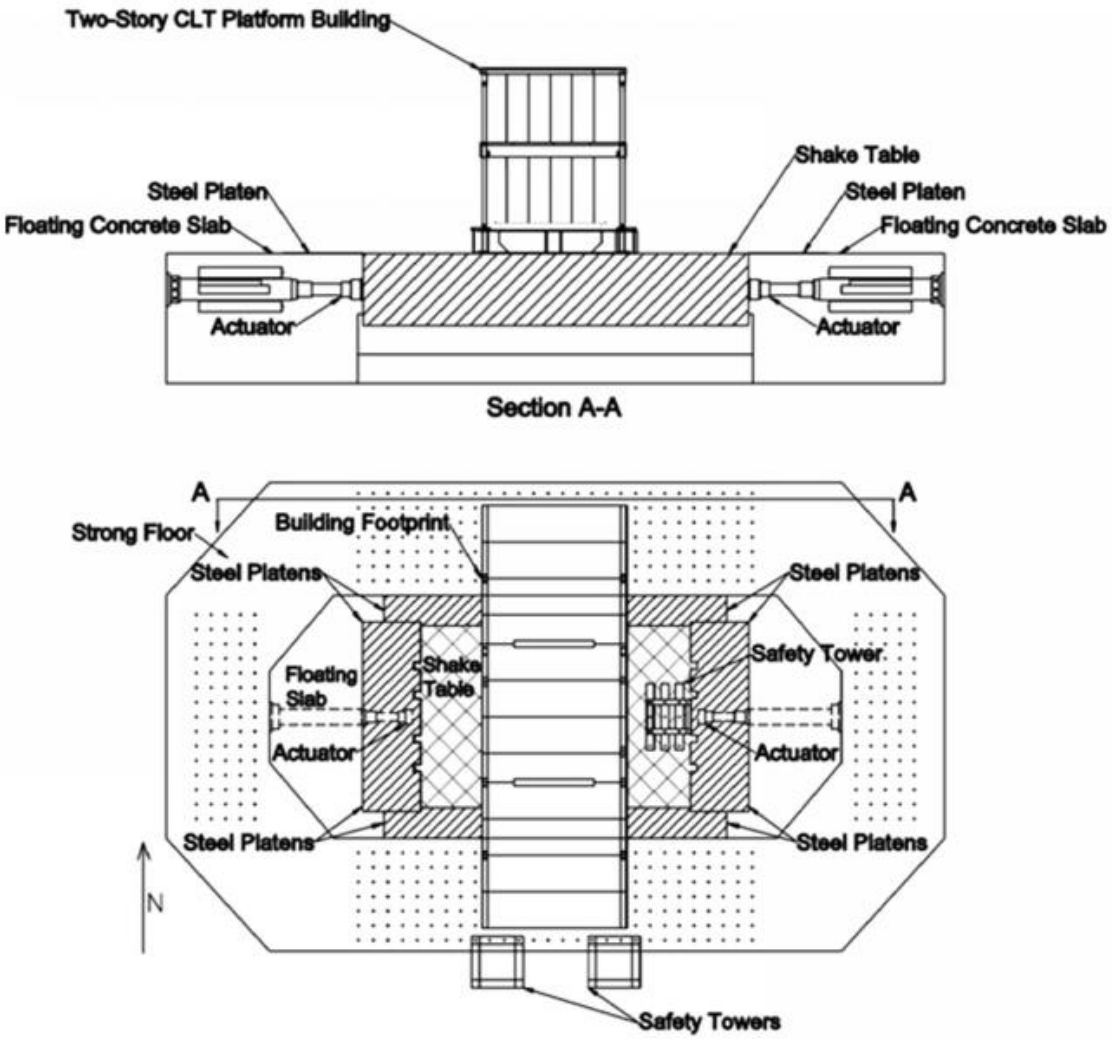

Figure 5.2.2 - Position of the two-story CLT Platform Building on the shake table.

5.3. Test description

5.3.1. Phase 3.1

Two shear walls were designated as the north and south wall system throughout the test program. The first story wall height was 3,200 mm (126 in) and second story wall height was 2.8 m (110 in). There were shear connectors installed at both the top and the bottom of the wall. The overturning restraint was provided by the ATS rods at the end of each wall similar to that used in stacked light-frame wood shear walls. The Phase 3.1 walls consisted of four (4) 900 mm x 3,200 mm (36 in x 126 in) CLT panels with a thickness of 105 mm (4-1/8 in), resulting in a total wall length of 3,700 mm (144 in), which is shown in the schematic of Figure 5.3.1. The shear capacity of the walls is provided by the inter-panel flat shear connectors, that are perforated metal plates placed half over a panel and half over the adjacent panel with screws fastening, along the vertical splices between panels and angle shear connectors at the top and bottom of the each panel. The base/top shear connectors were generic 76 mm x 57 mm x 3 mm

(3 in x 2-1/4 in x 3/25 in) L angle brackets with a length of 121 mm (4-3/4 in) with the number of connectors varying between the first and second story based on the calculated shear demands. Brackets were installed on the first and second story based on the required shear capacity. On the first story, the brackets were placed on both sides of the wall, resulting in a total of eight (8) brackets per panel and 32 per wall on the first story. The brackets on the second story walls were only located on the outside face of each wall and were spaced to ensure three brackets per panel on both the base and top, resulting in a total of six (6) brackets per panel and 24 per wall. The brackets were secured to each panel using 16 16D box nails (4.2 mm diameter x 89 mm). The brackets were connected to the diaphragm and the foundation by two 19 mm (3/4 in) diameter fully threaded, A36 bolts. The inter-panel shear resistance consists of inter-panel connectors vertically spaced at 406 mm (16 in). These inter-panel connectors are placed on both sides of each of the three inter-panel joints in the walls, resulting in a total of 14 connectors per vertical joint on the first story (total of 42) and 10 per vertical joint on the second story (total of 30). The overturning moment resisting system was comprised of vertical steel rods spanning the full height of the building. The tie down rods were located at the end of each wall on both sides, for a total of four (4) per wall and eight total and were allowed to reach at each floor (second flood diaphragm and roof level in this case) using a bearing plate to distribute the load. The diameter of the rods was not constant throughout the height of the building, with a coupler located above the first floor level bearing plate reducing the diameter from 31.8 mm (1-1/4 in) at the base to 19 mm (3/4 in) at the roof.

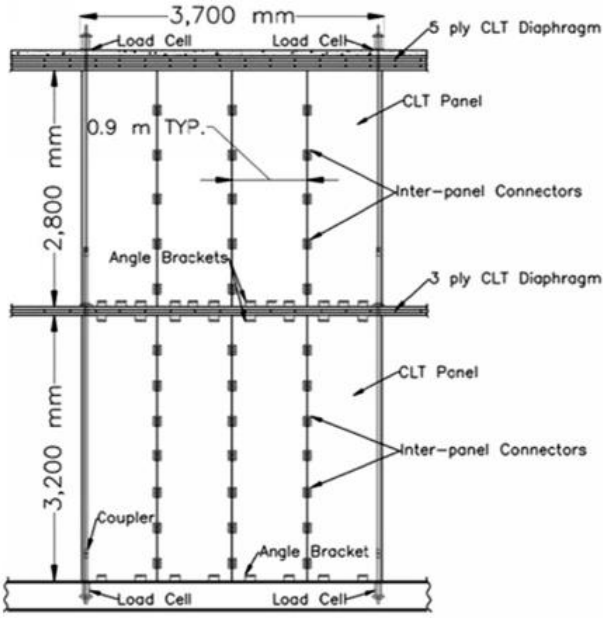

Figure 5.3.1 - Phase 3.1: 3.5:1 aspect ratio panels shear wall stack layout.

The rods were not designed for compression loading, only tension, so, to prevent buckling, the tie-down rods were allowed to slip through the oversized holes at the diaphragm when the corresponding side of the shear wall was in compression. The SFRS configuration for

Phase 3.1 is presented in the schematic of Figure 5.3.1.

5.3.2. Phase 3.2 test description

The Phase 3.2 wall system was similar in composition to the Phase 3.1 wall system but with CLT panels having a different aspect ratio (height/width). The wall configuration for Phase 3.2 consisted of two 1,520 mm x 3,000 mm (60 in x 126 in) CLT panels with a thickness of 105 mm (4- 1/8 in), resulting in a total wall width of 3 m (120 in) and an aspect ratio of 2.1:1, which can be seen in Figure 5.3.2. The first story had 16 angle brackets per panel with four located on the base and top of the panel on both sides. The second consisted of 12 brackets per panel with three brackets on the base and top of the panel as well as on both sides. The first story had eight (8) inter-panel connectors on each side of the joint between panels (total of 16) and six (6) per joint on the second story (total of 12). The ATS rods for overturning were increased to a 22.2 mm (7/8 in) diameter tie-down rod instead of a 19 mm (3/4 in) tie-down rod due to larger expected overturning moment, i.e. a function of aspect ratio of the panels making up the wall system for Phase 3.2 as shown in Figure 5.3.2.

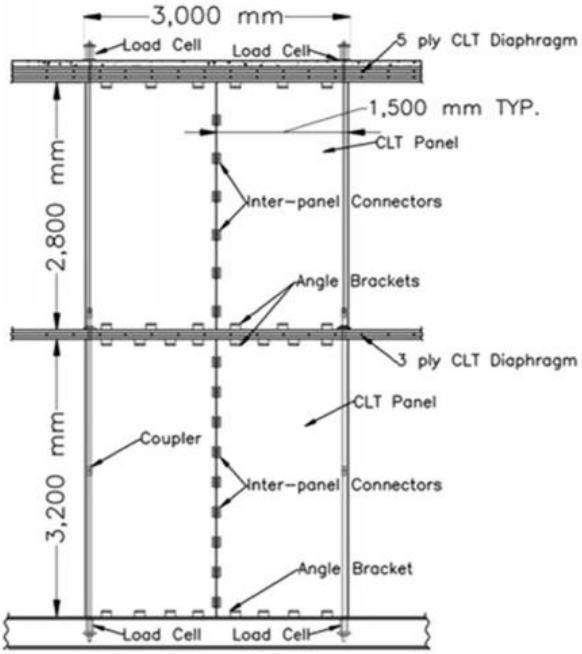

Figure 5.3.2 - Phase 3.2: 2.1:1 aspect ratio panels shear wall stack layout.

5.3.3. Phase 3.3

The Phase 3 wall system was identical to the Phase 3.1 wall system except for the addition of transverse CLT wall panels at the ends as shown in Figure 5.3.3.a. The transverse panels were added to examine the effect of these transverse walls on seismic performance. The first story transverse walls consisted of one CLT panel at each end of the shear wall. In order to avoid existing gravity frame beams, a 533 mm x 483 mm (21 in x 19 in) section was notched

out from the top corner of each panel to fit it around the beams. The walls were secured to the diaphragm on the top and the steel beam at the base by six angle brackets with three for the top and base respectively. The second story transverse walls were similar to the first floor with CLT panels on both ends of the shear walls. These panels were secured to the top and base diaphragms by three angle brackets on both the top and bottom. The Phase 3 wall system can be seen in Figure 5.3.3.

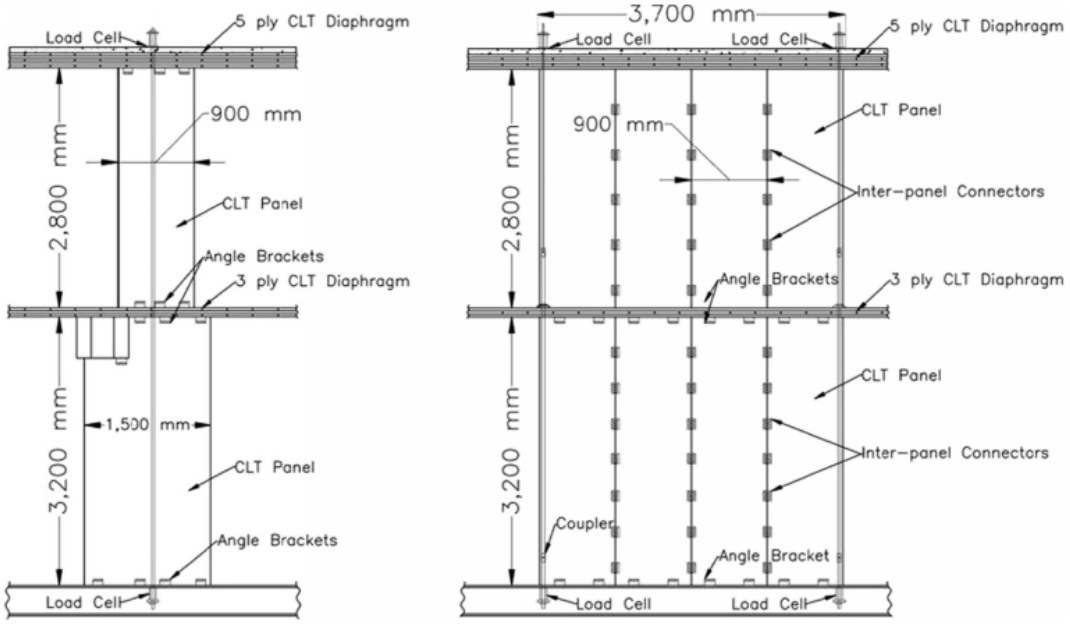

(a) (b)

Figure 5.3.3 - Phase 3: (a) Transverse CLT walls; (b) 3.5:1 aspect ratio panels shear wall stack layout.

5.3.4. Instrumentation

The response of the building during shaking was recorded by over 300 sensors placed in strategic locations throughout the building. As mentioned previously, the structure was part of a collaborative test program with various lateral systems and throughout the testing, the sensors installed to measure the response of the gravity frame and diaphragms remained unchanged. However, the sensors installed on the SFRS varied from each stage and in some cases within the stage. The diaphragms and gravity frame had 274 sensors installed throughout both floors of the building, and the quantity of each type of sensor can be seen in Table 5.3.1. Strain gauges were used to measure the deformation in the chord splices on the diaphragms as well as the rebar installed in the concrete of the composite roof. Linear potentiometers were used to measure the relative displacement between various components of the structure such as: CLT panels and the diaphragm, the diaphragm and gravity frame, and between the concrete and CLT panels in the composite roof diaphragm. String potentiometers were installed in the center of the diaphragm as well as on each corner of both floors to measure the global displacement of the building. They were also used to measure the relative vertical displacement between floors and the

relative vertical and horizontal displacement of the two farthest corners of the structure. Three directional accelerometers units were installed to measure the acceleration in the X, Y, and Z directions, and were installed in a similar fashion on each floor with one located at each corner of the diaphragm, as well as at quarter points along the centerline of the diaphragm.

Table 5.3.1 – Instrumentation on gravity frame and diaphragm.

Instrument	Quantity
Strain Gauge	133
Linear Potentiometers	63
String Potentiometers	42
Accelerometer	36

Figure 5.3.4 shows the location and details of the typical Phase 3.1 wall instrumentation. A total of 72 sensors were installed for Phase 3.1 (see Table 5.3.2) on both the north and south walls systems to capture the wall responses. Linear potentiometers were installed horizontally on the base and top of the first and second stories on both the north and south wall systems in order to capture any sliding motion. They were also installed vertically at each corner on the first and second stories on the south wall system to capture the uplift behavior of the walls. However, due to constraints on the quantity of sensors, the north wall system only had vertical linear potentiometers on two corners of the walls on both the first and second story. String potentiometers were installed in the horizontal and vertical directions on two of the three joints between the CLT panels on each of the four walls that comprised the north and south wall systems, to measure any relative panel displacement in either the vertical or horizontal directions. Two string potentiometers were also installed diagonally in opposing directions on both a first and second story wall on the north wall system to measure any panel deformation. A total of 16 load cells were installed in line with the anchor bolts on the base and top of each ATS anchor rod on both the north and south wall system to measure the tension in the rods caused by the overturning moment. Strain gauges were also installed strategically along the lengths of the rods as a redundant measurement to determine the tension in the tie down rods in case of load cell failure.

The Phase 3.2 SFRS sensors were installed in a similar fashion to Phase 3.1; however, there were some minor differences due to the smaller wall dimensions and fewer CLT panels making up each wall. With only one inter-panel joint in each wall, there were several unused string potentiometers previously utilized in Phase 3.1 for relative panel deformation.

These sensors were instead used to measure panel deformation on additional panels on both the north and south wall systems. All four panels comprising the two-story north wall system were measured for panel deformation as well as one panel from each floor on the south wall system. The total quantity of sensors for Phase 3.2 can be seen in Table 5.3.2.

Table 5.3.2 - Instrumentation on shear walls.

Instrument	Quantity for each phase		
	3.1	3.2	3.3
Strain Gauge	16	4	3
Load Cell	16	16	16
Linear Potentiometers	20	20	20
String Potentiometers	20	20	20
Accelerometer	0	0	0

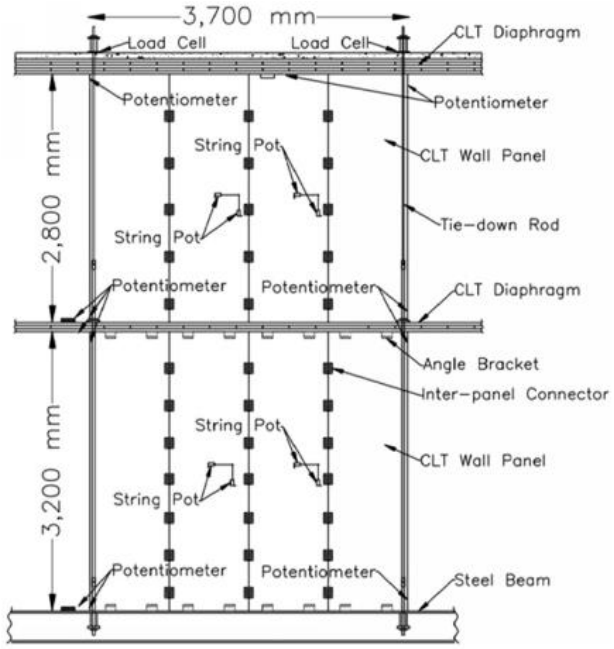

Figure 5.3.4 - Phase 3.1 instrumentation on south face of south shear wall (typ. across phases).

The Phase 3.3 string potentiometers, load cells, and strain gauges were installed in the same locations as Phase 3.1; however, the locations of some of the linear potentiometers changed due to the addition of transverse walls on either end of all four walls comprising the north and south wall systems. Some of the sensors measuring sliding were moved from the end of the walls towards the center due to the previous locations being blocked by the installed transverse walls. One potentiometer from each floor on the south wall system was moved to the end of the transverse wall on their respective floors to capture any potential uplift. The total quantity of sensors for Phase 3.3 can also be seen in Table 5.3.2.

5.4. Ground motion and testing program

Component 2 of 1989 Loma Prieta earthquake record from the Capitola recording station was used and scaled to various intensities for all testing according to ASCE 7-16. The scaling of the motion was done according to FEMA P695 for a location in San Francisco, California. Intensities were selected based on levels corresponding to a service level earthquake (SLE), design basis earthquake (DBE), and maximum considered earthquake (MCE), with mean return

periods of 72 years, 475 years, and 2475 years respectively. For the MCE motion, this led to a SDS and SD1 of 1.5 g and 1.0 g, respectively. The MCE scaled response spectra is presented in Figure 5.4.1, while the spectral accelerations for each phase is shown in Table 5.4.1. Due to time constraints for repairs, Phase 3.2 and 3.3 testing used only the SLE and MCE scaled ground motions, which optimized the amount of data collected with a minimal amount of repair.

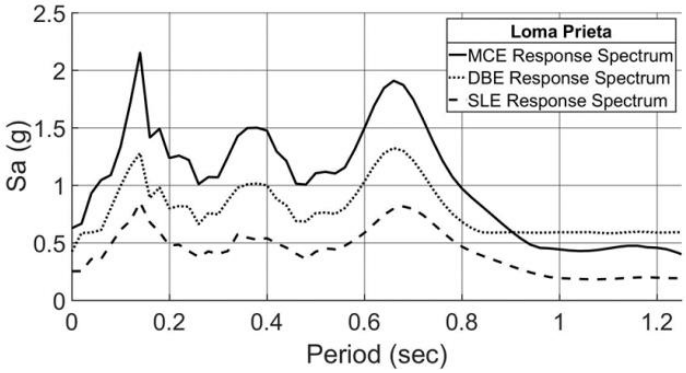

Figure 5.4.1 - Spectral accelerations for Loma Prieta scaled to SLE, DBE, and MCE levels.

Table 5.4.1 – Test sequencing and global story response for each phase.

				Average peak displacement[(c)] [mm]		Peak average inter-story drift[(e)] [%]		Peak story shear[(f)] [kN]	
Phase[(a)]	Test[(b)]	S_a [g]	PGA [g]	Story I	Story II	Story I	Story II	Story I	Story II
3.1	SLE	0,525	0,25	18	29	0,49	0,42	306	206
	DBE	0,92	0,42	51	94	1,4	1,4	582	456
	MCE	1,36	0,62	99	158	2,7	1,95	765	579
3.2	SLE	0,54	0,24	17	32	0,47	0,54	308	219
	MCE	1,29	0,66	93	159	2,54	2,15	873	643
3.3	SLE	0,68	0,265	40	48	1,08	0,59	301	190
	MCE	1,49	0,68	89	151	2,42	2,06	873	645

a) Phase 1 (3.5:1 aspect ratio). Phase 2 (2.1:1 aspect ratio). Phase 3 (4:1 aspect ratio with additional transverse walls).
b) Loma Prieta earthquake ground motion was used for all tests, and scaled appropriately to SLE, DBE and MCE levels respectively.
c) Average of the displacements recorded at the center, and both ends of each story
e) 3663 mm and 3043 mm were used for the height of the first and second story respectively.
f) 342,5 kN and 422,5 kN were used for the weight of the first and second story respectively.

The natural period of the test structure varied between tests due to structural damage and changes in wall configuration. White noise tests were conducted before and after every test in order to determine the natural period. Figure 5.4.2 presents a plot of the change in the natural period of the structure over the platform CLT testing program. Initially with Phase 3.1 (3.5:1 aspect ratio shear walls), the test structure had a natural period of approximately 0.38 seconds, which increased following testing with the peak natural period following Phase 3.1 being approximately 0.89 seconds. The installation of the Phase 3.2 shear walls, which had an aspect ratio of 2.1:1, returned the natural period of the structure to approximately 0.41 seconds. The peak natural period following Phase 3.2 testing was 0.73 seconds after the MCE level test. Phase 3, with the return to the 3.5:1 aspect ratio shear walls, and the addition of transverse CLT walls, reduced the natural period of the structure to 0.17 seconds. This decrease is most likely

due to the additional stiffness provided by the transverse CLT walls, including some potential "flanging" action during smaller deformations in and near the elastic range. The peak natural period for the structure following Phase 3 testing after the MCE level test was the shortest of the phases at 0.35 seconds. This indicates that the least amount of softening occurred in Phase 3 with the transverse walls in place.

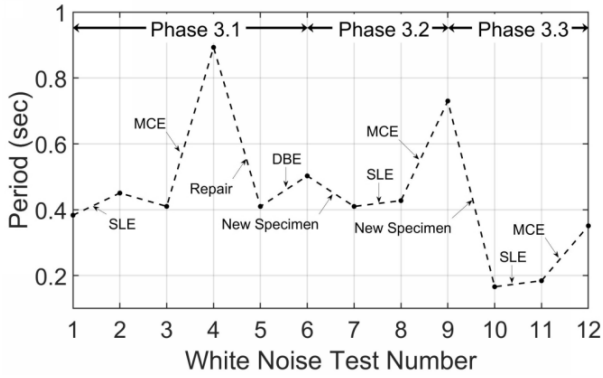

Figure 5.4.2 - Fundamental building period and the effect of repairs and different wall configurations.

5.4.1. Displacement profile

Figure 5.4.3 presents the displacement profile of the test structure for each test, with the profile constructed using the average maximum displacement of the story relative to the shake table. The horizontal displacement was measured at the north, south, and middle of the diaphragm on each story. Across all of the phases, primarily a first mode response was observed, with the peak interstory drift for each story occurring simultaneously to the peak displacement. Phase 3.1 and Phase 3.2 had similar peak MCE level average displacements of 158 mm (6.22 in.) and 159 mm (6.26 in), respectively, and Phase 3.3 had the smallest peak average displacement of 151 mm (5.94 in.). As mentioned previously, the objective of the testing was to demonstrate the performance of CLT shear walls using typical design techniques, in the case when ELF was used for the design. In the design, 2/3 of the MCE level spectral acceleration is reduced by a seismic reduction factor (R), developed over the course of the project, to account for the nonlinear response of the structure, specifically through its deformation capacity and ability to dissipate energy. The nonlinear response is confirmed by the results in Figure 5.4.3, as the MCE level motion is 1.5 times greater than the DBE level motion, but the maximum displacement for the Phase 3.1 MCE test (158 mm) is greater than 1.5 times the maximum displacement for the Phase 3.1 DBE test (94 mm). It was theorized in Popovski et al. [55] that the addition of walls transverse to the shear walls would improve the performance of the structure, and as can be seen in Table 5.4.1 and Figure 5.4.3, even though Phase 3.3 MCE had the largest peak ground acceleration (PGA) recorded by the table, its peak floor displacements were less than Phase 3.1 and Phase 3.2 on both floors.

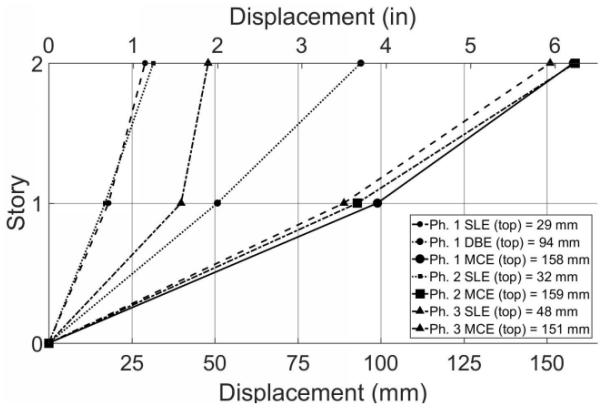

Figure 5.4.3 - Average displacement of first and second stories for each test.

5.4.2. Inter-story drift

The inter-story drifts (ISDs) of the test structure were obtained by finding the average relative displacement of each story. For the first story, this was done by taking the difference of the string potentiometers on the first floor level diaphragm and the table displacement feedback data, then averaging the results. The second story relative displacement was calculated in a similar way, except that instead the difference between the first and roof floor levels string potentiometers was used. The peak inter-story drift was then divided by the relevant story height, 3,663 mm (144 in) and 3043 mm (120 in) for the first and second stories, respectively, to obtain drift as a percentage of the story height. Table 5.4.2 shows the ISDs for all of the tests, and it can be seen that the first story ISDs were larger than the second story, which may imply slight soft story behavior of the structure, but could also have been influenced by the different story heights. This is particularly evident in the Phase 3.1 MCE level ISD results, where it can be seen in Figure 5.4.4 that the first story has an ISD 0.75% greater than the second story.

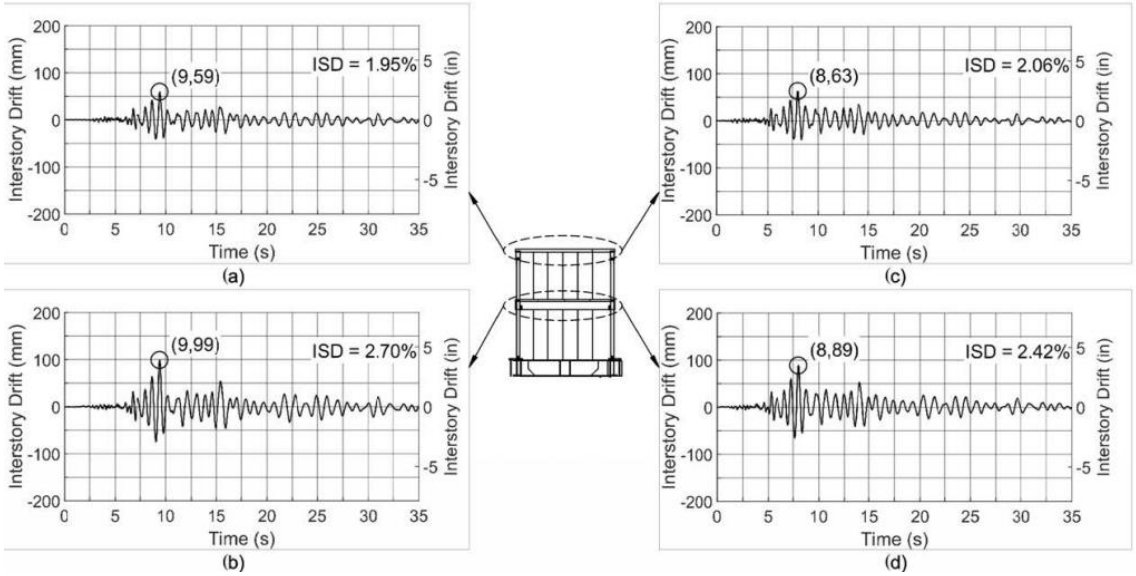

Figure 5.4.4 - Interstory drift: (a) Phase 3.1 MCE second story; (b) Phase 3.1 MCE first story; (c) Phase 3.3 MCE second story; (d) Phase 3.3 MCE first story.

The addition of transverse walls in Phase 3.3 improved the performance significantly of the first story even though the PGA was greater than in Phase 3.1.

5.4.3. Global hysteresis

Newton's second law was used to calculate the inertial force of each story by using the average of acceleration time histories recorded on both floors at each corner and along the center of the diaphragm at the north edge, center, and south edge. The shear force for each story was then calculated accordingly, and Table 5.4.1 presents the shear force for all seismic tests and both stories. It can be seen that the largest shear force of 873 kN (196 kips) occurred during Phase 3.3 and Phase 3.2 MCE. The maximum shear force in the first story of both Phase 3.2 and Phase 3.3 exceeded the design capacity of the shear connectors, however, it should be noted that the shear walls were designed to less than 2/3 of the design capacity that will be proposed. The walls were not in danger of failing and the overstrength seen in the testing could have had several possible origins. In Amini et. al [3] the R factor was determined using the average capacity of the connectors throughout testing, and it is possible the shear walls in the full scale test exceeded the average. The testing in the previously mentioned study was also done with minimal gravity loading, and the additional gravity loading here could have increased the capacity to the wall. Finally, the manufacturer of the CLT panels was not the same although the wood species was the same and both met current standards for manufacturing CLT.

Figure 5.4.5 compares plots of the floor displacements versus the story shear for Phase 3.3 MCE and Phase 3.1 MCE. Recall that Phase 3.1 and Phase 3.3 both had 3.5:1 aspect ratio panels, but Phase 3.3 also included the addition of transverse walls, which was done to simulate a real structure where there would be shear walls in both directions and to investigate their effect on performance.

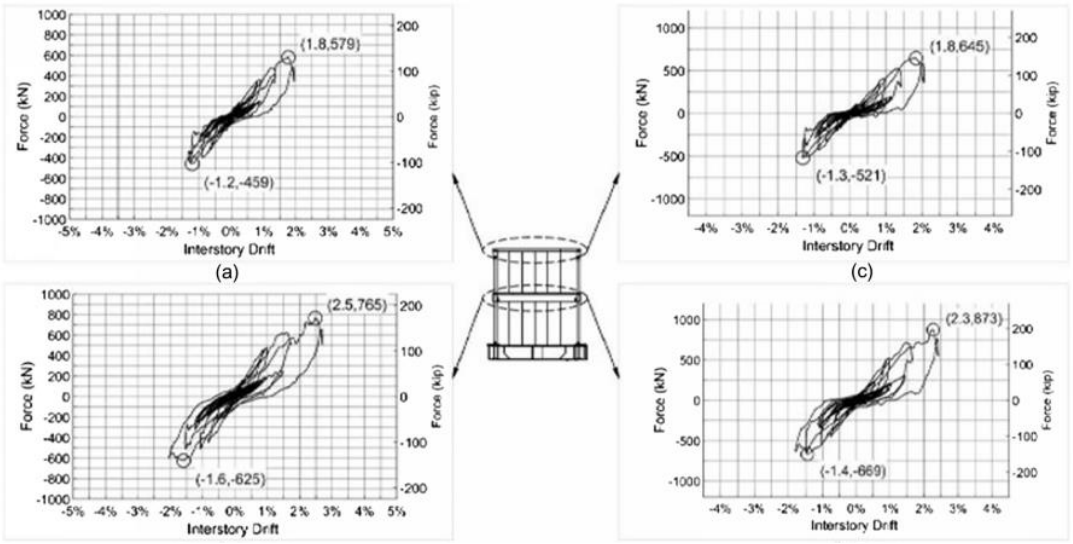

Figure 5.4.5 - Global hysteresis curves: (a) Phase 3.1 MCE second story; (b) Phase 3.1 MCE first story; (c) Phase 3.3 MCE second story; (d) Phase 3.3 MCE first story.

As can be seen, while the story shear is higher in Phase 3.3, the displacements are either similar or less than Phase 3.1. Since the PGA was larger in Phase 3.3, this implies that the transverse walls had no negative effect on performance, and in fact improved performance of the structure, which was expected but is quantified here.

5.4.4. Torsion

Figure 5.4.6 shows the deformed shape of the diaphragm indicating some torsion, with the south end of the second floor level displacing 35 mm (1.38 in) more than the center of the structure. It can also be seen that the torsion on the first story was not as large (25 mm), it was still however present and it should be noted that the north end of the structure did not experience much torsion across either story. The torsion experienced by the structure increased further into the testing program, but despite this, the CLT shear wall stacks still performed well.

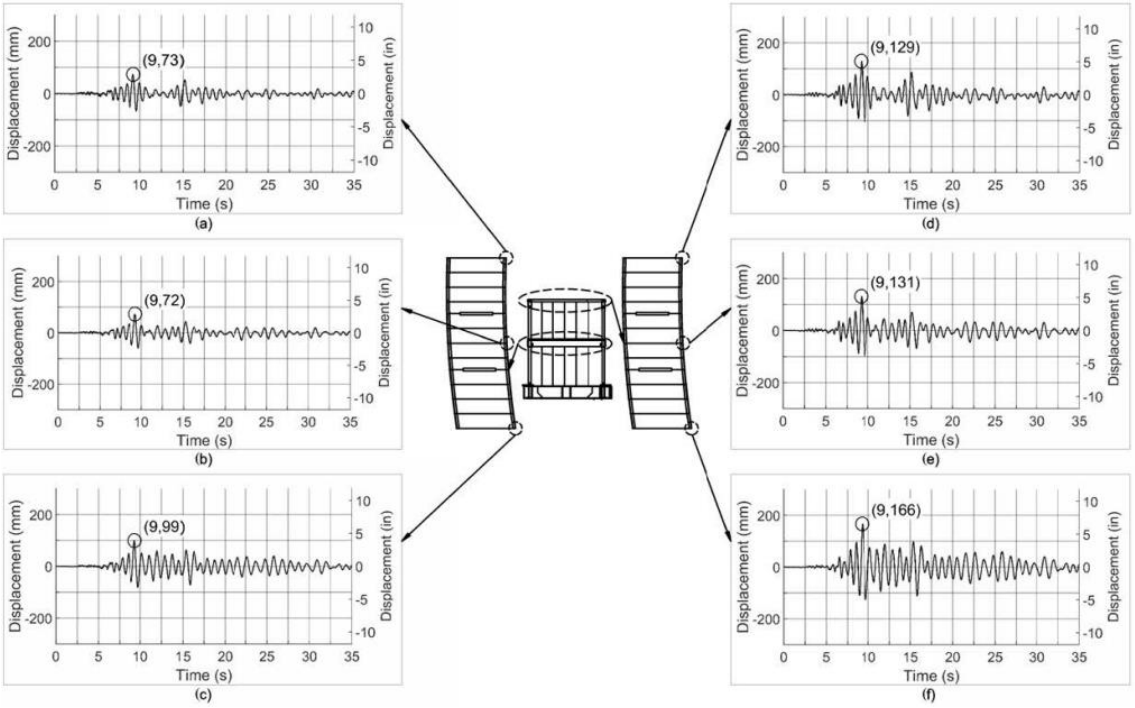

Figure 5.4.6 - 3.1 MCE Displacement: (a) first floor level northeast corner; (b) first floor level center east side; (c) first floor level southeast corner; (d) second floor level northeast corner; (e) second floor level center east side; (f) second floor level southeast corner.

5.4.5. CLT panel uplift

One of the principal objectives in the testing was to observe individual CLT wall panel behavior and investigate the effect of aspect ratio and in the case of Phase 3.3, the addition of transverse walls on that behavior. To capture any potential uplift of the panels, linear potentiometers were used at the four corners of the shear wall on both the first and second stories, and Table 5.4.2 summarizes the results. In addition, for Phase 3.3, linear potentiometers were installed on the transverse walls to capture any potential uplift. Figure 5.4.7 shows the

uplift recorded on the west side of the south shear wall stack during Phase 3.1 MCE, and it can be seen that the bottom of the panels experienced the most rocking, with the first story having the largest uplift values. The top of the panels experienced smaller uplift and hence less rocking, which was expected. Figure 5.4.8 shows the uplift recorded during Phase 3.3 MCE on both floors of the south shear wall stack as well as the uplift recorded at the base of the transverse walls. There was a concern that the addition of transverse walls on either end of the shear wall stack could inhibit the ability of the CLT panels to rock. Figure 5.4.8.a and b demonstrate that the CLT panels were still able to exhibit rocking behavior even with transverse walls present, and the behavior was similar to Phase 3.1.

Table 5.4.2 – Test sequencing and local story response for each phase.

		Peak uplift[a] [mm]		Peak vertical relative panel displacement[b] [mm]		Peak sliding[c] [mm]		Peak ATS rod force[d] [kN]	
Phase	Test	Story I	Story II	Story I	Story II	Story I	Story II	Story I	Story II
3.1	SLE	4,7	3,3	2,6	1,2	1,7	2,4	44,5	9,8
	DBE	13,2	12,5	7,8	4,7	8,1	9,0	105,1	31,3
	MCE	21,7	16,7	19,6	10,0	12,0	9,4	170,0	66,3
3.2	SLE	4,2	2,7	1,9	1,0	1,1	1,7	45,8	12,7
	MCE	26,1	12,2	13,6	9,9	56,1	32,7	237,6	74,4
3.3	SLE	3,7	2,7	2,1	1,4	2,6	1,1	31,6	10,2
	MCE	14,5	9,4	15,7	13,6	7,2	6,5	-	-

a) Uplift was measured at the upper and lower corners of each wall on both the first and second story
b) Vertical relative panel displacement is the vertical displacement measured at the inter-panel joint between CLT panels
c) Sliding was measured at the top and base of each wall on both the first and second story
d) Load cells were placed on the top and base of each ATS rod

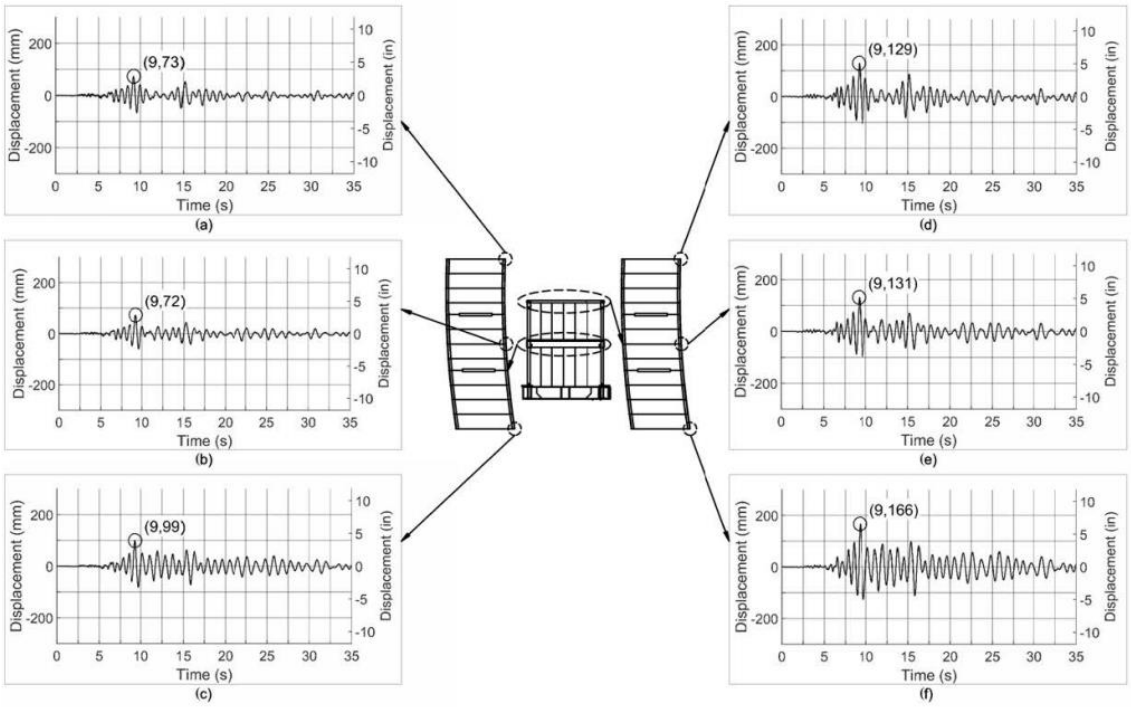

Figure 5.4.7 - Phase 3.1 MCE Wall Uplift: (a) First story shear wall top west corner; (b) First story shear wall bottom west corner; (c) Second story shear wall top west corner; (d) Second story shear wall bottom west corner.

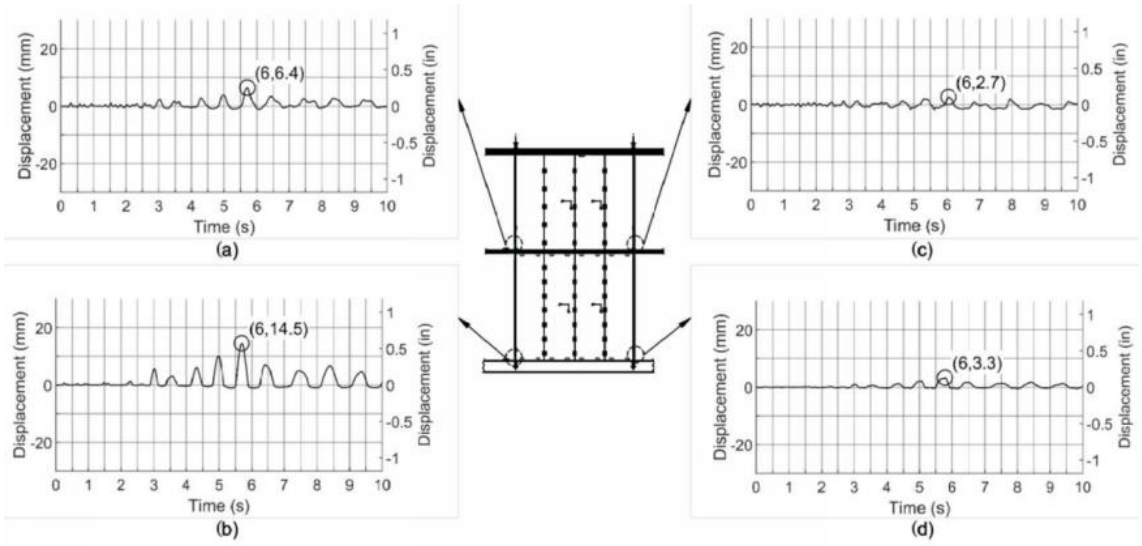

Figure 5.4.8 - Phase 3.3 MCE Uplift: (a) Second story shear wall bottom west corner; (b) First story shear wall bottom west corner; (c) Second story transverse wall top south corner; (d) First story shear wall bottom south corner.

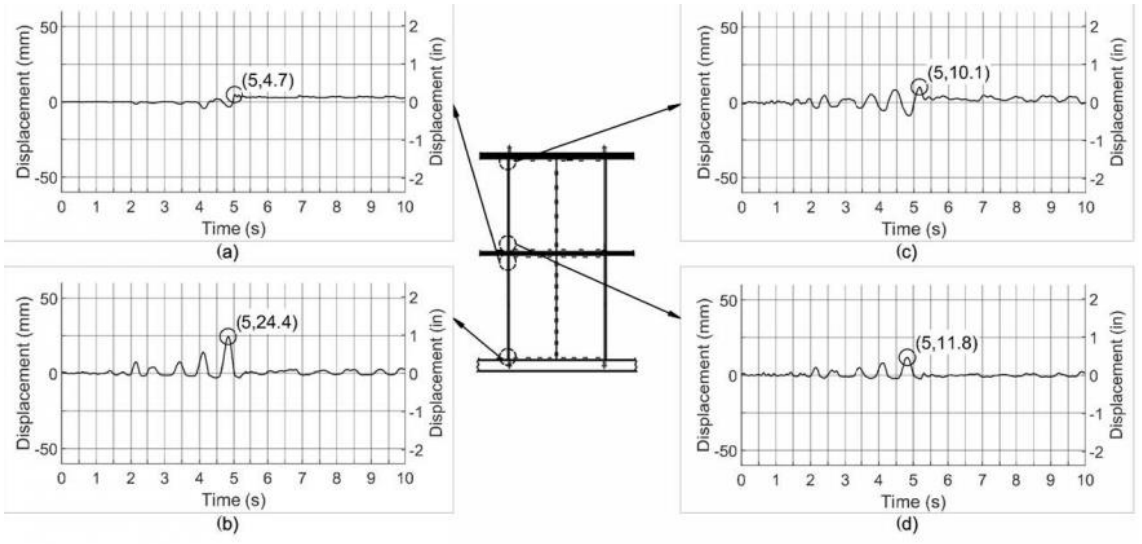

Figure 5.4.9 - Phase 3.2 MCE Uplift: (a) First story shear wall top west corner; (b) First story shear wall bottom west corner; (c) Second story shear wall top west corner; (d) Second story shear wall bottom west corner.

It was expected that the transverse walls would experience minimal uplift during testing, and Figure 5.4.9.c and d show that is indeed the case. The largest uplifts recorded during testing occurred during the Phase 3.2 MCE test, with a peak uplift of 24.4 mm (0.96 in) recorded at the bottom of the first story, but it should be noted that this measurement could have been affected by the nail shearing observed on the first story. Even though the uplift was the largest in Phase 3.2, the test structure still exhibited no risk of collapse. The uplift in Phase 3.2 followed a similar pattern to the other phases with the bottom of the CLT panel experiencing the most rocking behavior on both the first and second stories.

5.4.6. Sliding

The sliding of the shear wall panels was recorded using linear potentiometers positioned

horizontally at the base and top of each shear wall, and Table 5.4.2 summarizes the results. The panel sliding followed a similar pattern to the uplift, with the largest sliding occurring at the base of the panel at each story, and this can be seen in Figure 5.4.10 for Phase 3.1 MCE. The sliding behavior can be partially explained by nail withdrawal as the deformation of the angle brackets work the nails from the CLT. This was especially present for the Phase 3.2 MCE test, where nail shear was observed on the first story, resulting in a sliding of 56.1 mm (2.2 in) as seen in Figure 5.4.11, but although the sliding was large, the test structure was in no danger of collapsing with the tie down rods providing uplift restraint and likely some level of shear through bearing on the hole they passed through in the CLT diaphragm and, in the case of the lower shear walls, the steel support beam acting as a foundation into the shake table.

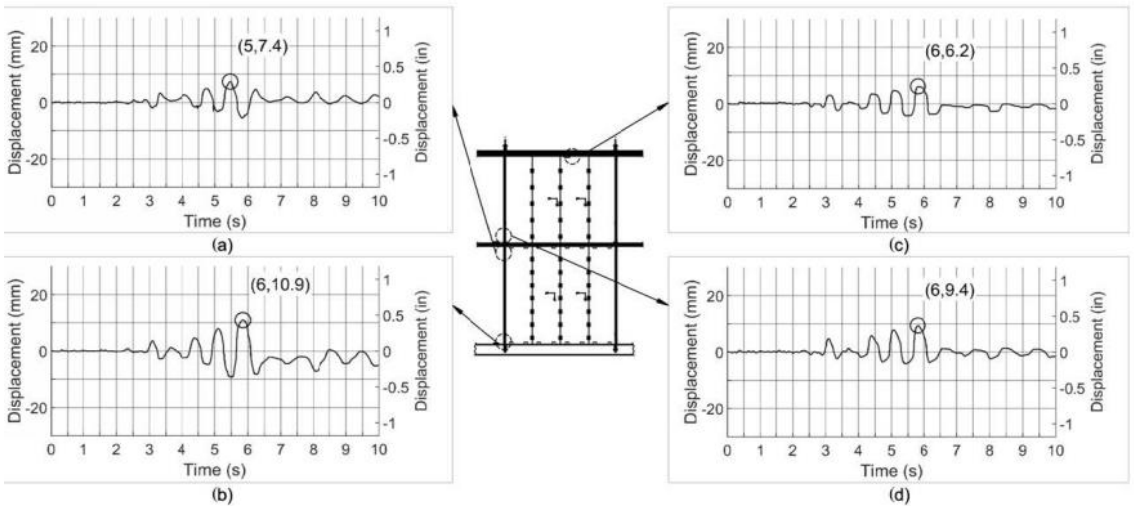

Figure 5.4.10 - Phase 3.1 MCE Sliding: (a) First story shear wall top west corner; (b) First story shear wall bottom west corner; (c) Second story shear wall top west corner; (d) Second story shear wall bottom west corner.

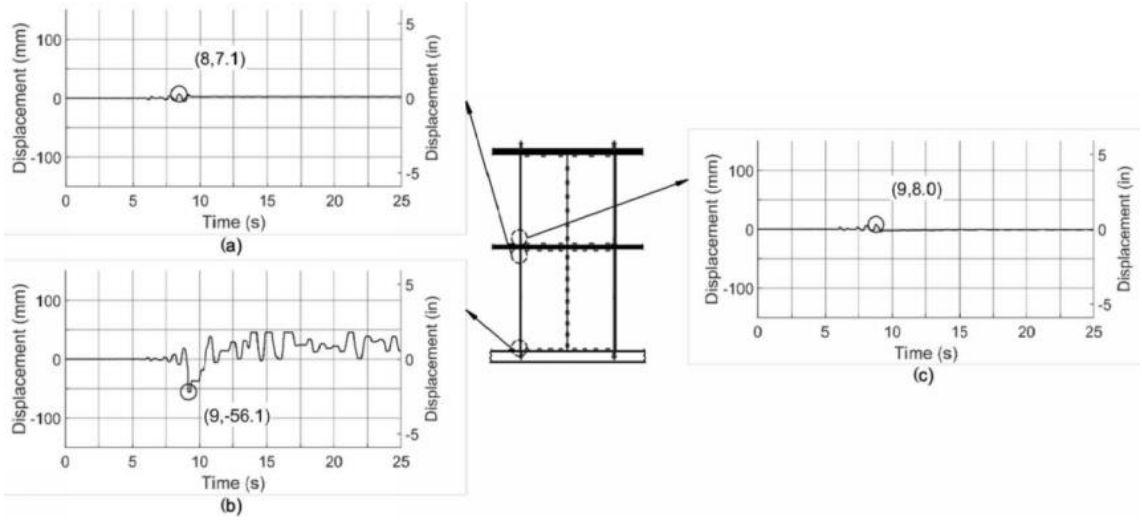

Figure 5.4.11 - Phase 3.2 MCE Sliding: (a) First story shear wall top west corner; (b) First story shear wall bottom west corner (nail shear failure occurred in brackets); (c) Second story shear wall bottom west corner.

5.4.7. Relative panel displacement

Relative panel displacement was measured in the horizontal and vertical direction using

string potentiometers at the inter-panel joints of each CLT panel for all tests and phases. No significant relative displacement was recorded or observed in the horizontal direction, so the vertical direction will be the primary focus, and Table 5.4.2 summarizes the results across the phases. Figure 5.4.12 presents the Phase 3.1 MCE results, and as can be seen, the first story experienced more relative panel displacement than the second story, which was expected given it deformed more overall. The displacement was also relatively consistent across the story with only a 3 mm (0.11 in) difference between the two recorded joints for Phase 3.1 MCE. The relative panel displacements for the 2.1:1 shear wall aspect ratio followed a similar trend to the 3.5:1 aspect ratio walls in Phase 3.1, the largest displacement occurred on the first story, this can be seen in Figure 5.4.13.

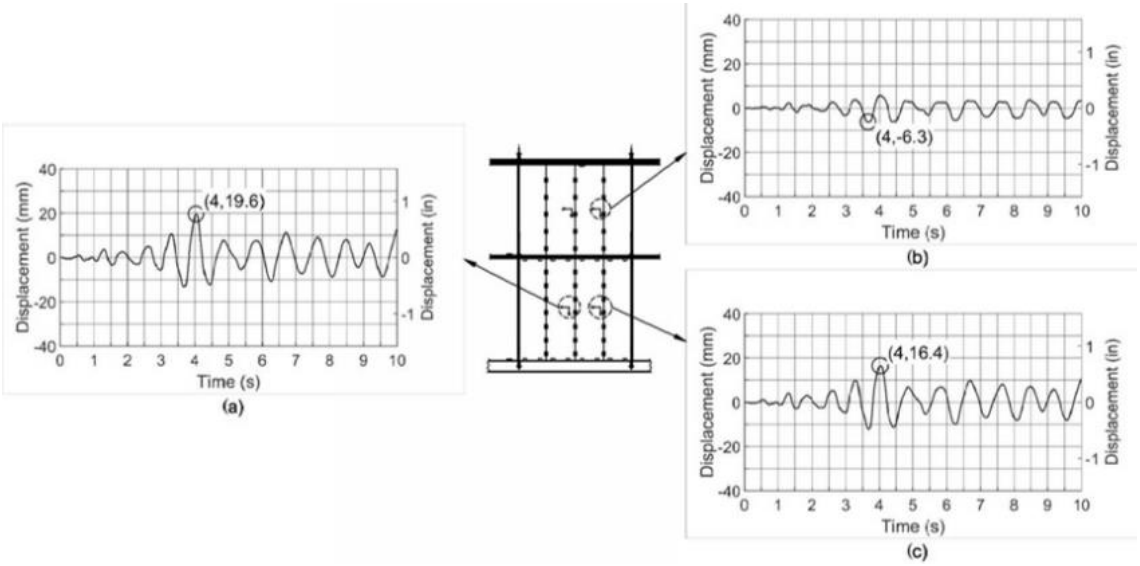

Figure 5.4.12 - Phase 3.1 MCE Vertical Relative Panel Displacement: (a) First story shear wall top west corner; (b) First story shear wall bottom west corner; (c) Second story shear wall top west corner; (d) Second story shear wall bottom west corner.

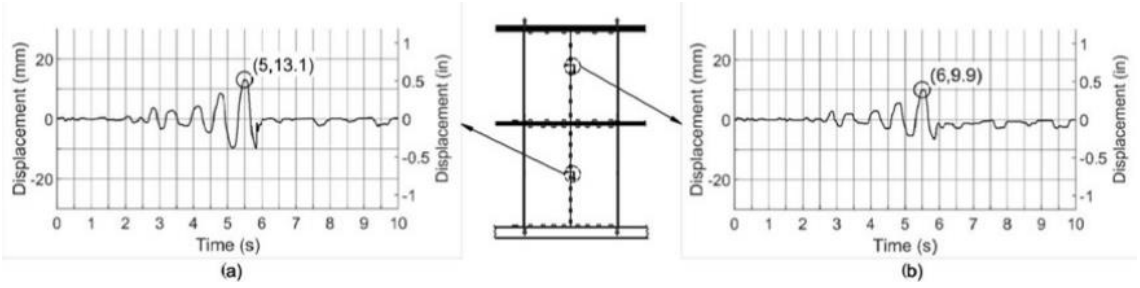

Figure 5.4.13 - Phase 3.2 MCE Vertical Relative Panel Displacement: (a) First story shear wall top west corner; (b) First story shear wall bottom west corner; (c) Second story shear wall top west corner; (d) Second story shear wall bottom west corner.

5.4.8. Forces in tie-down rods

ATS tie-down rods were installed in the SFRS, with a rod on each end of the wall and both faces, with a bearing plate providing a reaction point on each story, similar to standard construction for light-frame wood buildings. This was consistent throughout all the phases, and

in the design of the SFRS, it was assumed that the CLT wall panels worked as a continuous segment with the inter-panel connectors transferring shear, and because of this, tie-down rods were only required at the ends of the walls. The tie-down rods are designed to absorb tension from the overturning moment present in the structure, while the CLT panels and brackets transfer shear. The rods therefore are not designed to take any compression force, and are thus allowed to slide through at the bottom of the structure, allowing the CLT panels to absorb the compression load. The summary of the recorded forces in the rods can be seen in Table 5.4.2. No load cell data was available for the Phase 3.3 MCE level test, so data from strain gauges placed on the tie-down rods was used instead. The largest tension force in the rods was 237.6 kN (53 kips) recorded at the base on the first story during the Phase 3.2 MCE test, which was approximately 94% of the ultimate capacity of the rod. This test included the 2.1:1 aspect ratio walls, and it most likely due to the nail failure in the shear brackets, essentially forcing the hold downs to do 100% of the resistance in uplift. Although the shear brackets are assumed to only resist shear in the design approach for the platform CLT stacked walls herein, they do resist some overturning as the CLT panels rack. A large tension force of 170 kN (38 kips), or 68% of the rod's ultimate capacity, was also recorded during the Phase 3.1 MCE level test, and the tension both in this test and the Phase 3.2 MCE test were enough to cause some yielding in the A36 tie-down rods. Figure 5.4.14 presents the average tension force across both wall faces on the CLT panels from Phase 3.1 MCE level test at both the base and roof of the structure. It can be seen that the loading was not homogenous across the structure, and the east side received more load than the west side. This is a result of the torsion discussed earlier, and both Phase 3.2 and Phase 3.3 showed a similar trend. An objective of the test program was to determine if the addition of transverse walls in Phase 3.3 would decrease the loading in the tie-down rods. Unfortunately, load cell data for Phase 3.3 was unavailable due to technical difficulties. However, strain gauges were placed in strategic locations along the tie-down rods to act as a backup in such an event. Table 3 presents the strain gauge data for one of the tie-down rods for both the Phase 3.1MCE level test and Phase 3.3 MCE level test. It should be noted that in Phase 3.1 MCE level test the maximum recorded force (approx. 167 kN) was approaching the yield point of the tie-down rod, and due to this, it was not possible to convert the strain to force with a satisfactory degree of accuracy. However the difference in strains between the tests are rather significant, with the Phase 3.3 MCE level test experiencing strains an order of magnitude smaller, thus making the conversions to force unnecessary to analyze the performance of the structure. As anticipated, the addition of transverse walls reduced the strain in the tie-down rods, implying reduced force, and ultimately, reduced overturning moment and improved performance.

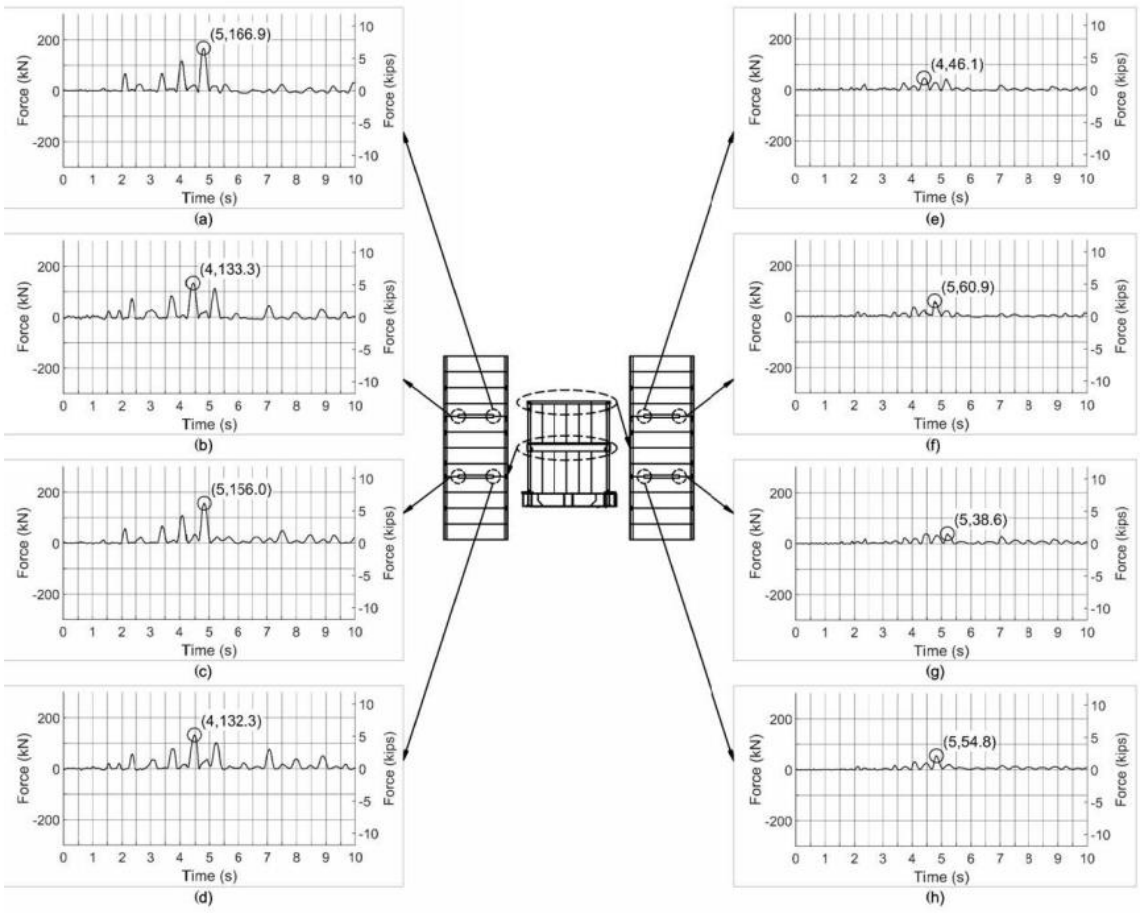

Figure 5.4.14 - Phase 3.1 ATS Rod Load Cells: (a) First story north wall east side; (b) First story north wall west side; (c) First story south wall west side; (d) First story south wall east side; (e) Second story north wall west side; (f) Second story north wall east side; (g) Second story south wall east side; (h) Second story south wall west side.

5.4.9. Overall performance

In all three phases presented herein, each of which consisted of several different ground motion intensities, the structure provided life safety as no significant damage have been spotted throughout the test. Phase 3.1 and Phase 3.3 CLT panels both clearly were governed by rocking behavior as had been demonstrated to occur in high aspect ratio panels. Partial nail pull-out and some steel angle bracket deformation was observed during Phase 3.1 and Phase 3.3 MCE level tests, but this was expected and results indicated that the connectors behaved as intended. It was also observed that the transverse walls installed in Phase 3.3 did not significantly affect the ability of the CLT panels to rock or the connections to perform as designed. Phase 3.2 and the lower aspect ratio panels were governed by sliding, and during the MCE level test, significant sliding and nail shearing was observed, resulting failure of the shear brackets at the base. Although this is far from an ideal behavior, it should be noted that the design used in this test was less than 2/3 the capacity eventually to be proposed for design of platform CLT systems in the U.S.; and also it is important to note that the stability of the structure was never in jeopardy. The tie-down rods experienced some yielding effects in both the Phase 3.1 and Phase 3.2 MCE level tests, but still performed as designed and resisted the overturning moment. In Phase 3.3,

there was no yielding observed due to the improvement in performance provided by the addition of the transverse walls. At SLE and DBE level tests, there was no observable damage in the connections in the shear wall stacks, and no yielding recorded in the tie-down rods. Towards the end of the testing, torsion in structure began to become more pronounced, and introduced some asymmetric loading into the structure, but the SFRS still performed such that there was never risk of collapse at MCE level shaking.

5.5. Concluding remarks

A full-scale two-story CLT platform building with two CLT panel shear wall stacks with tie-downs rods with three different shear wall configurations each tested, namely, 3.5:1 aspect ratio panels, 2.1:1 aspect ratio panels, and 3.5:1 aspect ratio panels with transverse walls installed on each end, being tested. All of the configurations were subjected to the 1989 Loma Prieta ground motion scaled to intensities corresponding to SLE, DBE, and MCE levels respectively, with spectral accelerations ranging from 0.52 g to 1.5 g. The design of the shear wall stacks used the equivalent lateral force procedure with the intent of providing life safety to would-be occupants. Each of the designs met the life safety criteria, and the structure was never in danger of collapse over the course of the testing program. This met the primary objective of the test to demonstrate the effectiveness of CLT shear-walls to provide life safety. The configurations performed as expected with the 3.5:1 aspect ratio being governed by rocking of the panels, and the 2.1:1 aspect ratio governed by sliding of the panels. However, the sliding in the 2.1:1 panels in Phase 3.2 was the result of nail shear failure in the base shear brackets, and thus no true conclusion that 2.1:1 aspect ratio panels has a sliding mechanism as its failure model can be drawn. This was more of a capacity issue given the shear wall capacities were designed at less than 2/3 of what is to eventually be proposed. This was mainly the result of the timing of the shake table test, which was an opportunity to perform the test with a gravity frame in place already, prior to completion of the design method for CLT platform construction being fully validated. However, as described in this study, a number of valuable conclusions were able to be drawn related to the behavior of this type of construction and connections for CLT, and accomplished the goal of providing insight into CLT panel aspect ratios. For example, it was also confirmed that the addition of transverse walls does not affect the ability of the panels to rock, and improves the performance of the tie-down rods. The results of this testing will be used to further refine the methodology for designing CLT SFRS using the equivalent lateral force procedure in the U.S., which will be used to suggest design provisions in the future.

METHODS FOR PRACTICE-ORIENTED LINEAR ANALYSIS IN SEISMIC DESIGN OF CLT BUILDINGS

SHORT SUMMARY

In the context of innovative seismic-resistant structures, Cross Laminated Timber (CLT) construction holds an important position at a global level, supported by important full-scale tests and studies of the non-linear behaviour of these structures for severe events, demonstrating excellent performance. The present study aims to transfer current knowledge in the form of modelling approaches applicable to design engineers presenting tools and methodologies pertinent to the daily procedures of professional practice, thus relating to linear static and dynamic analyses. Two different approaches of structural modelling are presented, validated and compared; the perspective is to cover two different points of view and conception of connections and calculation of the mechanical characteristics of members and connections. Both models are validated by comparing the time-history responses with the full-scale shake-table test results of a 3-storey CLT structure under three earthquakes, showing in both cases a reliable estimate of the structural response. Finally, a parametric study for the damping coefficient of the structural response is presented and the typical value of 5% is discussed.

6.1. Introduction

The primary deformation mechanisms of CLT structures under seismic loads are the rocking and sliding response of the wall panels. Such mechanisms are highly non-linear: rocking is associated to asymmetric resisting mechanisms like mono-lateral wood-to-wood contact between panels and tension-only hold-downs, while sliding depends on the friction characteristics between panels and can affect the initial stiffness of the structure and its energy dissipation capacity. Given that the current state-of-practice of seismic design still lies on the use of linear static or response-spectrum modal analysis, practicing engineers can face significant challenges in the definition and representation of a linear numerical building model. To consider the effective stiffness of the actual connections between the CLT panels, and to yield more accurate estimates of the load paths and the partition of the global shear within the walls of each storey, the modelling approach is a fundamental matter.

Within this context, this chapter presents two different approaches for the construction of

linear numerical models of CLT buildings and the definition of the mechanical properties of the structural components, including the connections. The two methodologies are evaluated based on the experimental data from a series of low-amplitude shake-table tests of a 3-storey full-scale CLT structure [10][40], by performing transient dynamic analyses of the corresponding linear models and comparing the numerical and experimental results in terms of global base shear and lateral roof displacement. The use of linear models is justified since the structure during these tests remained within the elastic range with no plasticity in the connections. Furthermore, the applicability of the typical value of 5% damping in the form of a classical matrix is investigated, calculating the numerical predictions for four different values of viscous damping ratios.

6.2. Test structure and experimental data

This chapter presents the test structure and the experimental data that were used for the validation of the two modelling approaches. A three-storey full-scale rectangular CLT structure with a double-pitched roof, as shown in Figure 6.2.1, was tested under shake-table tests in Tsukuba, Japan, as part of the SOFIE Project [40], which was a co-operative research project supported by the Trento Province, Italy, and coordinated and conducted by the CNR-IVALSA (Italian National Research Council – Trees and Timber Institute). Three different configurations of the test structure were implemented in the testing programme by varying the length of the door opening at the first storey. This study considers the second configuration (conf. B [10]) with a door opening of 2.23 m.

The structure consisted of 5-layer, 85 mm thick (**17**-17-**17**-17-**17**, bold numbers refer to fibres along the primary orientation) CLT wall panels with the primary orientation along the vertical direction and of 6-layer 142 mm thick (**27**-17-**27**-**27**-17-**27**) CLT floor panels. The roof was made of 5-layer 85 mm thick CLT panels, similarly to the walls. A detailed description of the various connections between the CLT panels is provided in chapter 6.3.1.

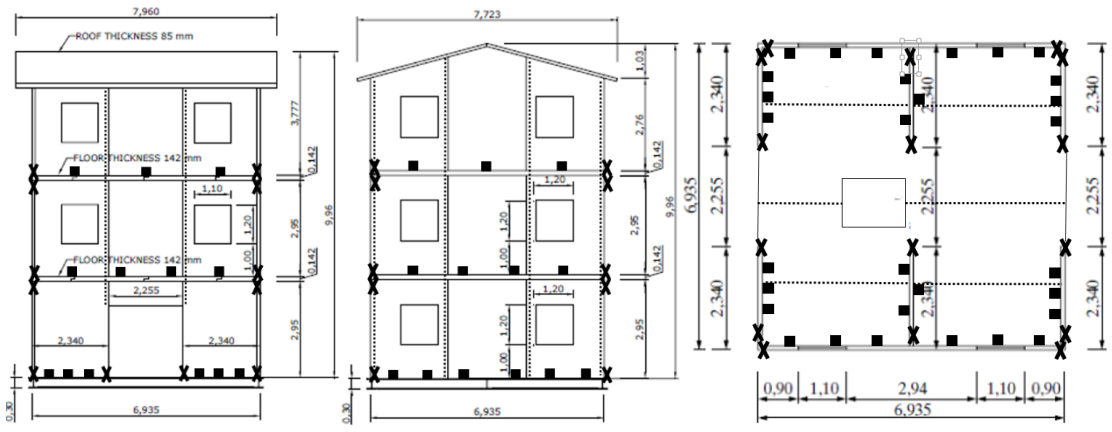

(a) (b) (c)

Figure 6.2.1 - North/South elevations (a), East/West elevations (b), and typical floor plan of Configuration B of the 3-storey structure with location of the metal connectors for the first storey (c) (from [40][62], measures in m).

With the scope of validating numerical models for linear dynamic analysis, three unidirectional shake-table tests with ground motions scaled to a Peak Ground Acceleration (PGA) of 0.15g were considered in this chapter, since the structure under these seismic motions did not exhibit any sign of plasticization in the connections, as verified by the researchers after the tests. The ground motions applied in sequence were Kobe (JMA station, 1995), El Centro (Imperial Valley, 1940) and Nocera Umbra (Marche, Italy, 1997). The pseudo spectral acceleration spectra of the effective table accelerations of these records are illustrated in Figure 6.2.2.a, while Figure 6.2.2.b shows the base shear versus roof displacement response of the test structure. The base shear was calculated from the acceleration measurements in each level, thus including the contribution of internal resisting and damping forces. First an average acceleration time-history was computed for each level, which was then multiplied by the total mass of each storey, taken equal to 21,93, 21,93 and 4,74 tons for the first, second and third storey, respectively. Finally, the three time-histories were summed and multiplied by (-1) to yield the base shear time-history.

The spectral ordinates at the fundamental period of the test structure in the shaking direction (T_2 = 0,183 s), as estimated from white-noise tests, are also identified in Figure 6.2.2.a. As observed in Figure 6.2.2.b, the structural response is coherent with the intensity of each motion in the fundamental period, but it can be clearly noticed that the effective lateral stiffness is slightly decreasing with the increase of the structural response. Since no inelastic response was identified in the connections, this non-linearity is attributed to the friction developed between wall and floor panels. This is the first time that such non-linearity is directly identified in the response of a test structure, mostly because research efforts are typically focused on large-intensity motions that result in a non-linear elastic structural response due to connection plasticization.

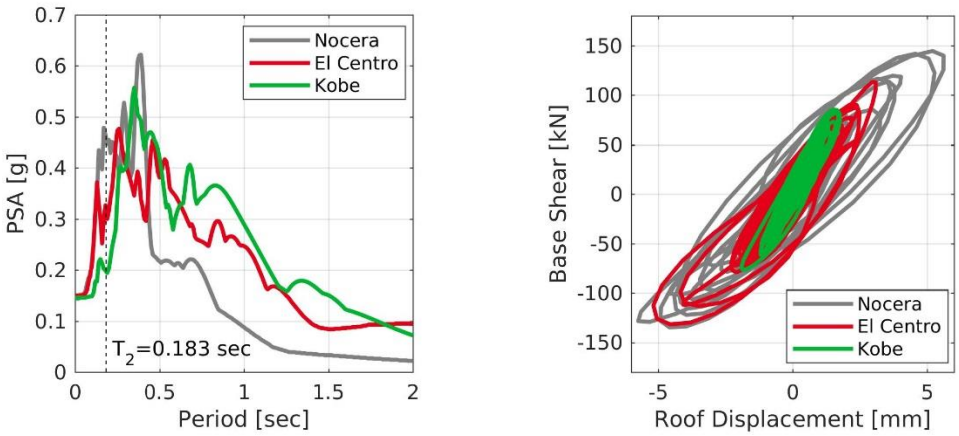

Figure 6.2.2 - Pseudo spectral acceleration spectra of the three ground motions considered (a), and base shear versus roof displacement response of the test structure (b).

6.3. Numerical models

Two different structural modelling approaches are described in the following sections.

The first approach, identified as the distributed-connection model, is based on a distributed representation of the various connections between the structural components. This model is suitable for structural design by practice engineers, since it is easy and fast to represent the desired connections, in terms of type of connectors and spacing, during the iterations implemented in a typical design workflow. It does not offer, however, the possibility to construct a model suitable for non-linear analysis in a sustainable amount of time, since that requires a discrete modelling of each connection.

The second approach on the other hand, identified as the component model [60], is based on a discrete representation of the connections between the structural components and has been conceived for research-oriented studies. Due to this characteristic, this model has the advantage that it can be easily and quickly adjusted for non-linear analysis, but it can be more time-consuming to adjust the connections between design iterations, since it requires mesh changes.

6.3.1. Distributed-connection model

The distributed-connection modelling approach has been designed for the practical creation of realistic three-dimensional CLT buildings with the Finite Element Method (FEM), to be used for design purposes under vertical, wind and seismic forces, considering the inherent assumptions adopted when performing linear static or linear dynamic analyses.

The geometry of the numerical model is composed of planar face entities that represent not only the CLT walls and floors, but also the wall-to-wall and wall-to-floor connections, as shown schematically in Figure 6.3.1.a. All face entities are meshed with linear 3- and 4-node shell elements that include out-of-plane shear deformations and each one has homogeneous orthotropic material characteristics. The thickness of the shell elements and the orthotropic material properties are defined according to the specific behaviour of the structural component represented, as explained later in this section. Each wall face with its adjacent connection faces shares the same nodes along the common edge forming a wall assembly, while wall assemblies and floor faces have coincident double nodes along the common edge, as indicated in Figure 6.3.1.b by the yellow lines. The coincident nodes are constrained to have the same displacement, transferring forces between them, but no constraint is imposed on the rotations resulting in a moment-free connection in the form of a cylindrical pinned support along the common edge. Thus, although floor-to-floor connections are not included in the current implementation, there is no bending stiffness and moment continuity between adjacent floor panels.

With this approach, each connection face represents a one-dimensional connection

element with distributed translational stiffness in the three orthogonal local directions *LTN*, where *L* the Longitudinal direction along the length of the face, *T* the Transverse direction along the width or height of the face, and *N* the Normal direction perpendicular to the face.

The wall-to-floor connections have length equal to the length of the wall panel attached to and height equal to one half of the thickness of the floor panel connected to. Two are the key material properties to be defined. The first is the in-plane shear modulus G_{LT} that is calculated from the shear stiffness provided typically by angle brackets or single dowel-type metal connectors that are spaced evenly along the horizontal (*L*) direction. The second is the modulus of elasticity E_T in the vertical (*T*) direction that is derived from the modulus of elasticity for compression perpendicular to grain of the CLT floor panel. This approach allows, thus, the calculation of the compressive stresses perpendicular to grain in the CLT floor panels placed between wall panels and the associated deformations, which in general can represent a limit for the application of this type of structures. It is, thus, excluded any contribution of hold-downs in the lateral stiffness of a building, assuming that the connections remain in compression under gravity and seismic loads, which is true for very small lateral displacements. This assumption has been deemed necessary for obtaining a single linear building model that can be practically used for all load cases of structural design, as mentioned earlier.

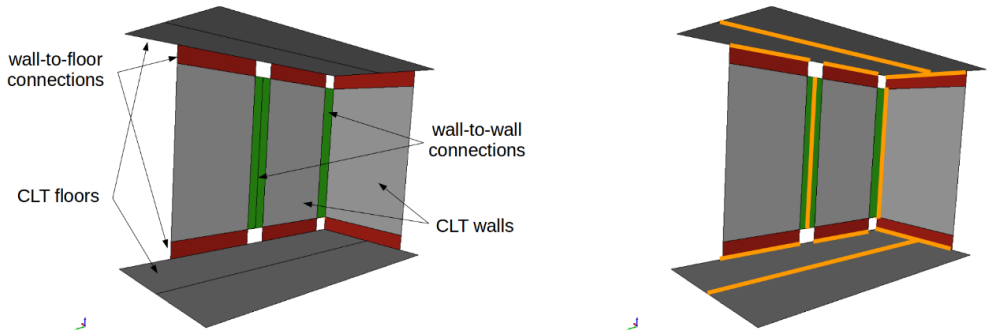

Figure 6.3.1 - Geometry and component identification (a) and location of common edges with coincident nodes, for a typical inter-storey CLT assembly (b).

The wall-to-wall connections between perpendicular walls have length equal to the height of the walls and width equal to one half of the thickness of the wall panel perpendicularly connected to. In this case, the in-plane shear modulus G_{LT} is calculated from the shear stiffness provided by the metal connectors spaced evenly along the vertical (*L*) direction. Instead, for connections between panels in the same plane, the two faces represent the typical vertical joint made with a panel stripe connected to each wall with metal connectors spaced evenly along the vertical (*L*) direction. The width of each connection face in this case is considered in the order of 25 mm.

The elastic properties of the equivalent orthotropic material used for the CLT wall and

floor panels have been calculated based on the effective mechanical cross-section properties that are derived from the basic material properties of the boards and the specific layer configuration of each type of panel. Table 6.3.1 lists the elastic material properties of the boards, which are based on the European C24 strength class [23], and Table 6.3.2 lists the effective flexural (*EI*), shear (*GA*) and axial (*EA*) cross-section properties per linear meter in each direction. The flexural and shear properties are based on the Timoshenko beam theory [72] that has been shown to yield accurate estimates of the elastic response of CLT panels [12], while the last is computed based on the basic composite theory [73]. Indices *L*, *T* and *N* are used to represent the longitudinal or primary direction, the transverse or secondary direction and the normal or direction perpendicular to panel.

Table 6.3.1 - Elastic orthotropic properties considered for the boards of the CLT panels.

Modulus of elasticity parallel to grain, E_0 [MPa]	Modulus of elasticity perpendicular to grain, E_{90} [MPa]	Shear modulus in planes parallel to grain, G_0 [MPa]	Shear modulus in plane perpendicular to grain, G_{90} [MPa]
11000,0	370,0	690,0	69,0

Table 6.3.2 - Effective mechanical cross-section properties of the CLT panels.

Panel ID	EI_L [kNm^2/m]	EA_L [kN/m]	GA_L [kN/m]	EI_T [kNm^2/m]	EA_T [kN/m]	GA_T [kN/m]
CLT-85	449,8	573580,0	9121,9	132,1	392870,0	5605,8
CLT-142	1210,5	903580,0	14971,1	230,5	403970,0	6109,4

The equivalent properties of the homogeneous orthotropic material for each panel, considering the same equivalent thickness, are listed in Table 6.3.3. The equivalent modulus of elasticity in *L* and *T* directions is selected to match the effective axial stiffness *EA*. The only Poisson's ratio that needs to be defined is ν_{LT}, since shell elements do not account for deformations perpendicular to plane. In this study, ν_{LT} is taken equal to zero assuming that deformations in each of the two principal directions are a direct result of stresses in the same direction. This is consistent with the fact that a single homogeneous material is considered based on the actual layers in each principal direction.

Table 6.3.3 - Equivalent elastic material properties for orthotropic shell elements.

Panel ID	E_L [MPa]	E_T [MPa]	E_N [MPa]	G_{LN} [MPa]	G_{TN} [MPa]	G_{LT} [MPa]
CLT-85	6748,0	4622,0	370,0	128,8	79,1	690,0
CLT-142	8454,8	2915,2	370,0	212,5	60,2	690,0

The type and distribution of the angle brackets located at the base of the wall panels for each storey is shown in Figure 6.3.2. Table 6.3.4 lists the characteristics of each type and the elastic stiffness under shear load. The latter is based on the stiffness of each connector, using the EC5 [23] formula for screws rather than for nails, similarly to [27], because of the saw-tooth shape of the Anker nails as opposed to the case of smooth nails.

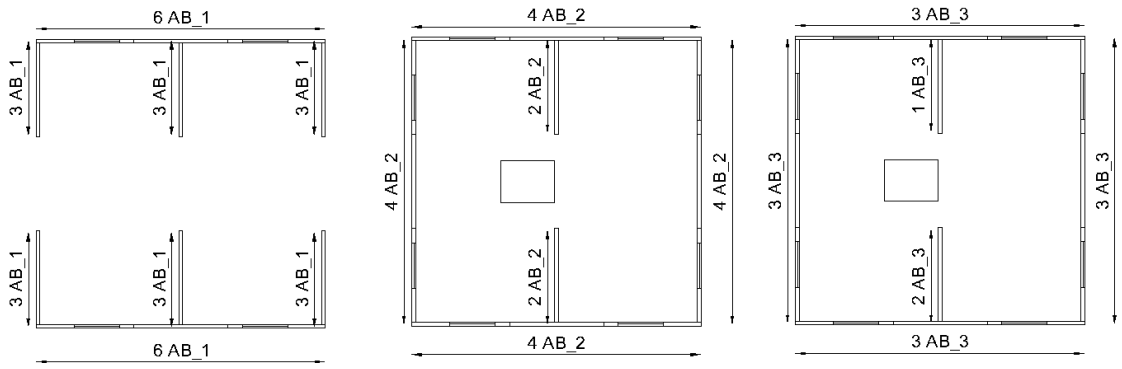

(a) (b) (c)

Figure 6.3.2 - Distribution of angle brackets at the base of the walls for the first (a), second (b) and third (c) storey.

The total stiffness of the angle bracket is computed by multiplying the single connector stiffness by an effective number of connectors, assuming no flexibility from the deformation and rotation of the angle brackets. A multiplier of 2 is also considered for steel-to-timber connections as per the EC5.

Table 6.3.4 - Properties of angle brackets.

Type and characteristics	Stiffness under shear load
AB1: BMF 90x48x3,0x116 angle bracket connected to the wall with 11 φ4x60 anker nails and to the foundation with one φ16 anchor bolt	11*2*420^1.5*4/23 = 32,9 kN/mm
AB2: BMF 105 angle bracket connected to the wall with 8 φ4x60 anker nails and to the floor with 8 φ4x60 anker nails	(8/2)*2*420^1,5*4/23 = 12,0 kN/mm
AB3: BMF 105 angle bracket connected to the wall with 5 φ4x60 anker nails and to the floor with 5 φ4x60 anker nails	(5/2)*2*420^1,5*4/23 = 7,5 kN/mm

Vertical joints between in-plane wall panels in the same assembly are realized with an internal LVL stripe connected to each panel with a row of screws. Table 6.3.5 lists the connection schedule for each storey and the elastic stiffness per linear meter under shear load. The latter is calculated from the stiffness of each row divided by 2 to apply the effect of the two springs in series.

Table 6.3.5 - Properties of vertical joints between in-plane wall panels in the same assembly.

Storey	Type and characteristics	Stiffness under shear load
1	2 φ8x80 @ 450 mm	420^1,5*8/23/0,45/2 = 3,3 kN/mm/m
2	2 φ8x80 @ 600 mm	420^1,5*8/23/0,60/2 = 2,5 kN/mm/m
3	2 φ8x80 @ 900 mm	420^1,5*8/23/0,90/2 = 1,7 kN/mm/m

Table 6.3.6 lists the connection schedule for each storey and the elastic stiffness per linear meter under shear load for the floor-to-wall connections at the top of the wall panels. Table 6.3.7 lists the connection schedule for each storey and the elastic stiffness per linear meter under shear load for the vertical joints between perpendicular wall panels.

Table 6.3.6 - Properties of floor-to-wall connections at the top of the wall panels.

Storey	Type and characteristics	Stiffness under shear load
1	φ10x260 @ 150 mm	420^1,5*10/23/0,15 = 24,9 kN/mm/m
2	φ10x260 @ 150 mm	420^1,5*10/23/0,15 = 24,9 kN/mm/m
3	φ10x260 @ 900 mm	420^1,5*10/23/0,90 = 4,2 kN/mm/m

Table 6.3.7 - Properties of vertical joints between perpendicular wall panels.

Storey	Type and characteristics	Stiffness under shear load
1	φ10x180 @ 150 mm	420^1,5*10/23/0,15 = 24,9 kN/mm/m
2	φ10x180 @ 150 mm	420^1,5*10/23/0,15 = 24,9 kN/mm/m
3	φ10x180 @ 150 mm	420^1,5*10/23/0,15 = 24,9 kN/mm/m

For the floor-to-wall connections the following method has been followed to obtain the equivalent material properties and the equivalent thickness of the shell elements. Considering an equivalent thickness equal to that of the wall attached to, the modulus of elasticity E_T in the vertical (*T*) direction is taken equal to 450 MPa as a more representative average value of the modulus of elasticity for compression perpendicular to grain of CLT floor panels [65]. The other two moduli in the horizontal in-plane (*L*) and out-of-plane (*N*) directions, E_L and E_N, are taken equal to 1% of E_T to minimize the contribution of these elements in the out-of-plane floor- and in-plane wall-bending mechanisms. The in-plane shear modulus G_{LT} is computed based on the corresponding shear stiffness of the connectors provided in Table 6.3.4 and Table 6.3.6, assuming that only shear deformations contribute to the lateral in-plane deformations of the connection face. Regarding the lateral out-of-plane deformations, the other two shear moduli, G_{LN} and G_{TN}, have the same values as G_{LT} for practical reasons and based on the fact that they have minimal effect on the global stiffness of the building. The three Poisson's ratios are all taken equal to zero.

The same method is applied for the wall-to-wall vertical connections, considering the same value of 450 MPa for the elastic modulus in the horizontal (*T*) direction and using the connection stiffness values provided in Table 6.3.5 and Table 6.3.7, for joints between in-plane and perpendicular wall panels, respectively.

The seismic mass of 21,93, 21,93 and 4,74 tons for the first, second and third storey, respectively, is evenly distributed to the CLT floor and roof panels of each level by adjusting the density of the homogeneous material to reflect the contribution of the mass of additional weights and of the self-weight of the portions of the CLT walls attributed to each floor.

The numerical model is implemented in the general, open-source, FEM solver Code_Aster [20], an industry-validated solver with a vast library of displacement-based isoparametric elements and a complete range of features for performing all major types of analyses, including the consideration of material and geometric non-linearities. The geometry and mesh of the numerical model are created using Salome-Meca, an open-source simulation

platform that includes specific modules for the generation of the geometry and mesh of the building model and for the visualization of the graphical results obtained by Code_Aster.

With the objective of proposing and implementing a detailed numerical model suitable for linear analysis by practicing engineers, a dedicated tool, Aetherium, has been developed to specifically facilitate the entire workflow, from the creation of the model, such as the assignment of object properties and the definition of boundary conditions, to the execution of the desired type of analysis and the extraction of specific results. Aetherium is based on a native geometry algorithm for managing all information related to each structural component at each point of the workflow and on specific script-driven operations to achieve the automatic creation of the specific input data needed for performing the analysis with Code_Aster. Figure 6.3.3 shows the geometry of the distributed-connection model of the test structure.

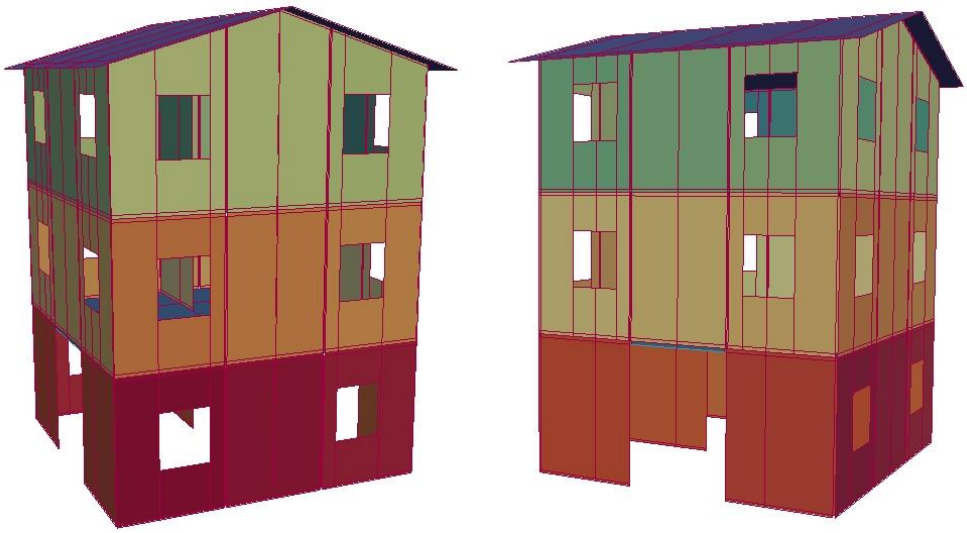

(a) (b)

Figure 6.3.3 - West view (a) and north view (b), of the geometry of the distributed-connection model.

6.3.2. Component model

The component model described is based on the meshing approach presented in [60], but using only connections with linear behaviour.

On the base of the geometry depicted, a FEM model has been created using the general-purpose software NextFEM Designer [44]. For wooden panels, 4-nodes linear shell elements have been used, whereas linear spring elements have been used to model metal fasteners and screw connections. The mesh is structured and has been easily created from inside the mentioned software.

The wooden material is assumed as isotropic. The Blaβ-Fellmoser formulas have been used to find an average Young modulus, which has been found equal to 5,7 GPa [7] for vertical walls. No mass is associated to these elements, since it has been lumped at floor levels only. For slab panels, they have been set as rigid, in order to avoid unrealistic local modes for these panels

as all masses are concentrated there. A conventional Young modulus of 10 times the one for vertical walls has been used for floor diaphragms and roofing panels.

The solver used in NextFEM Designer is OOFEM [48]. Figure 6.3.4 shows the geometry of the component model of the test structure.

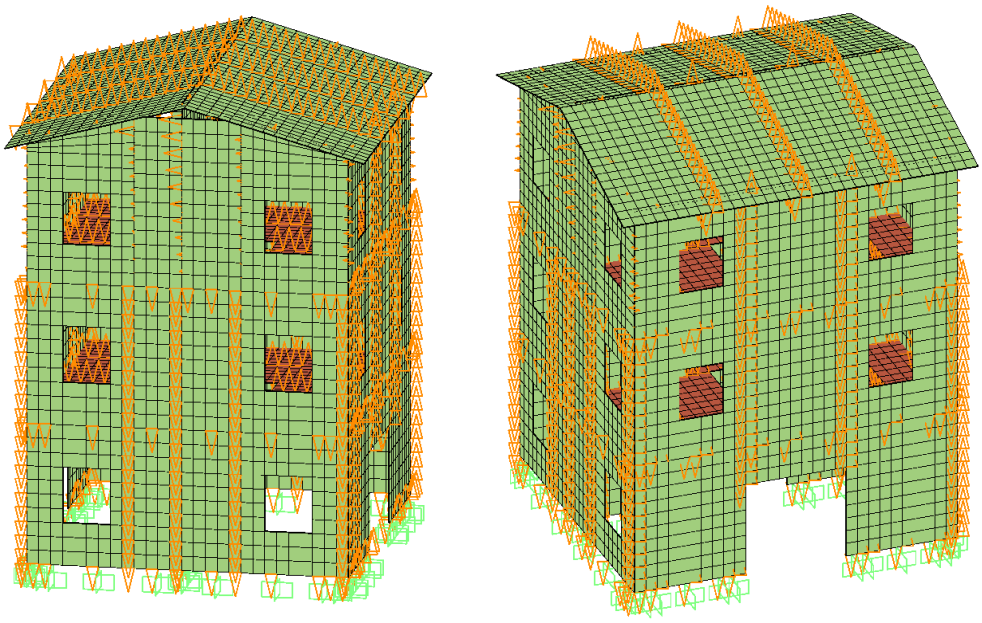

(a) (b)

Figure 6.3.4 - West (a) and North (b) views for the component model in NextFEM Designer [44].

As a linear elastic model, the following schematizations has been adopted:

- Friction has been neglected;
- No analysis is carried out before the modal analysis. In other words, modal forms are calculated considering the undeformed shape without applying vertical loads, as happens for any linear analysis used for design;
- The axial tension and compression stiffnesses of hold-downs and angle brackets have been averaged with the aim to have a single (elastic) value, and by using a conventional value of compression stiffness, equal to 100 times the tension stiffness. Hence, the resulting elastic conventional stiffness is 50 times the elastic one in tension;
- Shear and tension stiffnesses of hold-downs and angle brackets have been taken from the tests made on single connections [35];
- In order to ease the computation, screws linking floor diaphragms and underlying walls have been modelled through less springs, but accounting for the effective number of them in terms of equivalent stiffness;
- All screwed connections have been accounted as rigid, with a conventional stiffness of

100 kN/m, as the friction and the dowel action here (and the 45° inclination of the screws in the floor to underlying walls connection) perform a stiffer joint than the ones of the angle brackets and hold-downs.

Table 6.3.8 shows the values of the stiffnesses (tension/compression and shear) set for metal plates and screw connections.

Table 6.3.8 - Stiffnesses implemented for metal plate connections.

Connection	Tension/Compression stiffness [kN/mm]	Shear stiffness [kN/mm]
Angle brackets ground floor	136 = 50 * 2,72	1,8
Hold-downs ground floor	244 = 50 * 4,88	1,0
Screws for floor to wall connection	383 = (1screw/15cm) * 100 kN/m	383
Hold-downs upper side panels and upper floors	142 = 50 * 2,84	0,8
Angle brackets upper floors	156 = 50 * 3,12	1,5

6.4. Results

This section presents the results obtained from the two numerical models regarding the fundamental periods calculated from a modal analysis and the base shear and roof displacement time-history responses from the linear dynamic analyses with the three experimental motions.

6.4.1. Modal analysis results

The first three vibration periods of the numerical models along with the period of the structure in the shaking direction, associated with the second mode, are listed in Table 6.4.1, while the deformed shapes are illustrated in Figure 6.4.1 and Figure 6.4.2 for the distributed-connection and component model, respectively.

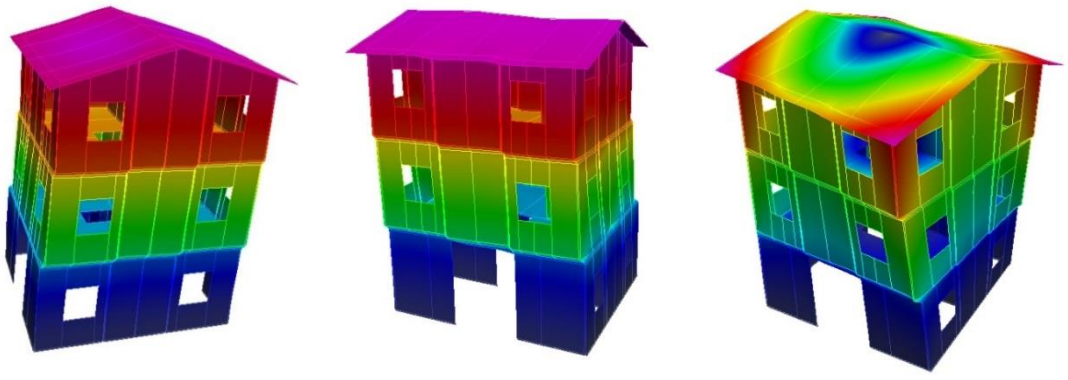

(a) (b) (c)

Figure 6.4.1 - Deformed shape for the (a) first [T_1 = 0,239 s], (b) second [T_2 = 0,199 s], and (c) third [T_3 = 0,137 s] mode of vibration for the distributed-connection model.

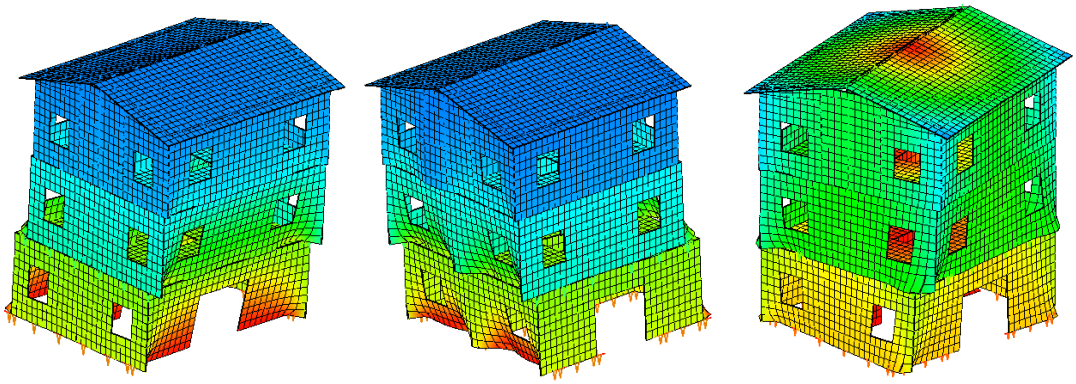

(a) (b) (c)

Figure 6.4.2 - Deformed shape for the (a) first [T_1 = 0,254 s], (b) second [T_2 = 0,223 s], and (c) third [T_3 = 0,152 s] mode for the component model.

Table 6.4.1 - Periods of vibration of the test structure, in the direction of shaking, and the numerical models.

Mode	Experimental [s]	Connection-distributed model		Component model	
		Value [s]	Diff.	Value [s]	Diff.
1	N/A	0,239	N/A	0,254	N/A
2	0,183	0,199	+8,7%	0,223	+21,9%
3	N/A	0,137	N/A	0,152	N/A

Both numerical models predict a fundamental period in the direction of shaking that is higher than the experimental one, by about 10% and 20% for the distributed-connection and component model, respectively. This discrepancy results in a little offset in the response when numerical model and real building are compared.

6.4.2. Time-history analysis results for 5% damping

This section presents the results of the two models in terms of base shear versus roof displacement response, under the three ground motions presented in chapter 6.2 that were scaled to a PGA of 0,15 g, are shown in Figure 6.4.3. The base shear has been calculated similarly to the experimental values; that is from the acceleration results in each level, thus including the contribution of internal resisting and damping forces. The damping in the numerical models is considered with a classical damping matrix in the form of Caughey damping [13] for both models, assigning a single reference value of the viscous damping coefficient desired to the first 9 fundamental modes of vibration. A value of 5% damping, typical in the structural design of buildings, has been considered for these analyses given that the connections of the structure remained elastic; there was, thus, no additional dissipation in the structural response, other than the internal inherent damping.

The predictions obtained from the distributed-connection model are closer to the experimental response, compared to the component model, which is attributed to the closer agreement of the former model, for this case, with the fundamental period of vibration of the

test structure. Nevertheless, in general both models demonstrate a relatively good agreement for El Centro and Nocera Umbra events, while over-estimate substantially the response for the Kobe event where the structure seems to respond in a higher stiffness regime, as discussed in chapter 6.2.

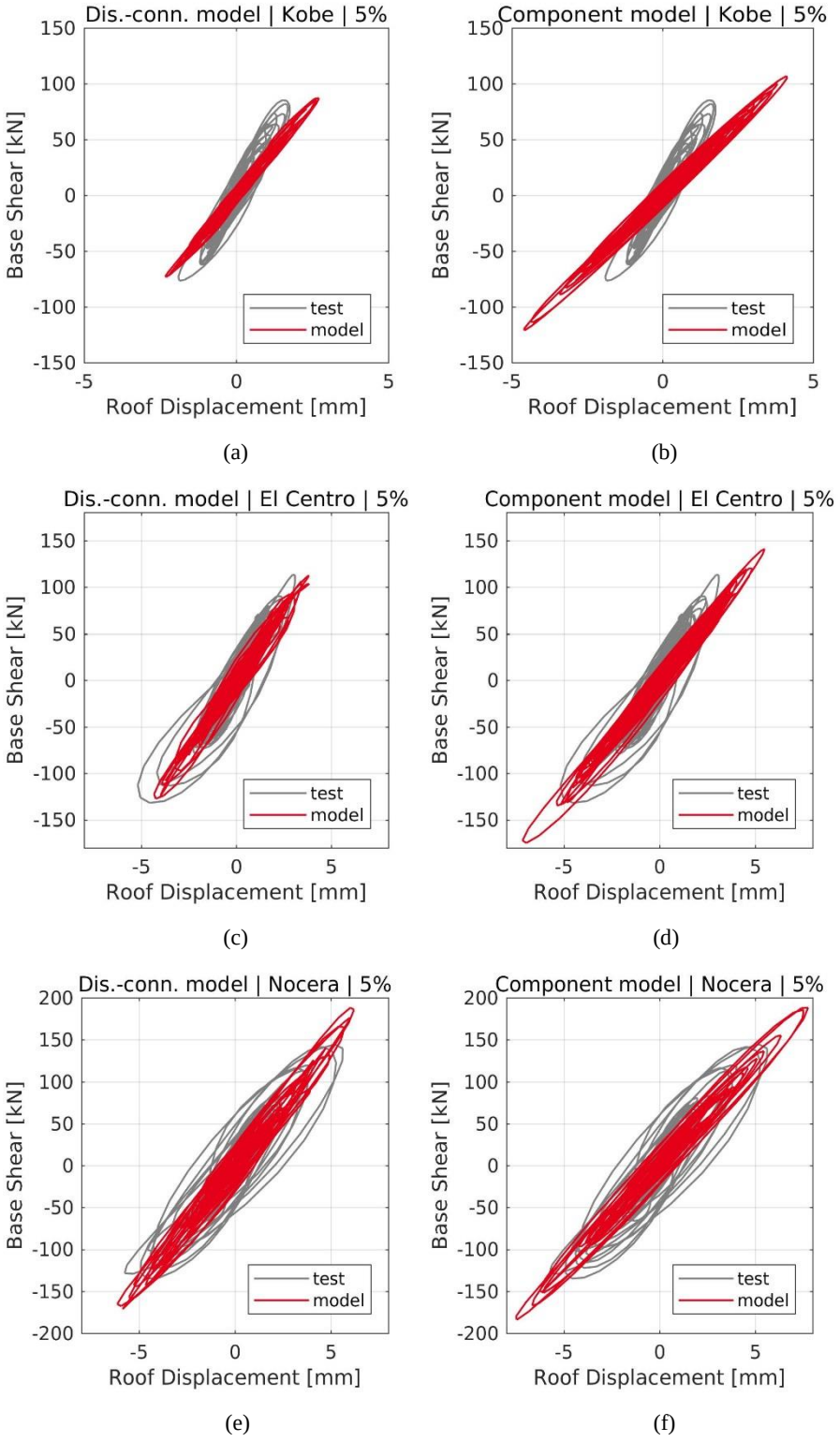

Figure 6.4.3 - Hysteretic loops for 5% damping for the distributed-connection model: Kobe (a), El Centro (c), Nocera Umbra (e). Hysteretic loops for 5% damping for the component model: Kobe (b), El Centro (d), Nocera Umbra (f).

It is observed, however, that the experimental loops have a higher dissipation capacity with thicker response cycles, a characteristic that is governed by structural damping. This can be seen qualitatively in Figure 6.4.4 that superposes the experimental loop obtained for the ground motion of Nocera Umbra, with the response, shown in dashed line, of a system having the area corresponding to a damping of 5% with the same displacement and force limits. As it can be clearly seen, the experimental response is much wider. A bigger size of these cycles together with the awareness that, in this kind of buildings subjected to seismic loads, wood pieces rub against each other, led to the consideration of friction as an important contribution for energy dissipation, especially for low intensity motion as the ones considered. For this reason, analyses with higher damping have been carried-out and presented in the following section.

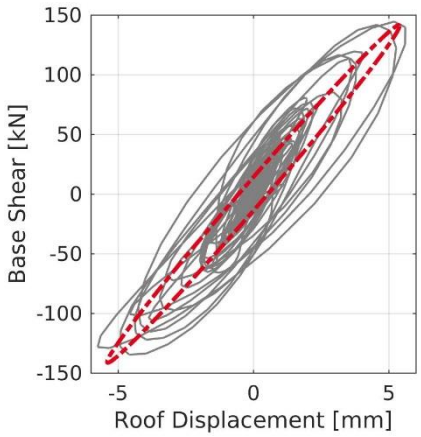

Figure 6.4.4 - Roof displacement vs. base shear diagram from the experimental response under Nocera Umbra and a loop with an equivalent damping of 5% for the same maximum displacement and base shear.

6.4.3. Parametric study for additional damping values

To better represent the real behaviour of the structure accounting for a higher dissipation, different values of damping have been tested numerically. More specifically additional values of 10%, 15% and 20% of viscous damping have been considered for both numerical models for the three seismic motions to identify the most suitable value for each case.

Table 6.4.2 - Comparison for the Kobe event in terms of maximum and minimum values of roof displacement d and base shear V [bold numbers indicate the best fit].

	Test	Distributed-connection model				Component model			
		$\zeta = 5\%$	$\zeta = 10\%$	$\zeta = 15\%$	$\zeta = 20\%$	$\zeta = 5\%$	$\zeta = 10\%$	$\zeta = 15\%$	$\zeta = 20\%$
d_{min} [mm]	-1,91	-2,34	-2,36	-2,17	-2,00	-4,61	-3,81	-3,36	-3,09
Error [%]		22,6	23,9	14,1	**5,1**	141,7	100,1	76,0	**61,9**
d_{max} [mm]	1,76	2,72	2,62	2,45	2,31	4,14	3,66	3,44	3,22
Error [%]		54,7	48,9	39,2	**31,4**	135,4	108,1	96,0	**83,1**
V_{min} [kN]	-76,47	-73,05	-74,79	-71,60	-68,38	-121,03	-102,47	-91,85	-86,53
Error [%]		-4,5	**-2,2**	-6,4	-10,6	58,3	34,0	20,1	**13,2**
V_{max} [kN]	85,33	87,21	85,34	82,55	79,95	106,92	98,17	94,38	89,91
Error [%]		2,2	**0,0**	-3,3	-6,3	25,3	15,0	10,6	**5,4**

Table 6.4.3 - Comparison for the El Centro event in terms of maximum and minimum values of roof displacement d and base shear V [bold numbers indicate the best fit].

	Test	Distributed-connection model				Component model			
		$\zeta = 5\%$	$\zeta = 10\%$	$\zeta = 15\%$	$\zeta = 20\%$	$\zeta = 5\%$	$\zeta = 10\%$	$\zeta = 15\%$	$\zeta = 20\%$
d_{min} [mm]	-5,18	-4,32	-3,72	-3,41	-3,13	-7,16	-5,79	-4,55	-3,93
Error [%]		-16,5	-28,1	-34,2	-39,4	38,4	11,8	-12,2	-24,1
d_{max} [mm]	3,09	3,84	3,13	2,43	2,11	5,49	4,56	3,66	3,11
Error [%]		24,2	1,2	-21,4	-31,6	77,6	47,7	18,6	0,6
V_{min} [kN]	-131,69	-127,27	-110,74	-106,50	-101,90	-174,73	-143,95	-117,47	-107,05
Error [%]		-3,4	-15,9	-19,1	-22,6	32,7	9,3	-10,8	-18,7
V_{max} [kN]	113,15	112,55	94,11	77,08	76,50	140,84	119,97	99,81	86,92
Error [%]		-0,5	-16,8	-31,9	-32,4	24,5	6,0	-11,8	-23,2

Table 6.4.4 - Comparison for the El Centro event in terms of maximum and minimum values of roof displacement d and base shear V [bold numbers indicate the best fit].

	Test	Distributed-connection model				Component model			
		$\zeta = 5\%$	$\zeta = 10\%$	$\zeta = 15\%$	$\zeta = 20\%$	$\zeta = 5\%$	$\zeta = 10\%$	$\zeta = 15\%$	$\zeta = 20\%$
d_{min} [mm]	-5,75	-6,14	-4,24	-3,42	-2,98	-7,50	-5,11	-4,25	-3,77
Error [%]		**6,8**	-26,2	-40,5	-48,1	30,6	**-11,1**	-26,0	-34,4
d_{max} [mm]	5,61	6,20	4,44	3,43	2,88	7,76	5,75	4,50	3,83
Error [%]		**10,5**	-21,0	-38,8	-48,7	38,2	**2,5**	-19,9	-31,8
V_{min} [kN]	-134,66	-171,15	-127,77	-106,33	-96,46	-183,95	-132,55	-115,10	-105,12
Error [%]		27,1	**-5,1**	-21,0	-28,4	36,6	**-1,6**	-14,5	-21,9
V_{max} [kN]	144,42	188,28	135,37	111,55	98,09	188,23	143,26	119,74	106,21
Error [%]		30,4	**-6,3**	-22,8	-32,1	30,3	**-0,8**	-17,1	-26,5

Figure 6.4.5 shows the analyses for which the best agreement with the experimental results was obtained, while a summarizing view of the maximum and minimum values of the roof displacements and base shear forces for both models for Kobe, El Centro and Nocera Umbra ground motions are shown in Table 6.4.2, Table 6.4.3 and Table 6.4.4 respectively.

Although the analyses with 5% damping demonstrate a relatively good agreement, a value of 10% seems to be on average more representative of the inherent damping of the system. More specifically, for the Kobe event the numerical loops for 20% damping illustrate a width comparable to the thickness of the test loops. For El Centro and Nocera Umbra the numerical loops are not as wide as the test loops but the response in terms of maximum values is closer, while the effective global stiffness is in good agreement.

A final comparison between experimental and numerical results in terms of roof displacement and base shear time-histories is shown in Figure 6.4.6 and Figure 6.4.6, respectively. This different aspect of visualization of the same results reveals that the agreement of the transient responses is, on the contrary of what the plots evidences, better for the Kobe event and less accurate for the El Centro and Nocera Umbra events. These observations lead to a strong indication that the test structure does remain linear elastic during the first event, while some type of nonlinearity is instilled in the response of the system during the latter two events. This is believed to be relevant to the friction that is primarily developed in the interface between

walls and floor panels.

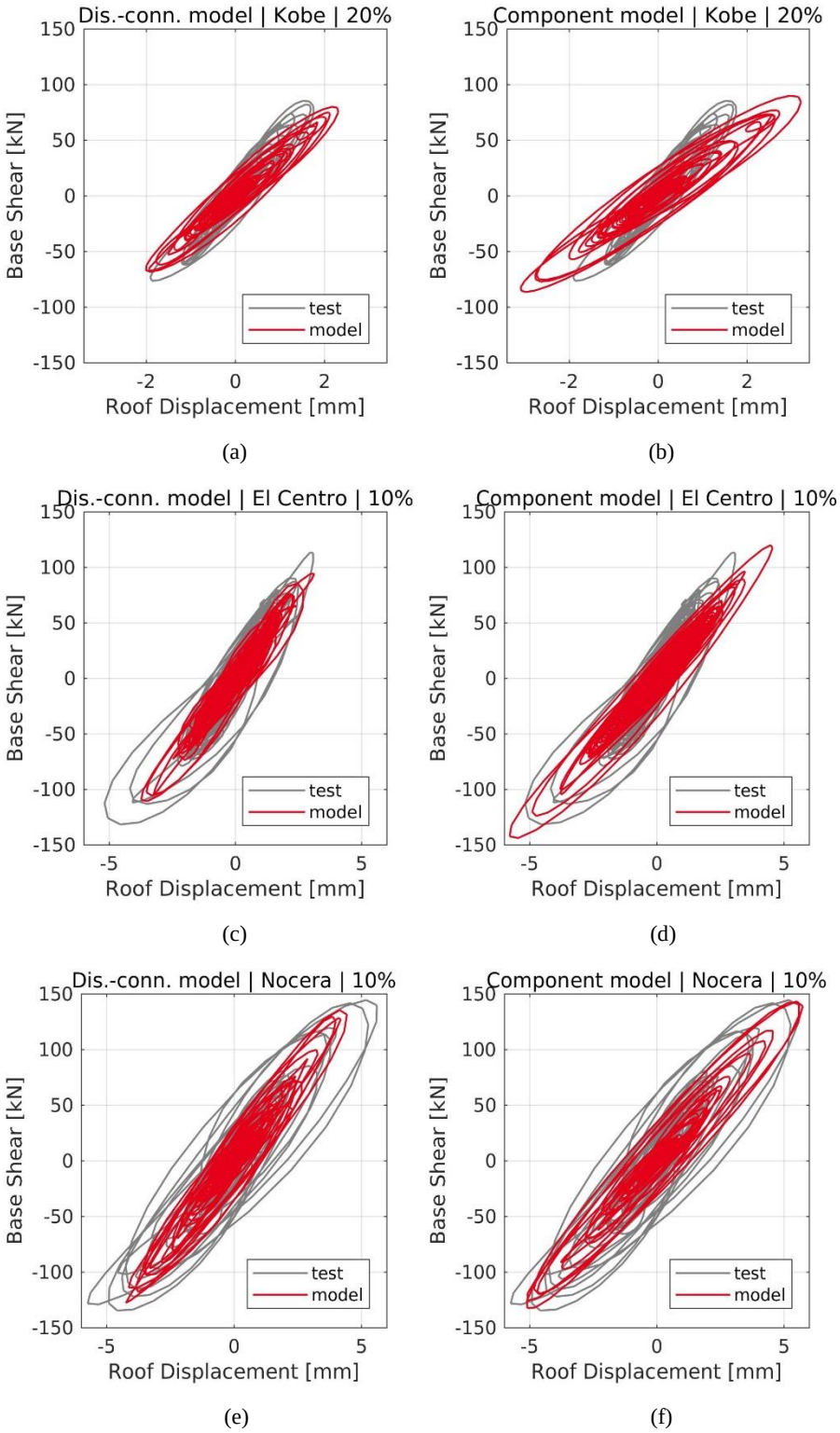

Figure 6.4.5 - Hysteretic loops for the distributed-connection model: Kobe – 20% (a), El Centro – 10% (c), Nocera Umbra – 10% (e). Hysteretic loops for the component model: Kobe – 20% (b), El Centro – 10% (d), Nocera Umbra – 10% (f).

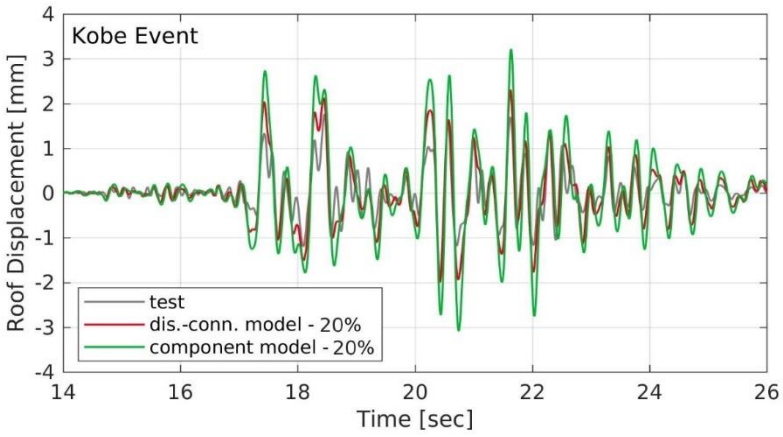

(a)

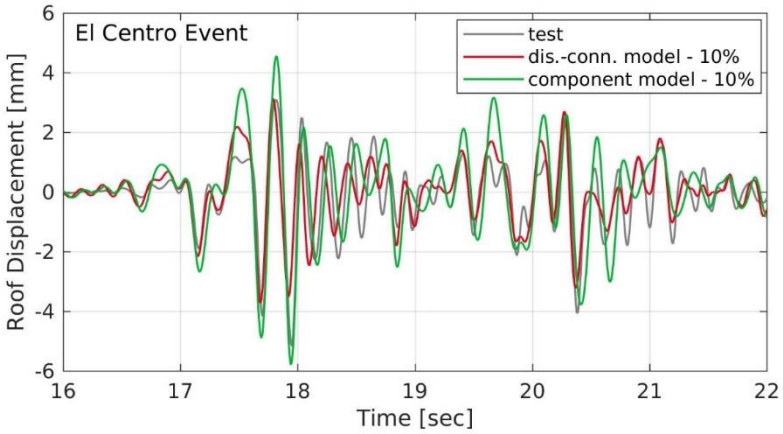

(b)

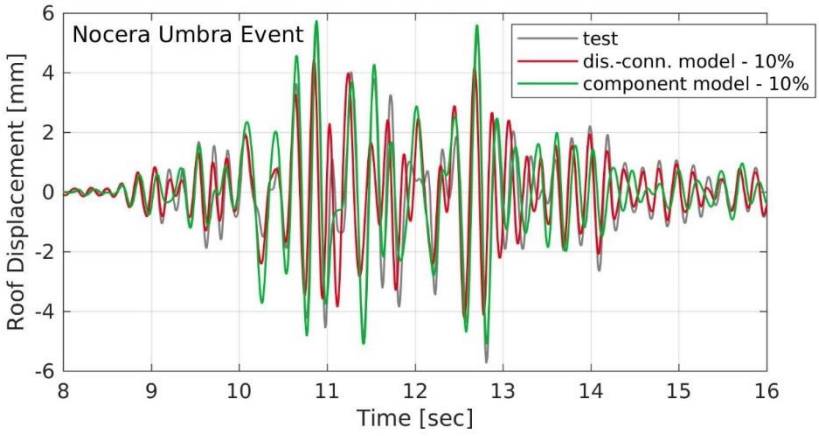

(c)

Figure 6.4.6 - Roof displacement time-histories for: Kobe – 20% (a), El Centro – 10% (b), and Nocera Umbra – 10% (c).

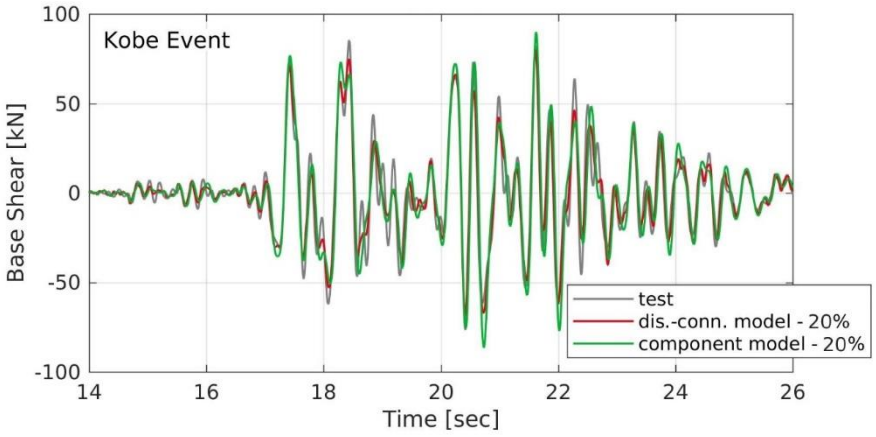

(a)

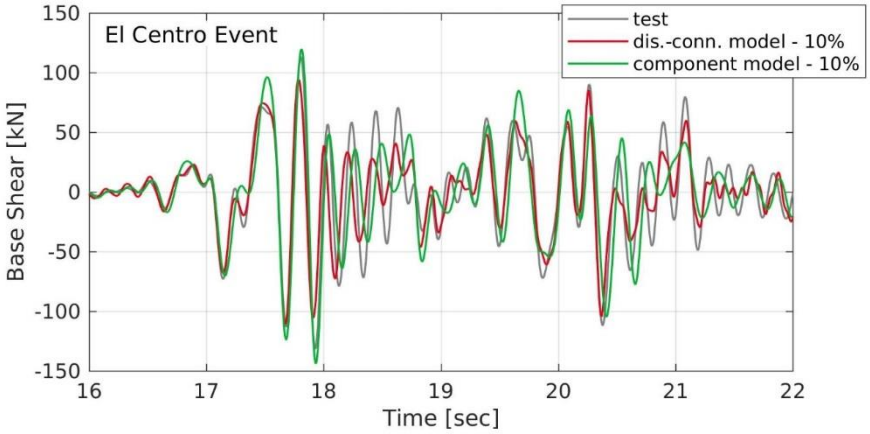

(b)

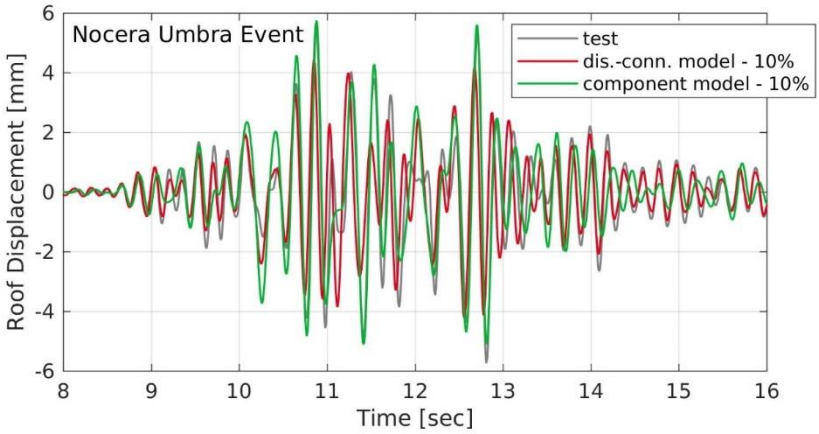

(c)

Figure 6.4.7 - Base shear force time-histories for: Kobe – 20% (a), El Centro – 10% (b), and Nocera Umbra – 10% (c).

For Kobe, the sliding in the interface between walls and floors seems to be restrained due to the low shaking and the stiffness of the building is driven mostly by the stiffness of the CLT panels. For El Centro, instead, and even more for Nocera Umbra, the resistance of friction could be exceeded in certain instants leading to a global stiffness that is the result of the additional connection stiffness in series with the panel stiffness. However, these are only assumptions and

further research of these aspects is needed for a better investigation of these very important phenomena, which cannot be easily accounted for in an equivalent way on linear analyses.

6.5. Concluding remarks

In this chapter, the dynamic response of the 3-storey CLT building tested within the SOFIE project [40] has been investigated through linear models built using two different approaches. In the first approach, the metal connectors between CLT panels have been modelled with shell elements, by distributing their stiffness along the wall edge. In the second approach, the walls have been connected by elastic spring elements, representing each one a single connector.

The results obtained from the transient dynamic analyses with the two approaches have been compared with the experimental results available from SOFIE project. Such comparison has been conducted on the base of the maximum and minimum base shear and roof displacement obtained.

The linear building models based on the described modelling approaches can provide reliable estimates of the structural response under low-amplitude seismic excitations. Moreover, it has been found that the analysed structure exhibited a higher energy dissipation than the simulation conducted with the 5% of damping ratio. For this reason, more linear analyses with higher damping ratios have been conducted. As a result, they evidenced a better estimation of the structural response.

Hence, one interesting aspect evidenced in the present work is that the equivalent damping ratio to be considered in a linear analysis of a CLT building could be used to take into account the energy dissipation provided by friction. Such effect is conservative, as it leads to higher equivalent damping ratios. By taking into account the principle of structural resilience [64], a seismic swarm that could hit the building will probably lower the damping in the structure. Such fact allows the designer to use the most common value of the damping ratio (5%) and to implicitly accept higher design displacements, as a result of the progressive deterioration of the friction effect between panel edges and as a conservative parameter. Obviously, the kind of structural behaviour showed in this work is related to the analysed building, and this work has to be extended to other static schemes and seismic events to draw general provisions.

The simplifications introduced in this work are oriented to the representation of the fundamental structural components with a practice-oriented approach, and not to a research-oriented modelling procedure. The use of conventional stiffnesses and any other simplifications are addressed to practicing engineers, with the final aim to allow that reliable results be obtained with common tools.

CONCLUSIONS

In this thesis, different aspects concerning CLT structures and their behavior have been investigated.

In chapter 3, a simplified method for the design of CLT connections is presented. This approach have proven to be reliable when compared to FE analyses, showing always a safety factor higher than one. It also gives information on the inter-story drift, the resistant axial force-bending moment domain and the neutral axis position for a given set of external loads.

In chapter 4, the design and behavior of the panel-to-panel connection and how an overlaying diaphragm influences its behavior is investigated. In the chapter a formula for the design of such connection is suggested basing on the characteristics of the other elements composing the assembly (i.e. panels and base connections). The formula has given acceptable results when used to predict the behavior of full-scale tests and, after a modification, it has shown good accuracy when predicting FE models behavior for a very large set of different parameters (e.g. connections arrangement, axial load, etc). In the second part of this chapter, the influence of the diaphragm and relative connection have been investigated. Connections have proven to play a very important role, whereas different type of diaphragm have not. The study highlighted. Results of assemblies with diaphragm and same assembly without diaphragm have been compared in terms of rocking capacity, lateral displacement contribution and rocking behavior

Chapter 5 presents the results of different full-scale shaking table tests of a 2-story CLT platform structure. These tests have been performed to evaluate the goodness of a novel design approach for these structures to be implemented in the US codes. The structure, subjected to seismic motion, ranging from 0.52 to 1.5 g, was never in danger to collapse. Phase 3.2, characterized by an aspect ratio of panels 2,1:1 gave different results from what expected due to the particular type of construction (i.e. walls placed in an already built structure), but, besides that, the tests gave valuable information and confirmed many predictions.

The last chapter, chapter 6, assess the influence of different modelling approaches and different value of damping in the prediction of the real behavior of CLT structures subjected to low intensity seismic motions. Damping, in this configuration, can be used to account for the energy dissipated through friction, as in full-scale tests it has been proven that this contribution is consistent and the structure itself show a higher energy dissipation than the one related to a common value of 5%. However, as the contribution of friction tends to lower for subsequent seismic motion, designers can use the value of 5%, accepting implicitly that the structure would

dissipate more than for what has been designed.

Further research should address the influence of the segmentation of the CLT diaphragm, walls formed with a higher number of panels, perpendicular walls and other story on the rocking behavior and capacity of wall assemblies.

Moreover, with lab tests, in order to devise reliable design procedures, researchers should study how different number and type of fasteners in a same metal plate connection influence its behavior and its capacity and how different arrangements of metal plates connection (i.e. number and disposition) influence the capacity and behavior of wall assemblies. These type of tests could give very useful hints on the design and numerical model of CLT structures when specific lab tests on the same connections or arrangements are not available.

ANNEX A – DESIGN EXAMPLE

8.1. Introduction

In this section, a brief example of a design made through the formulations proposed in chapter 3 and 4 is presented.

8.2. Example

Using the Italian design regulation (NTC2018) for the calculation of the seismic action on the structures, the following data is set:

- The building is regular in plan and elevation, hence the lateral force method is considered;
- The building is composed of two above the ground floors weighting, after the application of the seismic combination, 200kN each;
- The axial load is bore by columns and the lateral force by two 100mm thick, 3x3m^2 shear walls, respectively, so that the two design problems can be considered separately.
- The ordinate of the design spectrum at the period T_1 $S_d(T_1)$ is equal to 0.25g.

Developing the calculation:

$$F_h = WS_d(T_1)\lambda = (200+200)\cdot 0.25\cdot 1 = 100\text{kN} \qquad [8.1.1]$$

where

F_h Base shear force

$S_d(T_1)$ Ordinate of the design spectrum at the period

T_1 Fundamental period of the structure

W Weight of the structure

Each wall on the ground floor is loaded with 50kN in shear and 0kN in compression. Connections already presented in chapters 3 and 4 are used, placing two hold-downs at the edges of the wall and one angle bracket per meter along the base, as shown in Figure 8.2.1.

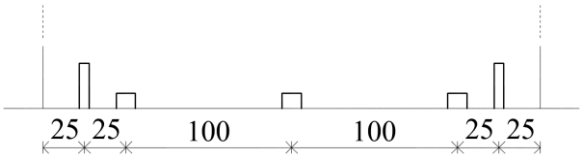

Figure 8.2.1 – Arrangement of the connection of the designed wall (measures in cm).

For this examples, the following parameters are considered:

- CLT strength in compression: 11N/mm^2;
- CLT Young modulus: 4600N/mm^2;
- Density of wood: 420kg/m^3;
- Stress distribution coefficient *k* equal to 0.23 (CLT on rigid support, see chapter 3.3.2.2).

In order to make the iterative process this method is characterized by automatic, a purposely developed software has been created. This software, once all the geometric and material parameters are set, draws the resistant domain for the given wall; calculates the values of bending moment, axial load and neutral axis position at the interface of the different sub-domains; calculates the neutral axis position, the compressive reaction force in the CLT panel and the sub-domain interested for the given external loads.

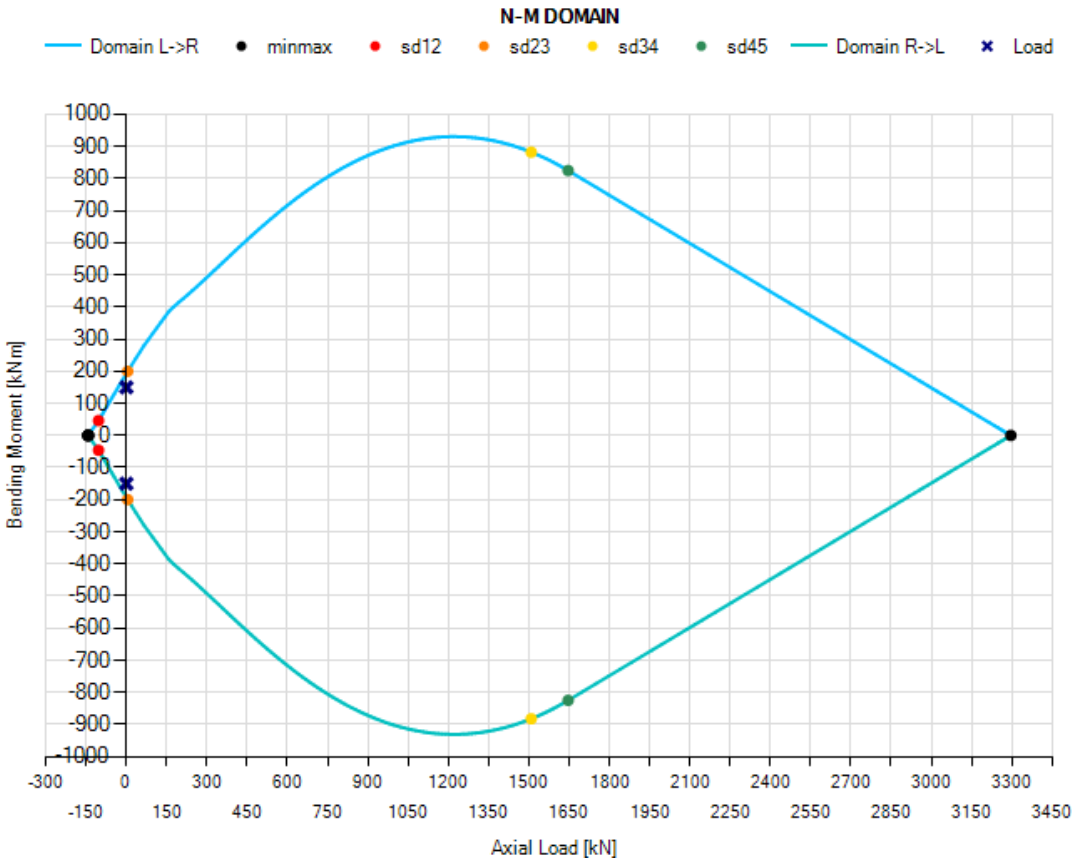

Figure 8.2.2 – Bending moment-axial load resistant domain for the given wall and verification of the calculated external loads (blue X) (figure taken from the purposely developed software).

For the given scenario and the loads set, the domain calculated is the one shown in Figure 8.2.2. As it can be seen from Figure 8.2.2, the point having the external loads as coordinates lays inside the resistant domain, so the supposed arrangement of connections satisfies the design conditions.

Now, let's suppose the shear walls are composed by two panels linked by six screws, as the one presented in chapter 4, each. In this example, the arrangement of connections just considered is not valid as the central angle brackets is placed between the panels. The configuration of base connections for the first attempt is the one shown in Figure 8.2.3.

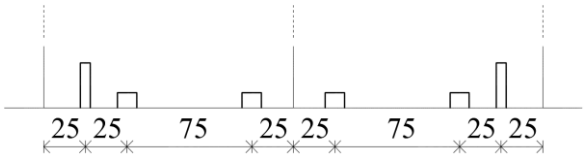

Figure 8.2.3 – First attempt arrangement of the connection of the designed segmented wall (measures in cm).

For the number of screws chosen, the behavior expected is coupled. For the hypotheses made in chapter 4.4, the capacity of the segmented shear wall is calculated by summing the capacity of each panel, obtained using the method presented in chapter 3. If the parameters for the two panels are used in the purposely developed software, the capacities obtained for the bending moment are 69.6kNm and 36.4kNm. In chapter 4.4.1. a corrective coefficient equal to 1.32 is suggested. The resulting capacity is the following:

$$M_{Rd} = \left(M_{Rd,left} + M_{Rd,right}\right) \cdot 1.32 = (69.6 + 36.4) \cdot 1.32 = 139.92 kNm \qquad [8.1.2]$$

The applied bending moment is greater than the resisting one, being equal to 150kNm.

The proposed solution is to considered two wider CLT panels, passing from 1.5m to 1.6m. The second attempt shear wall is depict in Figure 8.2.4.

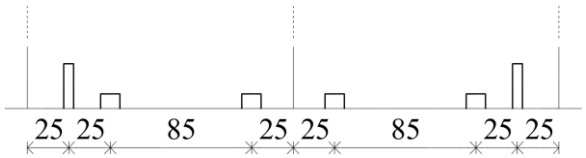

Figure 8.2.4 - Second attempt arrangement of the connection of the designed segmented wall (measures in cm).

Using this characteristics, the two separated capacities are 75.9kNm and 38.2kNm, that summed together and multiplied by the coefficient 1.32, give a total capacity of 150.61kNm, which satisfies the design requirements.

REFERENCES

[1] Al-douri K, Hamodi M, Hasuni H. Compression strength perpendicular to grain in cross-laminated timber (CLT). Master thesis, Växjö University, 2009.

[2] Amini M O, van de Lindt J W, Pei S, Rammer D, Line P, Popovski M. Overview of a Project to Quantify Seismic Performance Factors for Cross Laminated Timber Structures in the United States. RILEM Bookseries. 9. 2014. 531-541.

[3] Amini M O, van de Lindt J W, Rammer D, Pei S, Line P, Popovski M. Determination of Seismic Performance Factors for CLT Building Systems. 14th World Conference on Timber Engineering WCTE 2016. Vienna, Austria.

[4] Amini M O, van de Lindt J W, Rammer D, Pei S, Line P, Popovski M. Systematic experimental investigation to support the development of seismic performance factors for cross laminated timber shear wall systems. Engineering Structures, 172(2018):392–404. DOI:10.1016/j.engstruct.2018.06.021. 2018.

[5] ASCE. Minimum design loads for buildings and other structures. Reston, Virginia. 2010

[6] Barbosa A R, DeMeza B, Sinha A, Higgins C, Rodrigues L, Zimmerman R B, McDonnell E, Breneman S, Pei S, van de Lindt J W, Berman J, Branco J. Design and Shake-Table Experimental Results of CLT and CLT-Concrete Composite Diaphragms. 15th World Conference on Timber Engineering WCTE 2018. Seoul, Korea.

[7] Blaβ H J, Fellmoser P. Design of solid wood panels with cross layers. 8th World Conference on Timber Engineering WCTE 2004. Lahti, Finland, 2004.

[8] Blomgren H-E, Pei S, Powers J, Dolan J, Wilson A, Morrel I, Jin Z. Cross-Laminated Timber Rocking Wall with Replaceable Fuses: Validation Through Full-Scale Shake Table Testing. 15th World Conference on Timber Engineering WCTE 2018, Seoul, Korea.

[9] Casagrande D, Doudak G, Mauro L, Polastri A. Analytical approach to establishing the elastic behavior of multipanel CLT shear walls subjected to lateral loads. Journal of Structural Engineering 2018; 144(2): 04017193.

[10] Ceccotti A. New technologies for construction of medium-rise buildings in seismic regions: the XLAM case. Struct Eng Int 2008; 18(2):156–65. http://dx.doi.org/10.2749/101686608784218680

[11] Ceccotti A, Sandhaas C, Okabe M, Yasumura M, Minowa C, Kawai N. SOFIE project–3D shaking table test on a seven-storey full-scale cross-laminated timber building. Earthquake Engineering & Structural Dynamics 2013; 42(13): 2003-2021.

[12] Christovasilis I P, Brunetti M, Follesa M, Nocetti M, Vassallo D. Evaluation of the Mechanical Properties of Cross Laminated Timber with Elementary Beam Theories. Construction and Building Materials 2016; 122:202-213.

[13] Clough, R W, Penzien J. Dynamics of Structures, 2nd ed. (revised). Computers and Structures, 2003.

[14] CSA, O86-14. Canadian Standard for Engineering design in wood. CSA Publisher, 2014.

[15] CSI, “SAP2000 Integrated Software for Structural Analysis and Design,” Computers and Structures Inc., Berkeley, California, 2018.

[16] D’Arenzo G, Rinaldin G, Fossetti M, Fragiacomo M, Nebiolo F, Chiodega M. Tensile and shear behaviour of an innovative angle bracket for CLT structures. 15th World Conference on Timber Engineering. COEX exhibition and convention center. Seoul, South Korea. 2018.

[17] Dassault Systèmes Simulia Corp.. "Abaqus 2018 documentation." Johnston, Rhode Island, US, 2018.

[18] Dujic B, Pucelj J, Zarnic R. Testing of racking behavior of massive wooden wall panels. Proc., 37th CIB-W18 Meeting, International Council for Building Research and Innovation, Rotterdam, Netherlands. 2004.

[19] Dujič B, Strus K, Zarnic R, Ceccotti A.Prediction of dynamic response of a 7-storey massive Xlam wooden building tested on a shaking table. 11th World Conference on Timber Engineering WCTE 2010. Riva del Garda, Italy, CD

[20] Électricité De France - EDF. Finite element code_aster, Analyse des Structures et Thermo-mécanique pour des Etudes et des Recherches, open source on www.code-aster.org, 1989-2018.

[21] ETA Danmark A\S. European technical approval ETA-06/0106. Technical Approval for Simpson Strong-Tie Angle Bracket 90, http://www.strongtie.dk/, in Danish.

[22] European Committee for Standardization (CEN). Eurocode 2: Design of concrete structures - Part 1-1: General rules and rules for buildings. 2004.

[23] European Committee for Standardization (CEN). Eurocode 5: Design of timber structures - Part 1-1: General - Common rules and rules for buildings. 2014.

[24] European Committee for Standardization (CEN). Eurocode 8: Design of structures for earthquake resistance - Part 1: General rules, seismic actions and rules for building. 2004.

[25] FEMA, Federal Emergency Management Agency. Quantification of Building Seismic Performance Factors – FEMA P695. 2009.

[26] Follesa M, Fragiacomo M, Lauriola M P. A Proposal for Revision of the Current Timber Part (Section 8) of Eurocode 8 Part 1. CIB-W18, 44-15-1. Alghero, Italy. 2011.

[27] Follesa M, Christovasilis I P, Vassallo D, Fragiacomo M, Ceccotti A. Seismic design of multi-storey cross laminated timber buildings according to Eurocode 8. Ingegneria Sismica, 30 (4), pp. 27-53. 2013.

[28] Follesa M, Fragiacomo M. Force-based seismic design of mixed CLT/Light-Frame buildings. Engineering Structures 2018, 168(2018)628–642. https://doi.org/10.1016/j.engstruct.2018.04.091.

[29] Follesa M, Fragiacomo M, Casagrande D, Tomasi R, Piazza M, Vassallo D, Canetti D, Rossi S. The new provisions for the seismic design of timber buildings in Europe. Engineering Structures 2018, 168(2018)736–747. https://doi.org/10.1016/j.engstruct.2018.04.090.

[30] Fragiacomo M, Dujič B, Šušteršič I. Elastic and ductile design of multi-storey crosslam massive wooden buildings under seismic actions. Eng Struct 2011; 33(11):3043–53. http://dx.doi.org/10.1016/j.engstruct.2011.05.020

[31] Fragiacomo M, Rinaldin G. Advanced models for seismic analyses of timber buildings. Außergewöhnliche Einwirkung - Erdbeben - im Holzbau. Workshop on timber construction. Grazer Holzbau-Fachtagung–9. Gra FHT'11. Technical University of Graz, Austria

[32] Gagnon S, Pirvu C. CLT handbook: cross-laminated timber. Québec: FPInnovations, 2011.

[33] Gavrić I, Fragiacomo M, Ceccotti A. Capacity Seismic Design of X-Lam Wall Systems Based on Connection Mechanical Properties. CIB-W18, 46-15-2. Vancouver, Canada. 2013.

[34] Gavrić I, Popovski M. 2014. Design models for CLT shearwalls and assemblies based on connection properties. CIB-W18, 47-15-4, Bath, United Kingdom. 2014.

[35] Gavrić I, Fragiacomo M, Ceccotti A. Cyclic behaviour of typical metal connectors for cross-laminated (CLT) structures. Materials and Structures 2014; 48(15):1841–1857. DOI 10.1617/s11527-014-0278-7

[36] Gavrić I, Fragiacomo M, Ceccotti A. Cyclic behavior of typical screwed connections for cross-laminated (CLT) structures. Eur J Wood Prod 2015. 73(2):179–191. DOI 10.1007/s00107-014-0877-6

[37] Gavrić I, Fragiacomo M, Ceccotti A. Cyclic behavior of cross-laminated timber (CLT) wall systems: Experimental tests and analytical prediction models. ASCE Journal of Structural Engineering 2015; 141(11), 04015034, DOI: 10.1061/(ASCE)ST.1943-541X.0001246

[38] Granello G, Leyder C, Palermo A, Frangi A, Pampanin S. Design Approach to Predict Post-Tensioning Losses in Post-Tensioned Timber Frames. ASCE Journal of Structural Engineering 2018. 144. 10.1061/(asce)st.1943-541x.0002101.

[39] Hristovski V, Dujič B, Stojmanovska M, Mircevska V. Full-scale shaking-table tests of XLam panel systems and numerical verification: Specimen 1. ASCE Journal of Structural Engineering 2013; 139(11):2010–8. http://dx.doi.org/10.1061/(ASCE)ST.1943-541X.0000754

[40] IVALSA-CNR Trees and Timber Institute. SOFIE Project – new architecture with wood, http://www.ivalsa.cnr.it/sofie.html. 2008 (in Italian).

[41] Izzi M, Rinaldin G, Polastri A, Fragiacomo M. A hysteresis model for timber joints with dowel-type fasteners. Engineering Structures 2017; 157(18)170–178. https://doi.org/10.1016/j.engstruct.2017.12.011

[42] McKenna F, Scott M H, Fenves G L. Nonlinear finite element analysis software architecture using object composition. Journal of Computing in Civil Engineering 2010, 24(1):95-107, http://dx.doi.org/10.1061/(ASCE)CP.1943-5487.0000002

[43] Miura S, Isoda H, Tsuchimoto T, Nakagawa T, Kitamori A, Suzuki K, Tsuda C. Lateral Structural Performance of Narrow Size Cross Laminated Timber Connected with Tensile Bolts. Journal of Structural and Construction Engineering (Transactions of AIJ) 2016; vol. 81, no. 721, 2016, pp. 585-593.

[44] NextFEM Designer Users' manual, v. 1.20b, 2018, Internet site: nextfem.it.

[45] Okabe M, Yasumura M, Kobayashi K, Haramiishi T, Nakashima Y, Fujita, K. Effect of vertical load under cyclic lateral load test for evaluating Sugi CLT wall panel. 12th World Conference on Timber Engineering WCTE 2012. Auckland, New Zealand, 2012, DVD.

[46] Ozcelik O, Luco J E, Conte J P, Trombetti T L, Restrepo J I. Experimental characterization, modeling and identification of the NEES-UCSD shake table mechanical system. Earthquake Eng. Struct. Dyn. 2008; 37(2), 243-264.

[47] Pampanin S, Palermo A, Buchanan A, Fragiacomo M, Deam B. Code Provisions for Seismic Design of Multi-Storey Post-tensioned Timber Buildings. CIB-WG18, 39-15-6. Florence, Italy. 2006.

[48] Patzák B. OOFEM - an object-oriented simulation tool for advanced modeling of materials and structures. Acta Polytechnica, 52(6):59–66. 2012.

[49] Pei S, Popovski M, Van de Lindt J W. Performance Based Design and Force Modification Factors for CLT Structures. CIB-W18, 45-15-1. Växjö, Sweden. 2012.

[50] Pei S, van de Lindt J W, Popovski M, Berman J W, Dolan J D, Ricles J, Sause R, Blomgren H, Rammer D R. Cross-Laminated Timber for Seismic Regions: Progress and Challenges for Research and Implementation. Journal of Structural Engineering 2014; E2514001

[51] Pei S, van de Lindt J W, Barbosa A R, Berman J, McDonnel E, Dolan J, Zimmerman R, Sause R, Ricles J, Ryan K. Full-Scale Shake Table Test of Mass-Timber Building with Resilient Post-Tensioned Rocking Walls. 15th World Conference on Timber Engineering WCTE 2018, Seoul, Korea.

[52] Piazza M, Schickhofer G, Flatscher G, Campos Costa A, Candeias P X. Seismic performance of multi-storey timber buildings - TUGraz building. Final Report. SERIES - Seismic Engineering Research Infrastructures for European Synergies. TUGraz, Graz, Austria. 2013.

[53] Polastri A, Giongo I, Piazza M. An innovative connection system for cross-laminated timber structures. Structural Engineering International 2017; 27:4, 502-511. DOI: 10.2749/222137917X14881937844649.

[54] Polastri A, Giongo I, Angeli A, Brandner R. Mechanical characterization of a pre-fabricated connection system for cross laminated timber structures in seismic regions. Engineering Structures 2017; 167(2017):705-715. https://doi.org/10.1016/j.engstruct.2017.12.022

[55] Popovski M, Gavrić I. Performance of a 2-Story CLT House Subjected to Lateral Loads. Journal of Structural Engineering 2016; 142 (4). https://doi.org/10.1061/(ASCE)ST.1943-541X.0001315

[56] Pozza L, Scotta R, Vitaliani R. A non linear numerical model for the assessment of the seismic behavior and ductility factor of X-Lam timber structures. International Symposium "Timber Structures from Antiquity to the Present" edited by J. Chilton and I. Mungan, Istanbul (Turkey), June 25-27, pp. 151-162, 2009.

[57] Pozza L, Scotta R, Trutalli D, Polastri A, Smith I. Experimentally based q-factor estimation of cross-laminated timber walls. Proc ICE Struct Build 2016; 169(7):492–507. http://dx.doi.org/10.1680/jstbu.15.00009.

[58] Pozza L, Saetta A, Savoia M, Talledo D. Coupled axial-shear numerical model for CLT connections. Constr Build Mater 2017; 150:568–82. http://dx.doi.org/10.1016/j.conbuildmat.2017.05.141

[59] Rinaldin G, So.ph.i. program, internet site: giovanni.rinaldin.org

[60] Rinaldin G, Amadio C, Fragiacomo M. A component approach for the hysteretic behaviour of connections in cross-laminated wooden structures. Earthquake Eng Struct Dyn 2013; 42(13):2023–42. http://dx.doi.org/10.1002/eqe.2310

[61] Rinaldin G, Poh'sie G H, Fragiacomo M, Amadio C, Pontarin F. Non-linear modelling of the three and seven storey X−Lam buildings tested within the SOFIE project. 13th World Conference on Timber Engineering WCTE 2014. Quebec City, Quebec, CA. 2014.

[62] Rinaldin G, Fragiacomo M. Non-linear simulation of shaking-table tests on 3- and 7-storey X-Lam timber buildings, Engineering Structures 2016; 113(16)133-148 http://dx.doi.org/10.1016/j.engstruct.2016.01.055

[63] Rinaldin G, Amadio C, Macorini L. A macro-model with nonlinear springs for seismic analysis of URM buildings. Earthquake Engng Struct. Dyn. 2016; 45 no.14: 2261-2281. DOI: 10.1002/eqe.2759

[64] Rinaldin G, Fragiacomo M, Amadio C. On the accuracy of the N2 inelastic spectrum for timber structures. Soil Dynamics and Earthquake Engineering 2017; 100(17)49-58 http://dx.doi.org/10.1016/j.soildyn.2017.05.026

[65] Schickhofer G, Brandner R, Bauer, H. Introduction to CLT, Product Properties, Strength Classes. Cross Laminated Timber - a competitive wood product for visionary and fire

safe buildings: Joint Conference of COST Actions FP1402 and FP1404, Stockholm, Sweden. 2016.

[66] Shen Y-L, Schneider J, Tesfamariam S, Stiemer SF, Mu Z-G. Hysteresis behavior of bracket connection in cross-laminated-timber shear walls. Constr Build Mater 2013; 48:980–91. http://dx.doi.org/10.1016/j.conbuildmat.2013.07.050

[67] Simpson Strong-Tie. Strong-Rod™ Systems for Multi-Storey Overturing Restraint, Canadian Edtion, Simpson Strong-Tie. 2016.

[68] Šušteršič I, Fragiacomo M, Dujič B. Influence of the connection behaviour on the seismic resistance of multi-storey crosslam buildings. 12th World Conference on Timber Engineering WCTE 2012. Auckland, New Zealand, 2012, DVD.

[69] Šušteršič I, Fragiacomo M, Dujič B. Seismic analysis of Cross-Laminated multistory timber buildings using code-described methods: influence of panel size, connection ductility, and schematization. J Struct Eng 2016; 142(4):E4015012. http://dx.doi.org/10.1061/(ASCE)ST.1943-541X.0001344

[70] Tamagnone G. Numerical analysis of X-Lam buildings under seismic loads and validation of design procedures. Master thesis, Politecnico di Torino, Italy. 2015.

[71] Tamagnone G, Rinaldin G, Fragiacomo M. A novel method for non-linear design of CLT wall systems. Engineering Structures 2018; 167(18)760-771 https://doi.org/10.1016/j.engstruct.2017.09.010

[72] Thiel A, Schickhofer G. CLTdesigner – A Software Tool for Designing Cross Laminated Timber Elements: 1D-Plate-Design. 11th World Conference on Timber Engineering WCTE 2010. Riva del Garda, Italy. 2010.

[73] Thiel, A. ULS and SLS Design of CLT and its Implementation in the CLT designer. In: Harris R, Ringhofer A, Schickhofer G (ed.), Focus Solid Timber Solutions – European Conference on Cross Laminated Timber (CLT), Graz, Austria. 2013.

[74] Tomasi R. Seismic behaviour of connections for buildings in CLT. COST Action FP1004 Conf. on the State-of-the Art in CLT Research. Univ. of Bath. Bath, North East Somerset, UK. 2013.

[75] van Bakel R, Rinaldin G, Leijten A J, Fragiacomo M. Experimental-numerical investigation on the seismic behaviour of moment-resisting timber frames with densified veneer wood-reinforced timber joints and expanded tube fasteners. Earthquake Engng Struct. Dyn. 2017; 46:1307–1324 DOI: 10.1002/eqe.2857

[76] van de Lindt J W, Furley J, Amini M O, Pei S, Tamagnone G, Barbosa A R, Rammer D., Line P, Fragiacomo M, Popovski M. Experimental seismic behavior of a two-story CLT platform building: shake table testing results. 15th World Conference on Timber Engineering. COEX exhibition and convention center. Seoul, South Korea. 2018.

[77] Vassallo D, Follesa M, Fragiacomo M. Seismic design of a six-storey CLT building in Italy. Engineering Structures 2018, 175(2018)322–338. https://doi.org/10.1016/j.engstruct.2018.08.025.

[78] Yasumura M, Kobayashi K, Okabe M, Miyake T, Matsumoto K. Full-scale tests and numerical analysis of low-rise CLT structures under lateral loading. J Struct Eng 2016; 142(4):E4015007. http://dx.doi.org/10.1061/(ASCE)ST.1943-541X.0001348

[79] Zarnani P, Valadbeigi A, Hashemi A, Darani F M, Yousef-beik S M M, Bagheri H, Quenneville P. Rotational performance of Resilient Slip Friction Joint (RSFJ) as a new damage free seismic connection. 15th World Conference on Timber Engineering WCTE 2018. COEX exhibition and convention center. Seoul, South Korea. 2018.